BUNDESAMT FÜR
SEESCHIFFFAHRT
UND
HYDROGRAPHIE

Tsunami - a study regarding the North Sea coast

Autoren:
Ingrid Bork
Stephan Dick
Eckhard Kleine
Sylvin Müller-Navarra

Berichte des
Bundesamtes für Seeschifffahrt und Hydrographie
Nr. 41/2007

In der Reihe „Berichte des Bundesamtes für Seeschifffahrt und Hydrographie“
werden Themen mit Dokumentationscharakter aus allen Bereichen des BSH veröffentlicht.
Durch die Publikation nimmt das BSH zu den Inhalten der Beiträge keine Stellung.
Die Veröffentlichungen in dieser Berichtsreihe erscheinen nach Bedarf.

Der Tsunami – a study regarding the North See coast im Internet:
www.bsh.de (Menü: Produkte → Bücher → Berichte des BSH)

ISSN-Nr. 0946-6010

Abstract

North Sea storm surges with water levels of 4 to 5 m NN (German ordnance datum) are annually recurring events that are dealt with by the official prediction services. The subject of this study is the behaviour of a hypothetical tsunami of comparable height traversing a wide, shallow shelf. The period of a tsunami ranges between that of wind waves and that of the semidiurnal tide dominating in the North Sea. Analytical wave theories, which have been developed for sea and swell, do not describe tsunami completely. Numerical models used to forecast storm surges are suitable in principle to simulate the propagation of medium-length waves in the North Sea. This mainly requires an adaptation of grid spacing to the shorter wave lengths. As an example, the propagation of three positive signals with a period of 1800 s, which is typical of tsunami caused by slope failure, and wave heights of 5 to 8 m, has been simulated. Models of this type have limited applicability on the continental slope and are not suitable for near-shore areas. Despite all restrictions regarding the analytical estimations and numerical simulations used, the conclusion appears justified that significantly less wave energy would be present in the German Bight after a hypothetical tsunami has crossed the wide and shallow shelf of the North Sea than be the case on a coast with a steep, narrow shelf that was hit by a comparable tsunami.

1 Introduction

In December 2004, when the disastrous tsunami occurred in the Indian Ocean, the coastal population and the authorities were totally unprepared. Immediately after the disaster, the German Federal Ministry of Education and Research (BMBF) commissioned the Helmholtz Association of National Research Centres to develop a tsunami early warning system for the Indian Ocean. A commission to develop a warning system for the Mediterranean Sea and the Atlantic Ocean was established later. Scientists at the Federal Maritime and Hydrographic Agency of Germany (BSH, Bundesamt für Seeschifffahrt und Hydrographie), the agency issuing the official water level predictions for the North and Baltic Seas, raised the question whether a tsunami from the Atlantic Ocean might also pose a hazard to the German coasts.

At first glance, the occurrence of a tsunami in the North Sea may appear quite unlikely. But there is evidence that the European waters have witnessed tsunami in the past. For example, a tsunami was triggered by the Lisbon earthquake in 1755. The best studied event in northern Europe is the tsunami caused by the Storegga submarine slide about 8000 bp (before present, i.e. before 1950).

The propagation of long waves with amplitudes of up to one metre, tidal waves, and external surges into the North Sea is well understood and is taken into account in the daily water level predictions. Tsunami are long waves, with shorter wavelengths and significantly greater wave heights than the semidiurnal tide prevailing in the North Sea. Prior to this investigation, the lead time between the entry of a tsunami into the North Sea from the north and its arrival on the German coasts had been estimated at 10 hours. It had also been assumed that a tsunami would lose much of its energy on the wide, shallow North Sea shelf.

In order to provide well-founded answers to questions raised by the public and to obtain quantitative data, the BSH carried out its project “Tsunami - a study regarding the North Sea coast“ between 24 January 2005 and 31 August 2005. The scope of the study was limited to information that is relevant to the German coasts. It included mainly:

- literature and internet research
- compilation of possible tsunami sources
- compilation of historical tsunami events
- theoretical descriptions of the behaviour of waves propagating from deep to shallow waters, wave propagation and damping on wide shelves
- estimated travel times and wave heights
- development of a tsunami modelling concept based on BSH models
- model simulations using a model system adjusted to the problem.

After the tsunami issue had also been discussed at other institutions, the BSH hosted the workshop “Tsunami – Eine Gefahr für unsere Küsten?“ (Tsunami - a hazard to our coasts?), which was limited to German institutions. Its aim was to enter into a discussion about recent findings and possibly define research topics regarding the German coasts. (CD of the workshop of 21 June 2005 is available from the BSH).

2 Selected literature and web sites

Not a single tsunami warning has been issued since the beginning of official water level predictions for the North Sea coast, i.e. since 1879, when the first tide table was published. The operational models for water level predictions run at the BSH thus were not designed for tsunami simulations and those in charge of the predictions had no experience in tsunami forecasting. Therefore, some books are introduced below which discuss the subject briefly but in sufficient detail. Also the web sites listed in chapter 10 were chosen under the same aspect. Of particular interest in this regard are the risk assessments and reports provided by other North Sea countries. More specific work is referred to in the text.

In the aftermath of the disastrous 1960 tsunami in Chile, the International Union of Geodesy and Geophysics (IUGG) held an international meeting parallel to a conference on tsunami hydrodynamics. The proceedings of the conference are still worth reading. In his keynote address, Cox (1961) summed up the status of tsunami research at the time. The final resolution is particularly interesting (Resolutions 1961). Although tsunami events were considered to be primarily a problem of countries bordering the Pacific Ocean, the IUGG recommended that European countries should investigate the possibility of tsunami occurrence in the Atlantic Ocean and Mediterranean Sea.

40 years later, tsunami research was still getting little attention in Europe. McNeil, in the "Encyclopaedia of Ocean Sciences" (2001), dedicates less than half a page to the subject of tsunami:

„Tsunamis are long-period waves generated primarily by submarine earthquakes. The name comes from a Japanese word meaning ‚harbour waves', however, it is now used in the scientific literature to exclusively describe seismic sea waves.

Tectonic activity in the seafloor creates a vertical movement in the seafloor and a resultant vertical movement across a wide area of the sea's surface. This leads to the formation of a train of long-period waves. Periods of over an hour are not uncommon. These waves can travel very large distances from the earthquake's epicenter and, as they near the coast, their amplitude is increased by local topographic features.

Considerable damage to property and loss of life have been recorded as the result of tsunamis. Warning systems have been developed mainly around the Pacific Ocean. Provided the epicenter and the time of occurrence are known good estimations can be made of the time the tsunami will reach coastal areas."

The "Encyclopaedia of Physical Science and Technology" contains a good and concise description (15 pages) of subjects ranging from the "Characteristics of Tsunamis" to "Tsunami Forecasting" (Ward 2002).

Another summary is provided by Camfield (1990) in the Handbook of Coastal and Ocean Engineering.

A book that has been widely read among experts after the tsunami of December 2004 is "Tsunami – The Underrated Hazard" (Bryant 2001). When compiling section 3 of this report, much of the information about possible tsunami causes was taken from this book. Especially chapter 2 of the book, entitled "Tsunami Dynamics", is worth reading.

A precise description of analytical wave theory and the approximations on which it is based has been provided by Peregine (1972). More recent theories are discussed by Liu et al. (2002). Mader (2004) provides a good compilation of such theories, together with a survey of numerical models used in tsunami research. The CD enclosed with the book contains some smaller programmes and the results of many tsunami simulations, e.g. the Lisbon tsunami, and tsunami caused by meteoritic impacts in the North Atlantic Ocean (also on the Internet, 10.5: MAD04). It also contains all papers published in the journal „Science of Tsunami Hazards" from 1982 to 2003 (on the Internet, 10: STH82 and 10: STH06 for more recent volumes). A paper dealing with the tsunami of December 2004, which focuses on early

warning and numerical simulations, was published in “Spektrum der Wissenschaft“ in April 2006 (Geist et al. 2006). A book on numerical methods to simulate tsunami wave run-up (Liu et al., 2007) will be published in the fall of 2007.

Studies on submarine slides and tsunami generation have been compiled in Volume 21 of the NATO Science Series (Yalciner et al. 2003). It includes a supplement to the European Tsunami Catalogue (Maramai et al. 2003). A compilation of tsunami in the southern East Atlantic Ocean up to 1963 is provided by Berninghausen (1964).

In 2005, the journal „Marine Geology“ dedicated a special issue to the results of a tsunami symposium (2003), including examples from the Atlantic Ocean and Europe.

Of particular interest to forecasting services are the risk assessments and official reports published by other states (see list of Internet addresses in section 10.1). They exceed the scope of this report. The modelling results given in the reports of the UK (Kerridge 2005, Smallman 2006) and Denmark (Buch et al. 2005) supplement the simulations described in section 7.

The selection of links in section 10 is, of course, arbitrary because the search word “tsunami“ produces a very large number of sites. Besides, the focus in section 10 is on the specific scope of this report. Internet pages listed cover

0 Literature
1 Reports of other institutions and risk assessments
2 Databases and catalogues
3 Internet pages of research institutions and projects
4 Models
5 Tsunami simulations and benchmark problems, and
6 Waves.

3 Sources of relevance to the North Sea

Before considering the establishment of a tsunami warning service for the German North Sea coast, possible causes of tsunami that may affect the North Sea have to be studied and evaluated.

The following is a collection of possible causes of tsunami events, i.e. volcanic eruptions, submarine slides, and meteoritic impacts, under the aspect of their potential occurrence in the North Atlantic Ocean and Arctic Ocean.

In the past, the most devastating destruction has been caused by tsunamigenic events close to the coast, e.g. the Lisbon tsunami in 1755. The UK reports (Kerridge 2005, Smallman 2006) also discusses simulations of tsunami events caused by North Sea earthquakes. However, in the present report, it is assumed that tsunami affecting the North Sea are generated outside the North Sea. An exception might be tsunami caused by meteoritic impacts.

3.1 Earthquakes

Submarine earthquakes are the best-known causes of tsunami events. However, most submarine earthquakes do not result in tsunami.

An earthquake in the subduction zone between tectonic plates and near transform faults (Fig. 3.1.1) will only cause a tsunami if it generates a vertical displacement of the seabed. Such displacements are rare near transform faults, where the plates slide past each other. The only subduction zone in the North Atlantic Ocean is the Caribbean Arc system, and the longest transform fault in this region extends from the Azores into the Mediterranean Sea (see Fig. 3.1.2).

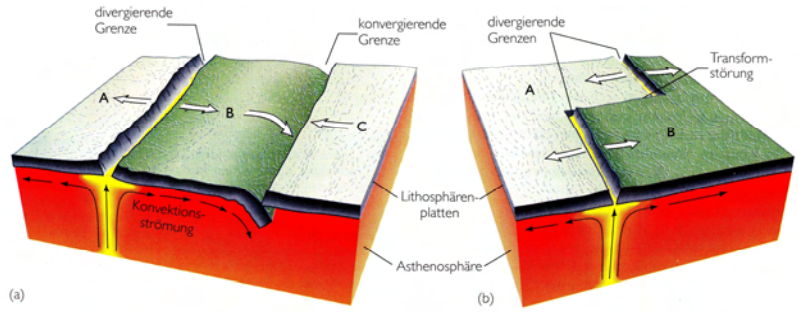

Fig. 3.1.1: Types of plate boundaries (Press et al. 1995, Fig. 1.14)

The earthquake magnitude it takes to produce a significant elevation of the water level depends on the depth of the earthquake epicentre. Strong earthquakes and tsunami felt as far as the North Sea are rare events. However, the Lisbon earthquake of 1755, which had a Richter magnitude of 8.5-9, caused a devastating tsunami. The epicentre of the earthquake was located on the shelf, close to the boundary between the Azores and Gibraltar plates. About 40-60 minutes after the earthquake, the water retreated from the coast and returned a few minutes later as a 15 m wave. More waves followed. The tsunami also propagated along the western European coasts. About 4 hours later, a 3-4 m high wave with a period of 10-20 minutes travelled through the English Channel towards the North Sea. Besides the tsunami caused by vertical water displacement, the seismic waves of this earthquake triggered seiches in Scottish, Swedish, and Finnish lakes (Bryant 2001). Model hazard assessments (Smallman 2006) give extreme sea levels around the Cornish coast from 3.4 to 5.2 m.

In the Caribbean region, the Caribbean plate is moving toward the North American plate. Tsunami are frequent in this region (Grundlay et al. 2005), but their effect on northern Europe is minor.

Earthquakes at other plate boundaries hardly ever trigger tsunami that reach the North Atlantic Ocean. However, the tsunami of December 2004 was also recorded on the European coasts. Model simulations showed that it reached the continental shelf off Ireland after about 30 hours (Geist et al. 2006).

The reported periods of 10-20 minutes are characteristic of earthquake-induced tsunami, but also periods of more than one hour are not unusual (McNeil 2001).

Earthquakes have also occurred in the North Sea itself. Huge waves were reported in the Channel at the time of the 1580 earthquake. The authors of the British report (Kerridge 2005) concluded, however, that most likely the 1580 earthquake did not cause a tsunami, and that the huge waves observed had other sources.

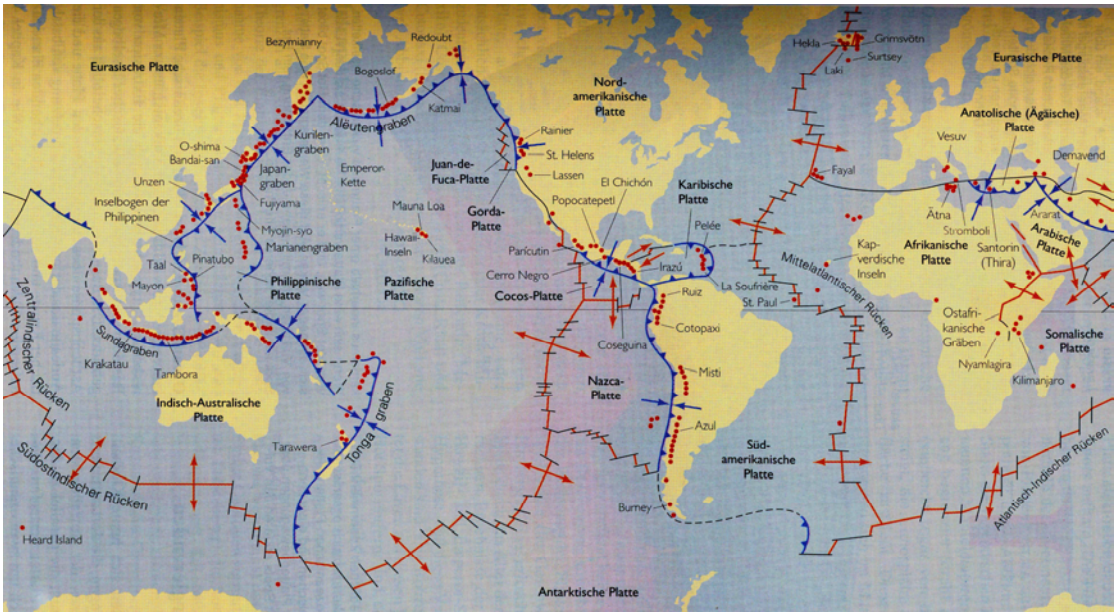

Fig. 3.1.2: Plate boundaries (blue: convergent, red: divergent, black: transform fault) and active volcanoes (Press et al. 1995, Fig. 5.27)

3.2 Volcanic eruptions

Volcanic eruptions may cause tsunami by different mechanisms (cf. Table 7.1, Bryant 2001, Latter 1981).

- A tsunami can be triggered by seismic tremors accompanying an eruption.
- Volcanic eruptions may lead to pyroclastic flows. Most of these flows consist of two parts: a mixture of hot rock and gas that moves along the ground and a cloud of hot ash that rises above it. Both parts can result in a tsunami when they reach an ocean surface. In the past, hot ash having a higher density than sea water has caused large tsunami remote from the eruption site due to large masses of ash sinking to the seabed and flowing along the bottom.
- Underwater volcanic eruptions in the upper 500 m of the water column result in tsunami due to pressure fluctuations. Steam explosions followed by huge tsunami occur when water comes in contact with hot magma.
- The collapse of a vulcano summit may form a caldera. Water rushing into such calderas has been the cause of historical tsunami.
- During slope failures on high, steep volcanoes, the avalanching slope material reaches very high flow speeds before it enters the water. The resulting tsunami may be extremely high.
- Lateral eruptions may cause major debris flows into the water.
- Also mixtures of ash and water from crater lakes or ash and glacier ice from the crest of the volcano (lahars) have triggered high local tsunami.
- Another potential cause is lava flows into the ocean.

All of the above events require the volcano to be located in or close to the ocean. According to a map of historic volcano eruptions (Latter 1981), tsunami have occurred in the North Atlantic Ocean after volcanic eruptions on Martinique (Monte Pelée) and Iceland. The Russian tsunami catalogue (10.2: HTA03) lists seven tsunami which were triggered by Icelandic volcanoes. Imsland (1988), however, considers the tsunami risk from Icelandic volcanoes to be very low or even non-existent.

Tsunami generation by atmospheric pressure waves following a volcanic eruption at a large distance from the volcano has been observed. So far, there has been no evidence of such phenomena in the North Atlantic Ocean.

3.3 Slope failures

Earthquakes may trigger slope failures on steep, vulnerable continental slopes and coasts. Volcanic eruptions may be involved in slope failures in several ways. Prehistoric slope failures have been attributed to meteoritic impacts. Also a potential de-stabilisation of slopes by mining of mineral resources has been discussed. Gas hydrates have an influence on local slope stability in the area of the hydrate reservoir. They are very vulnerable to changes in ambient conditions, especially pressure conditions. These may be influenced by climatological changes or by the exploitation of gas hydrates or other natural resources. Also minor slope failures triggered by various factors may change pressure conditions within the slope, thus modifying the ambient parameters for the gas hydrates and causing secondary slope failures (Parlaktuna 2003).

The mechanism of tsunami generation by slope failure is movement of the slope material itself or the impact of rapidly moving material on the water. The oscillation period increases with the size of the slide and steepness of slope (Bryant 2001).

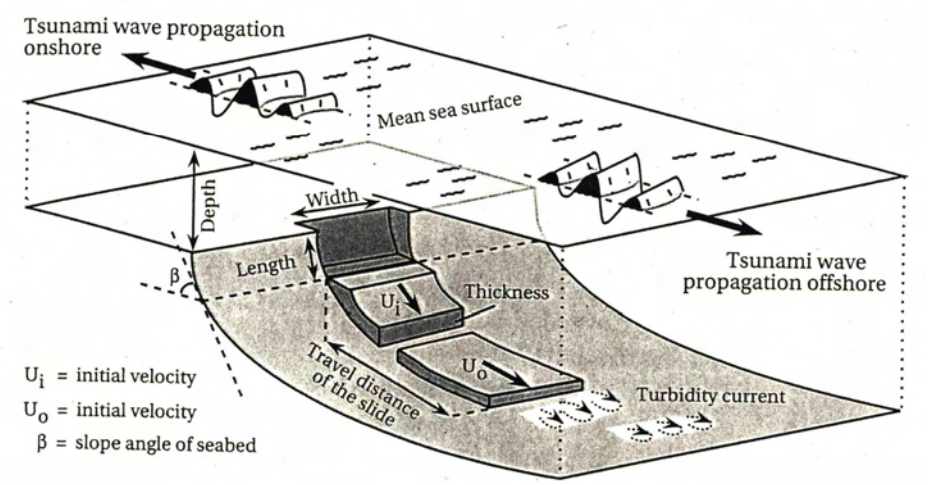

Fig. 3.3.1: Schematic representation of a submarine slide (Bryant 2001, Fig. 6.3)

Several large slope failures occurred on the Norwegian continental slope in the past. One of them is the Storegga slide around 8000 bp which caused a well-known tsunami. From the thickness of the sediment layer flowing down the slope, a wave height of 2.30 m was computed for the tsunami in the deep ocean. Its oscillation period was 2 to 3 hours, which is clearly longer than that of tsunami caused by earthquakes (Blasio et al. 2003). Reconstruction based on geological data, with different assumptions regarding slide velocity, yielded computed water levels between 5.3 and 18 m near Scotland (Harbitz 1992). With sea level rising 0.30-0.35 m per century (Streif 2003), the North Sea level at 8000 bp was about 20 m below the present mean sea level. Off Scotland, it was only 6 m below current mean sea level (Long et al. 1989). This has been taken into account in the above reconstruction. Model computations indicate water levels from 3 m to 5.5 m on the coast of East Scotland (Harbitz 1992 and Bondevik et al. 2005). According to computations by Henry et al. (1992)

using recent bottom topography, the Storegga tsunami reached the central North Sea 6 hours after crossing the shelf edge. The possible recurrence of a slope failure at the Norwegian continental shelf break on the order of the Storegga slide is discussed controversially (see section 10.1).

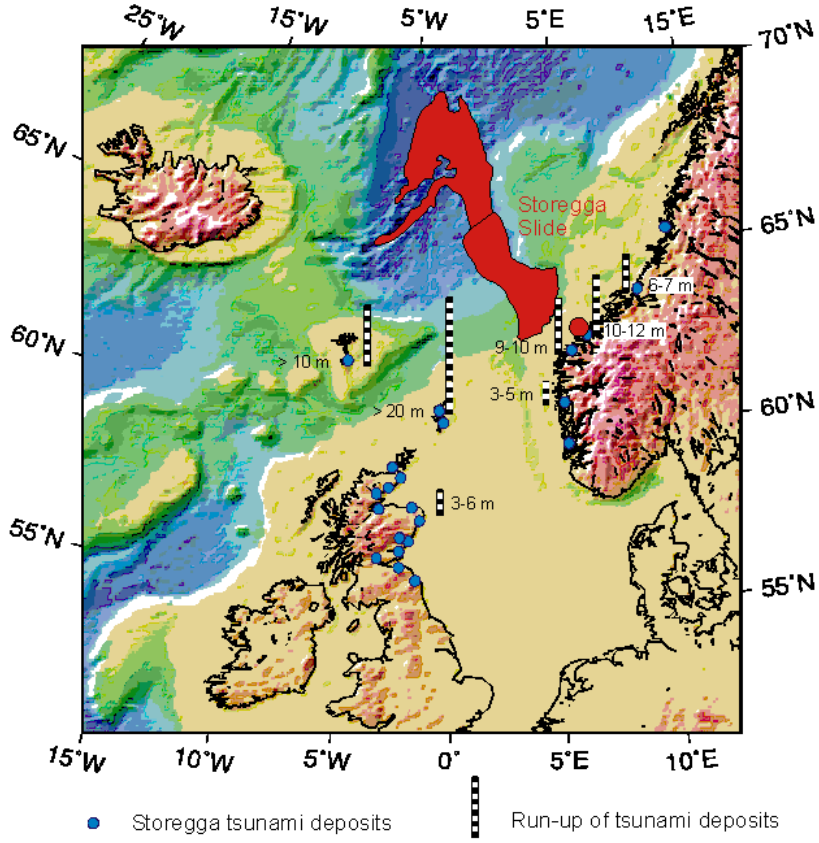

Fig. 3.3.2: Storegga slide; height of deposits above recent sea level (Bondevik et al. 2005)

The volumes of coastal slides are smaller. Theoretical slides off the Norwegian coast were modelled by Rubino et al. in 1998. The expected height of tsunami caused by such slides was found to be 1-2 m, their wavelengths 10 km, and their period about 10 minutes.

A submarine slide near Newfoundland caused by an earthquake was recorded on 18 November 1929, at 20:32 UTC (Ruffmann 2005). Typical periods of the waves generated by the slide were between 12 and 25 minutes. The resulting tsunami had amplitudes of 3-8 m at Newfoundland and was recorded as far as Portugal. Unfortunately, all European coastal gauge station records from those days have disappeared (Fine et al., 2005). In model simulations, the tsunami reached the German North Sea coast after about 16 hours (Fine et al. 2005). However, no evidence of the tsunami has been found in the original, analogue records of the Cuxhaven gauge station (Fig. 3.3.3).

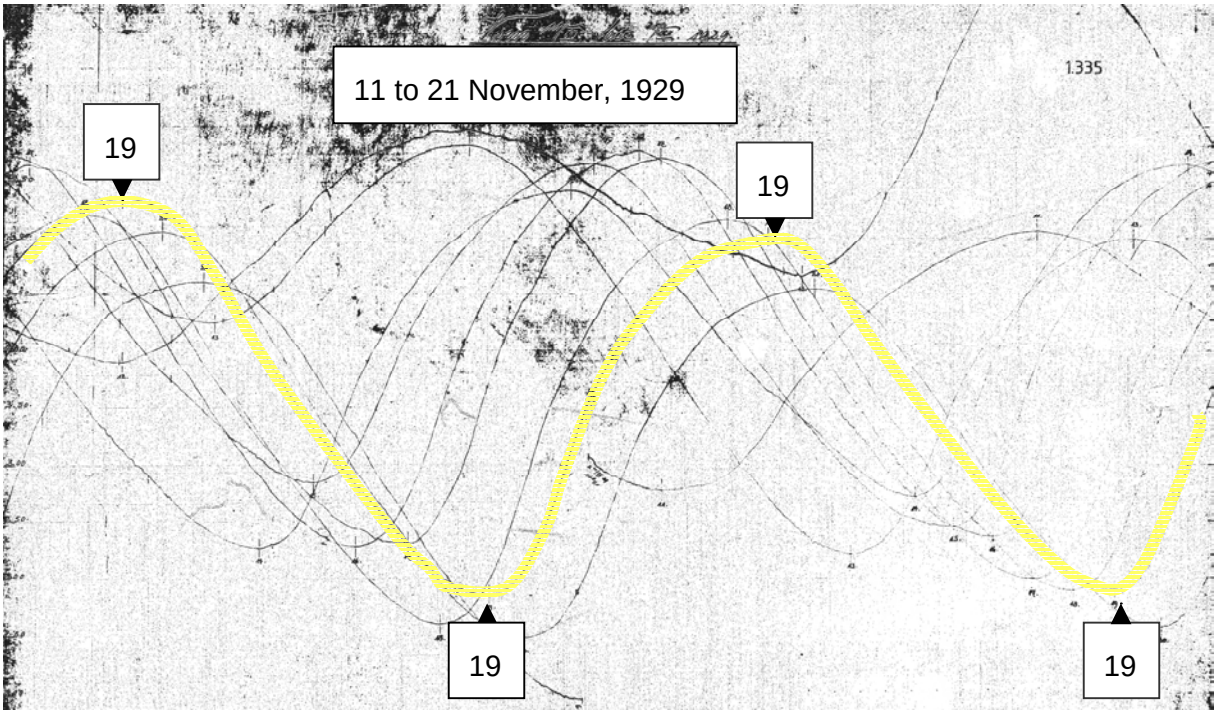

Fig. 3.3.3: Analogue records of the Cuxhaven gauge station from 11 to 21 November, 1929. Curve 19 indicates the day after the Newfoundland slide (Wasser- und Schifffahrtsamt Cuxhaven).

A dramatic scenario of a hypothetical submarine slide on the North-West European continental margin followed by a catastrophic tsunami has been described by Bryant (Bryant 2001). The UK report (Kerridge 2005) is less dramatic in its discussion of submarine slides in this area. Nevertheless, the authors do consider these slides a potential hazard for the Irish and Scottish coasts, but allocate a low probability of occurrence to such events.

On the Canary Islands, evidence for major underwater slides and deposits attributable to a tsunami event has been found onshore at a height of 35-75 m (Bryant 2001). However, the probability of future tsunami events is discussed controversially (Ward et al. 2001, Wynn et al. 2003 and 10.1: TUD06). Model computations of Ward et al. (2001) do not show any significant waves in the Channel or near Scotland caused by a tsunami propagating from the Canary Islands.

Another event occurred in Alaska (Lituya Bay, 1958), where 0.3 km^3 of rock slid into the bay from 600–900 m height, causing a wave run-up of 524 m on the opposite side of the bay (Bryant 2001). The wave travelling out of the bay into the open ocean was about 30 m high (Mader 2004). In principle, such rock slides generate substantially higher tsunami than submarine slides (Sabatier 1986, Fine et al. 2003). Tsunami of such origin have also occurred in Norwegian fjords, but their energy has been much lower.

3.4 Meteoritic impacts

About 8,200 (±200) years ago, a swarm of meteorites struck the Earth. According to geological studies and ancient myths, seven regions of the Earth were hit. One of them is located between Iceland and Norway (Bryant 2001).

In seismic data of the North Sea, Allen (Stewart et al. 2002) identified an impact crater dating back 60–65 million years (Silverpit structure). Although the asteroid reconstructed from the data was small, it was big enough to generate a tsunami in the North Sea (10.3: LOR02).

In 1993, the underwater meteoritic crater Mjølnir was discovered in the Barents Sea. The impact was dated at the Volgian-Ryazanian boundary (Smelror et al. 2001) i.e. about

140 million years ago. Simulations of the tsunami triggered by this event and its propagation in the Paleobarents Sea resulted in maximum water levels of about 100 m in northern Norway. In these simulations, the surface elevation outside Bergen was 30-50 m (Glimsdal et al. 2007,10.3: ICG10).

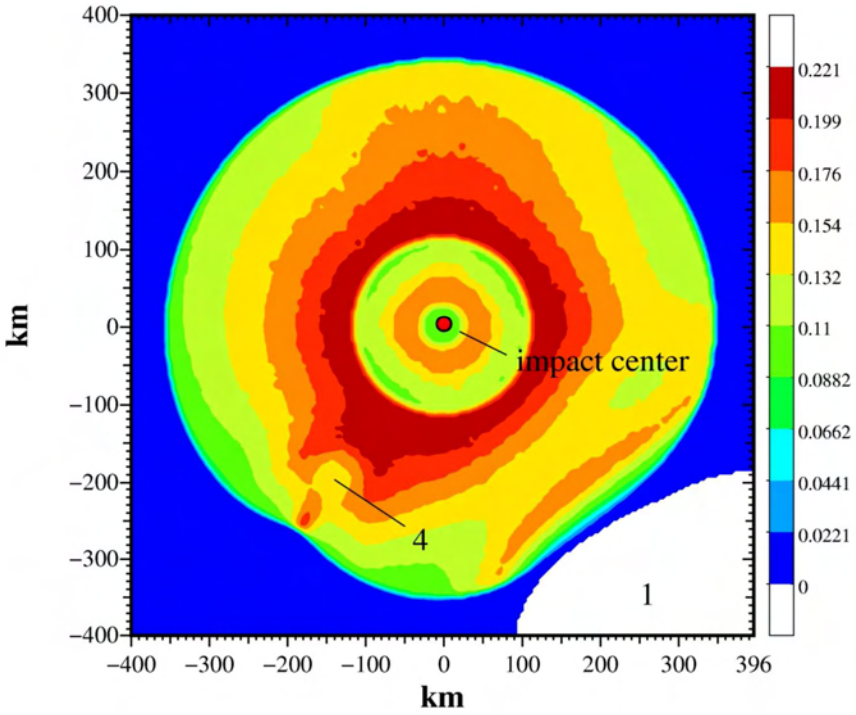

Fig. 3.4.1: Simulation of Mjølnir impact north of Norway (1), maximum vertical surface displacement in km during the tsunami propagation from 17 min to 1 h 10 min after impact (Glimsdal et al. 2007, upper left of Fig. 19)

Meteoritic impacts in different regions of the North-East Atlantic Ocean (Mader 2004: ATLAST.MVE, EURAST.MVE, ICEAST.MVE) were simulated as well. The resulting tsunami propagate in the area between Iceland and Scotland and reach the North Sea after different periods of time, depending on the impact location. Wave height depends on the type and size of the falling body and on the distance from the initial disturbance. For example, an asteroid of 500 m diameter can generate a tsunami which, 500 km from the impact location, is 37 m high and has a period of 180 s (Bryant, 2001, Table 8.2). A tsunami computed by Ward et al. (2003), triggered by an assumed impact of the asteroid “1950 DA” off the U.S.A., generates waves that are still 20 m high off Ireland. However, agreement on quantitative assumptions has not yet been reached in the scientific community.

4 Historic tsunami affecting the North Sea

The tsunami of December 2004 gave rise to a discussion on possible tsunami in the North Sea, mainly because it hit the coastal and island population completely unprepared. No collective memory of a tsunami event existed although major tsunami had occurred in this region in the not too distant past. The Krakatoa volcano erupted in 1883. Then, in 1907, a tsunami of intensity 4 (on a scale from –5 to +5; from 2001: scale from 1 to 12) caused 400 deaths. In 1941, another tsunami of intensity 4 in the Andaman Sea north of Sumatra had a death toll of 5,000 (10.2: NGDC).

Prior to the event of December 2004, the German public and many scientists saw no association between tsunami and the North Sea. Therefore, historic tsunami events affecting the North Sea will be outlined in the following.

The most recent major tsunami which travelled as far as the North Sea were the tsunami caused by a slope failure off Newfoundland (1929) and that triggered by the Lisbon earthquake in 1755. However, it is primarily the proven impact of the Storegga slide which has raised the awareness of a potential threat. It dates back about 8,000 years and probably contributed to the destruction of the land bridge between Denmark and England (Derbyshire et al. 2003).

65 million years ago, a meteoritic impact off Yucatan (Mexico) caused a devastating tsunami in the prehistoric Atlantic Ocean. However, the region now covered by the North Sea was affected only by the climatic change caused by the meteoritic impact. A much smaller asteroid hit the prehistoric North Sea 65-60 million years ago. The Mjølnir impact was about 140 million years ago. Part of the Paleo-North Sea (Ziegler 1990) is included in model simulations (Glimsdal et al. 2007).

Since 1952, several smaller tsunami have been recorded in Norwegian fjords, the most recent one in 1999 (Maramai et al. 2003). The most recent entries in the Russian database, with the source region Iceland, date back to 1924 and 1934.

The North Sea earthquakes of 1927 and 1931 discussed in the UK report (Kerridge 2005) did not even cause local-scale tsunami.

5 Tsunami behaviour upon reaching shallow water

Possible causes of tsunami that may affect the North Sea region have been compiled In section 3. Literature data on the probability of occurrence is either contradictory or not available (see section 10.1). Additional research in this field will be needed. Despite the paucity of data, the assumption will be discussed in this section that a tsunami entering the North Sea would not have impacts on the German coasts comparable to those of the catastrophic tsunami of December 2004 which destructed the coastline of the Indian Ocean. Possible analytical tsunami descriptions will be discussed first. Then, using different modelling concepts and simulations, the modification and propagation of a theoretical tsunami wave travelling from the deep ocean to the coast is discussed with a focus on special features regarding the North Sea.

5.1 Wave theoretical interpretation

The propagation of very long waves – tidal waves and external surges – into the North Sea is the subject of daily water level forecasts. Such waves have characteristic lengths *L* of the order of 1,000 km, and wave heights *H* of 2 metres when entering the North Sea, and up to 4 m at the German coast. The dominant co-oscillating tide in the North Sea is the semidiurnal tide. Sea and swell in the open North Sea have periods *T* on the order of 10 s (Couper 1983) and integral wave lengths of up to 250 m. Tsunami are „in between“. Depending on their origin, their periods are on the order of 100 s (meteoritic impact), 10 minutes (earthquake), and 30 minutes (slope failure). Ward (2002) defined a „tsunami window“ by periods from 100–1,000 s. A single tsunami has a narrower spectrum. Therefore, it is often characterised by a single period. Typical wavelengths of a wave with a period of 30 minutes range between 400 km in the deep sea and 20 km in shallow water (see Table 5.1.1). Disregarding meteoritic impact, the period of tsunami is longer than that of wind waves by about the factor 200, and shorter by the factor 20 than that of the semidiurnal tide. Models used for daily routine water level forecast thus seem to be closer to the description of tsunami than wave theories. On the other hand, tsunami are hardly influenced by the Earth's rotation. The inertial period at the pole is about 12 hours and increases toward the equator. Therefore, classical irrotational wave theories have been used to understand tsunami (e.g. Voit 1987). They have been developed for a range extending from short wind waves to swell, and initially only consider single waves, i.e. progressing waves with a defined wave length, wave height, and wave period.

5.1.1 Wave theories

Starting from the three-dimensional mass and momentum balance equations (e.g. Pichler 1984):

$$\frac{\partial \rho}{\partial t} + \nabla \cdot (\rho \vec{v}) = 0 \text{ und } \frac{\partial \rho \vec{v}}{\partial t} + \nabla \cdot (\rho \vec{v} \vec{v}) + 2\vec{\Omega} \times \rho \vec{v} = -\nabla p - \rho \nabla (\phi + \phi_G) + \vec{F} \qquad (1)$$

(ρ density, $\vec{v} = (\vec{v}_h, v_v)$ velocity, p pressure, $2\vec{\Omega}$ angular velocity of the earth, ϕ gravitational potential, ϕ_G tidal potential, $\vec{F}$ frictional force),

many wave theories are based on simplified advection equations for incompressible, inviscid fluids:

$$\nabla \cdot \vec{v} = 0 \text{ and } \rho_0 \frac{\partial \vec{v}}{\partial t} + \rho_0 \vec{v} \nabla \vec{v} = -\nabla p - \rho_0 \nabla \phi \text{ with boundary conditions} \qquad (2)$$

$v_v = \frac{\partial \eta}{\partial t} + \vec{v}_h \nabla \eta$, $p = 0$ at the water surface (η elevation of the water surface),

$v_v = -\vec{v}_h \nabla h$ at the bottom (h undisturbed water depth).

For analytical progress it is frequently assumed that the water initially is at rest and the velocity field is irrotational. In an inviscid fluid, motion then remains irrotational.

Each particular wave theory neglects certain processes. By neglecting advection (non-linear term) in the equations and in their boundary conditions, changes in wave shape are suppressed. Solutions to linear equations (Airy waves) thus preserve the shape of the surface elevation. A simple wave whose propagation speed is a function of its period is called dispersive (more precisely: frequency dispersive). Whether an approximation leads to dispersive waves can only be seen when the solution has been obtained (Whitham 1999). By neglecting local vertical acceleration, $\partial w/\partial t$, linear equations become hydrostatic linear equations whose solution is non-dispersive. More complex approximations such as the Boussinesq equations (e.g. Boussinesq 1871), and their special forms Korteweg de Vries (Korteweg et al. 1895, 10.6: WEI05) and KP equations (Kadomtsev et al. 1970), are both dispersive and shape changing but, for both properties, only approximately (cnoidal and solitary waves). Other non-linear non-hydrostatic theories (e.g. Stokes 1847) apply only to very small surface elevations and hence are not of interest in this context. Linear Boussinesq equations are shape preserving and, to first order, dispersive.

In linear non-hydrostatic and non-linear hydrostatic equations, the manifold influences of variable bottom topography, reflection, refraction, diffraction, and energy concentration (shoaling) are taken into account through the bottom boundary condition. Of the Boussinesq type, only more complex equations (Peregine 1972, Madsen et al. 1991, Madsen et al. 1992, Liu et al. 2002) can be applied to variable bottom topography.

Fig. 5.1.1 shows several solutions of analytical wave theories for shallow water (Komar 1976, Table 3.1). The first three wave types are simple periodic waves with L, T, H and the undisturbed depth h as parameters, while the fourth solution, a limit of the cnoidal wave, is a solitary wave valid only for $L \to \infty$.

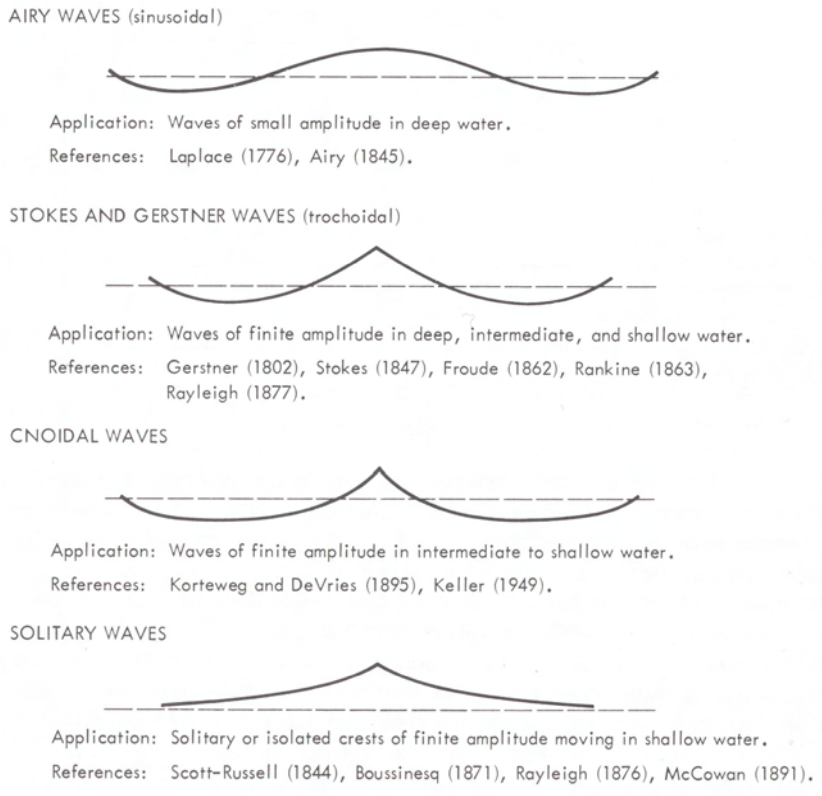

Fig. 5.1.1: Wave theories (Komar 1976, Table 3.1)

A solitary wave, which is a long single wave, seems to be well suitable to describe a tsunami because, in a solitary wave, the water particles move horizontally as, for example, in long Airy waves, but unlike the latter they move only in the direction of wave propagation (Fig. 5.1.2). The waves are waves of translation, with a mass transport exceeding that of the Stokes drift (mass transport because particle trajectories do not close) of wind waves.

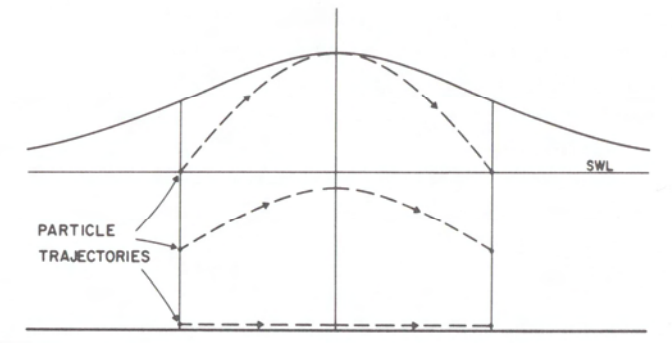

Fig. 5.1.2: Trajectories of water particles during passage of a solitary wave (Komar 1976, Fig. 3.15). Surface elevation: $\eta = \sec h^2\left(\sqrt{\frac{3}{4}\frac{H}{h}}\frac{x}{h}\right)$.

5.1.2 Equations of wave theories

With regard to section 6.2, the main differences among the individual wave theories are presented below using a very simple version of equations 2 for irrotational flow (Cartesian co-ordinates, two-dimensional with $\vec{v} = (u, w)$ and constant depth h_0, and $\nabla\phi = (0,0,g)$).

Non-linear hydrostatic:

$\nabla \cdot \vec{v} = 0$, $\rho_0 \frac{\partial u}{\partial t} + \rho_0 u \frac{\partial u}{\partial x} = -\frac{\partial p}{\partial x}$ and $0 = -\frac{\partial p}{\partial z} - \rho_0 g$ with boundary conditions

$w = \frac{\partial \eta}{\partial t} + u\frac{\partial \eta}{\partial x}$, $p = 0$ at $z = \eta$ and $w = 0$ at $z = -h_0$.

From $\nabla \cdot \vec{v} = 0$ it follows that $w = -\int_{-h_0}^{z} \frac{\partial u}{\partial x} dz$.

Irrotationality $\nabla \times \vec{v} = 0$ in this simple example takes the form $\frac{\partial u}{\partial z} = \frac{\partial w}{\partial x}$.

With $\frac{\partial w}{\partial x} = 0$ (hydrostatic), it follows from irrotationality that $\frac{\partial u}{\partial z} = 0$. Pressure is

$p = p_0 + p'_{hs} = -\rho_0 g z + \rho_0 g \eta$.

Linear non-hydrostatic:

$\nabla \cdot \vec{v} = 0$, $\rho_0 \frac{\partial u}{\partial t} = -\frac{\partial p}{\partial x}$ and $\rho_0 \frac{\partial w}{\partial t} = -\frac{\partial p}{\partial z} - \rho_0 g$ with boundary conditions

$w = \frac{\partial \eta}{\partial t}$, $p = 0$ at $z = \eta$ and $w = 0$ at $z = -h_0$.

Irrotationality allows a solution via the introduction of a scalar velocity potential (e.g. Komar 1976). Instead, $\nabla \cdot \nabla p' = 0$ may be considered (Gill 1982). The solution for pressure in both cases thus is:

$$p = p_0 + p' = -\rho_0 g z + \rho_0 g \eta \frac{\cosh L/2\pi(z + h_0)}{\cosh L/2\pi h_0}.$$

p' differs from p'_h by a factor approaching 1 for small $L/2\pi h_0$.

Boussinesq equations:

$\nabla \cdot \vec{v} = 0$, $\rho_0 \frac{\partial u}{\partial t} + \rho_0 u \frac{\partial u}{\partial x} = -\frac{\partial p}{\partial x}$ and $\rho_0 \frac{\partial w}{\partial t} = -\frac{\partial p}{\partial z} - \rho_0 g$ with boundary conditions

$w = \frac{\partial \eta}{\partial t} + u \frac{\partial \eta}{\partial x}$, $p = 0$ at $z = \eta$ and $w = 0$ at $z = -h_0$.

It follows from $\nabla \cdot \vec{v} = 0$ that $w = -\int_{-h_0}^{z} \frac{\partial u}{\partial x} dz$, from irrotationality $u = u(z = 0) + \int_{z}^{0} \int_{-h_0}^{z'} \frac{\partial^2 u}{\partial x^2} dz'' dz'$.

Expressed by the approximation for w, the pressure is:

$$p = p_0 + p'_B = -\rho_0 g z + \rho_0 g \eta - \rho_0 \int_{z}^{0} \int_{-h_0}^{z'} \frac{\partial^2 u}{\partial t \partial x} dz'' dz'.$$

p'_B differs from p'_h by a summand vanishing with $\frac{\partial w}{\partial t} \to 0$. A solution to the equations is possible by assuming $\frac{\partial u}{\partial x} = \frac{\partial u(z = 0)}{\partial x}$ and it is determined by the choice of $u(z = 0)$. The additional terms in this simple version of the Boussinesq equations as compared to non-linear hydrostatic equations can be deduced from the local temporal derivative of u and from the horizontal pressure gradient (cf. Peregine 1972).

5.1.3 Applicability of the equations to tsunami events

The various approximations of equations 2 apply only to a certain region of the parameters wave height, wave length, and undisturbed water depth. In section 5.1.1, a solitary wave was stated to be a possible way of describing a tsunami. It is the solution to simple Boussinesq equations.

Let a tsunami be a simple wave characterised by the parameters H, L, and h. With suitable scaling of the equations (Voit 1978), the orders of magnitude of the individual terms in (2) can be estimated through these parameters, and simplifications evaluated. The non-linear terms in the horizontal momentum equations and in the surface boundary conditions are on the order of $0.5H/h$, in the vertical momentum equation $0.5H/h \cdot h^2/L^2$ and in the bottom boundary conditions 1. The order of magnitude of the local temporal change of horizontal motion with this scaling is 1, that of vertical motion h^2/L^2. Komar (1976) accordingly determined the range of validity of different wave theories in dependence on the two important parameters h/L and H/h (Fig. 5.1.3). Compare also Mader (2004, Table 1.1); Fröhle et al. (2002, Table A.3.1); and Peregine (1972).

Consequently, h^2/L^2 toward zero (i.e. h/L <0,05) marks the hydrostatic limit case of equations 2, $0.5H/h$ toward zero (i.e. H/h <<1) the linear limit case. However, both parameters alone are not sufficient to determine the range of validity of individual wave theories. According to Ursell (1953), it is the relative order of magnitude of non-hydrostatics (local temporal change of vertical velocity) h^2/L^2 and non-linearity $0.5H/h$, the so-called Ursell parameter U, which determines the necessary generality of the equations.

$h^2/L^2 << 0.5H/h$ $(U >> 1)$ allows a hydrostatic approximation, and $h^2/L^2 >> 0.5H/h$ $(U << 1)$ allows linear equations. $h^2/L^2 \sim 0.5H/h$ $(U \approx 1)$ is the prerequisite to the validity of simple Boussinesq equations (Ursell 1953). In Fig. 5.1.3, the plotted red line represents $\frac{0.5H}{h}\frac{L^2}{h^2} = 1$, with values >1 to the left of it and values <1 to the right. It is also common to interpret *U* as the relation between wave steepness H/L and relative water depth h/L, i.e. $U = \frac{H}{L}\left(\frac{L}{h}\right)^3$.

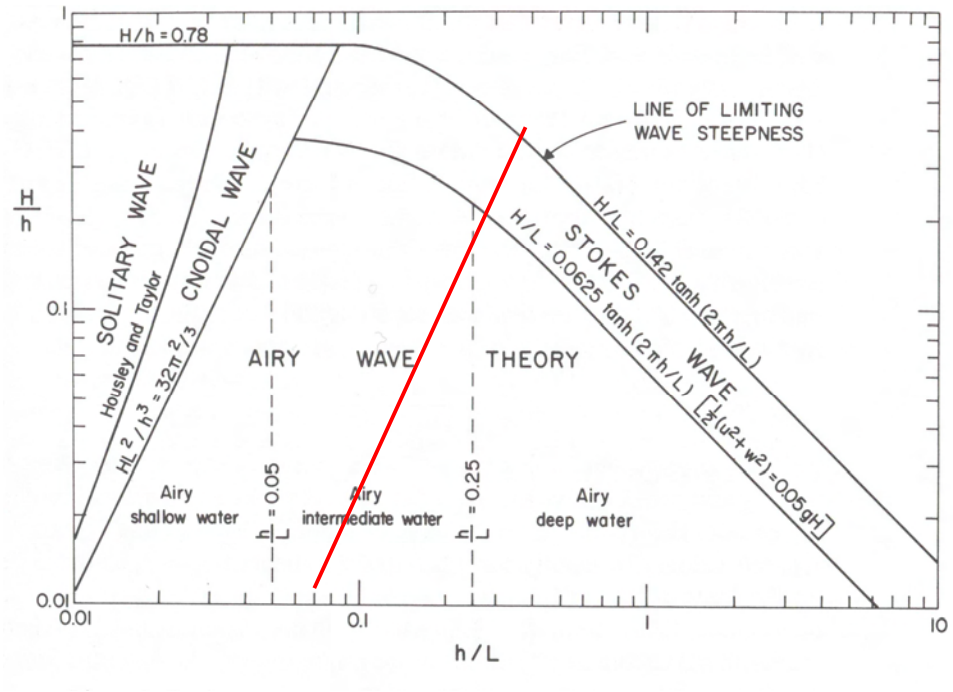

Fig. 5.1.3: Range of validity of different wave theories as a function of H/h and h/L (Komar 1978, Fig. 3.17)

Of the above frictionless and irrotational wave theories, the theory of cnoidal waves has the highest generality. It applies to non-breaking waves, i.e. in the case of long waves up to $H/h = 0.78$ (Miche 1944). The other waves referred to are limiting cases of this theory based on simplifying assumptions. „Airy deep water" in Fig. 5.1.3 marks the validity of linear non-hydrostatic wave theory, „Airy shallow water" the region of linear hydrostatic wave theory. Komar assumed a wider range of validity of linear theory than Ursell, i.e. $U \approx 50$ $(U = 16\pi^2/3)$. Fröhle et al. (2002) set the limit at $U = 13$. Solitary waves are located in the left part of Fig. 5.1.3. They are single waves, cnoidal waves in the limit *L* toward infinity. In Fig. 5.1.3, an idea of Munk (1949) is taken up according to which steep-crested waves separated by long, flat troughs may be considered to constitute single solitary waves. Fig. 5.1.3, the boundary line for the validity of the theory of solitary waves has been established at $H/h = 1600(L/h)^{-2.5}$ (Housley und Taylor 1957).

Let tsunami be simple long waves with typical periods of 10 to 30 minutes. Then the parameter h/L (estimating L by $T \cdot \sqrt{gh}$) for depths of less than 8,000 m is smaller than 0.05 (Table 5.1.1). In Fig. 5.1.3, this limits possible theories for the description of tsunami to „Airy shallow water", „cnoidal wave", and „solitary wave". With regard to solitary waves, it should be noted that h/L theoretically declines to zero due to $L \to \infty$, while for tsunami h/L declines to zero with h, while L decreases.

Fig. 5.1.3 is limited to values of $h/L \geq 0.01$. Tsunami having a period of 10 minutes (and wavelength $T \cdot \sqrt{gh}$) reach this value in water of 500 m depth (Table 5.1.1). For $h/L = 0.01$, the boundary to solitary waves on the H/h-axis is at $H/h = 1600(L/h)^{-2.5}$, which equals 0.016. At a depth of 500 m, this value corresponds to a wave height of 8 m. However, with $U \approx 50$ in Fig. 5.1.3, the boundary toward linear hydrostatic theory on the H/h-axis is $H/h = 100h^2/L^2$ equalling 0.0105, and hence the application of linear hydrostatic theory would be allowed for wave heights below 5 m in 500 m depth.

Estimates for the parameters which enter Fig. 5.1.3 are based on the assumption of a flat bottom. Variable depth additionally limits the validity of solutions. For instance, generalised Boussinesq equations (Peregine 1972) apply only to bottom slopes of $\Delta h/L_h \leq h/L$ due to the way the bottom boundary condition is approximated. The continental slope typically has a value of 0.025 (Dietrich et al. 1975). Thus, the solution to a Boussinesq equation generalised for variable depth is no model for a tsunami in that area. The special types of equation, Korteweg–de Vries and KP, cannot be generalised at all for variable bottom topography (Peregine 1972). Mofjeld et al. (2000) use hydrostatic linear equations to study the influence of bottom topography on simple waves.

Water depth [m]	*L (10 minutes)*	*h/L (10 minutes)*	*L (30 minutes)*	*h/L (30 minutes)*
5000	132.9	0.0376	398.7	0.0137
2000	84.0	0.0238	252.1	0.0079
1000	59.4	0.0168	178.3	0.0046
500	42.0	0.0119	126.1	0.0040
200	26.6	0.0075	79.7	0.0025
100	18.8	0.0053	56.4	0.0018
50	13.3	0.0038	39.9	0.0013
20	10.3	0.0024	25.2	0.0008
10	5.9	0.0017	17.8	0.0006

Table 5.1.1: Parameter h/L with $L = T\sqrt{gh}$ in km for two typical tsunami periods.

Water depth [m]	*U (10 m, 10 min.)*	*U (1 m, 10 min.)*	*U (10 m, 30 min.)*	*U (1 m, 30 min.)*
5000	0.7	0.1	6.4	0.6
2000	4.4	0.4	39.7	4.0
1000	17.7	1.8	158.9	15.9
500	70.6	7.1	635.7	63.6
200	441.5	44.1	3973.1	397.3
100	1765.8	176.3	15892.2	1589.2

Table 5.1.2: Ursell parameter $\frac{0.5H}{h}\frac{L^2}{h^2}$ with $L = T\sqrt{gh}$ for two typical H and T values.

In large parts of the shelf, with an estimated $L = T\sqrt{gh}$, values of h/L <<0.01 are obtained (Table 5.1.1), which are outside the parameter range in Fig. 5.1.3. Considering the Ursell

parameter U (Table 5.1.2), it is found that non-linear influences prevail on the shelf and, with h/L <0.01, hydrostatic non-linear theory is adequate.

All wave theories referred to in this section are severely limited by a breaking criterion, which is h/L =0.78 for long waves. At 10 m water depth, it limits wave heights to maximally 7.8 m, and to 0.78 m in 1 m of water. Therefore, the description of tsunami by the analytical theory of long waves in frictionless media, in particular as solitary waves, is no longer valid in shallow water.

Also the interpretation of tsunami as simple waves with a given period, determined by the process that generated them, ceases to be valid in coastal regions, where wave period rather is a function of location (Munk 1962), because frictional effects prevail (Sabatier 1986). In other respects, too, the interpretation of tsunami as simple waves is simplistic. Despite a relatively narrow spectrum, a tsunami is a superposition of simple waves having different periods. As such, it has been described as a soliton. Such waves preserve their overall shape in spite of major non-linearities, whose influence is compensated by dispersion i.e. by the change in shape of the composed signal due to different propagation speeds of single waves (Fig. 5.1.4). A soliton thus is described well by Boussinesq equations. In real tsunami, however, such equilibrium is rarely present. In addition, a soliton is not a good model for a tsunami because it is a positive signal and thus fails to reproduce the initial receding of water (wave trough) which is often observed on the coast.

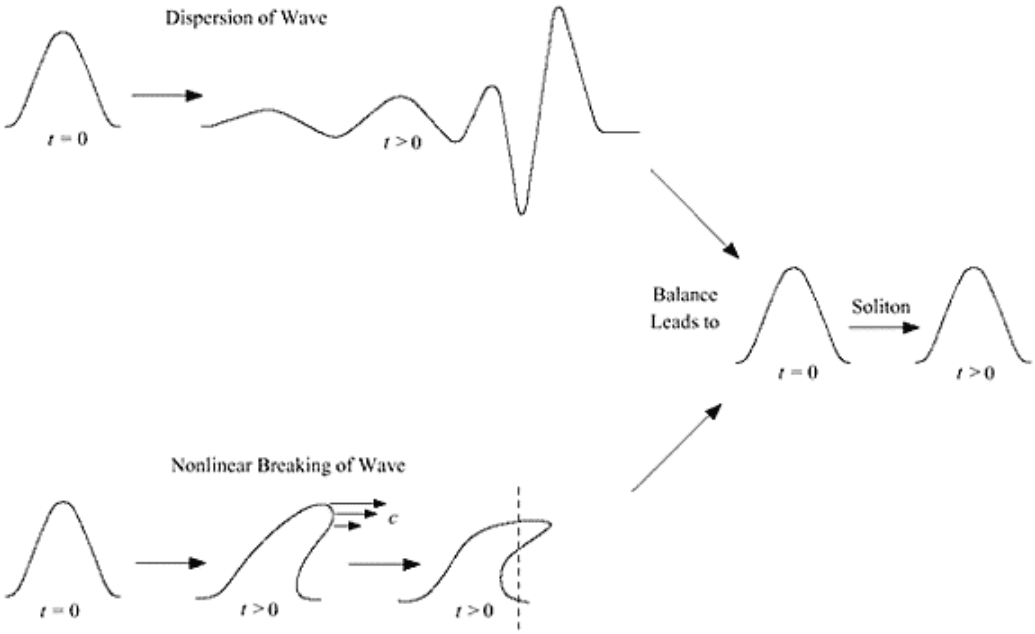

Fig. 5.1.4: Equilibrium in a soliton (Brunelli 2000, Fig. 3, Lomdahl 1984, Fig. 1).

Earthquake triggered tsunami often are generated in deep water, with an impulse-type initial elevation of the water surface. In incompressible, frictionless media, an initial surface elevation represented as a delta function develops a shape that can be described by an Airy function. The first excursion of this function is negative, as desired (Gill 1982). Another way of generating an initial wave trough is to consider the viscosity of water. In a viscous fluid, the dissipation and non-linear propagation of an impulse-type signal, in the most simple, one-dimensional case, is described by a non-linear diffusion equation (Burgers equation, Burgers 1974) for the scalar velocity potential (Whitham 1999). With a suitable initial distribution, its solution gradually develops a surface elevation termed „N-wave“ based on its shape, which also has a leading wave trough (Fig. 5.1.5).

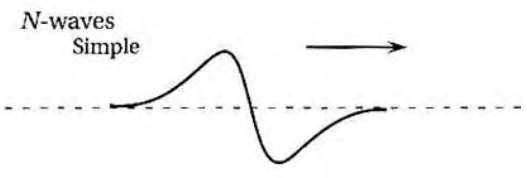

Fig. 5.1.5: N-wave (Bryant 2001, Fig. 2.4).

However, this too does not always approximate a tsunami correctly. During slope failures the period of seabed motion is relatively long, and the initial phase of the tsunami is described adequately by hydrostatic theory. Model computations have shown that in this case a wave crest comes first, followed by a seaward wave trough (Ward 2002). Solitary waves may then form in the closer far field (Rubino et al. 1998).

Summarising the above, it may at best be possible in limited evolution phases of a tsunami to describe it analytically as a single wave or wave train. In the following, different wave theories, in conjunction with other model concepts and simulation results, will continue to be used to discuss the propagation and modification of a tsunami travelling into shallow-water areas like the North Sea.

5.2 Propagation and modification in the deep ocean

Especially the impulse-type excursion of the water surface following an earthquake does not constitute a solution in analytical wave theory. If it is interpreted as a linear superposition of simple waves, the individual waves propagate in all directions with their specific phase velocities. In the deep ocean, part of the spectrum will be short waves. Short waves ($h/L > 0.25$) have a period-dependent phase velocity $gT_{short}/2\pi$. Short partial waves with small periods thus lag behind waves with greater periods. This process is called frequency dispersion. It weakens the primary signal of a tsunami. According to this theory, the dominant long-wave signal ($h/L < 0.05$) propagates in a dispersion-free way, i.e. with a velocity $\sqrt{gh}$ that is only depth dependent.

Fig. 5.2.1 shows a tsunami as the solution to linear Boussinesq equations. It is part of a two-dimensional, frictionless computation by Pedersen (10.5: PEDpT), which will be used in the following to demonstrate important evolution phases of an exemplary tsunami.

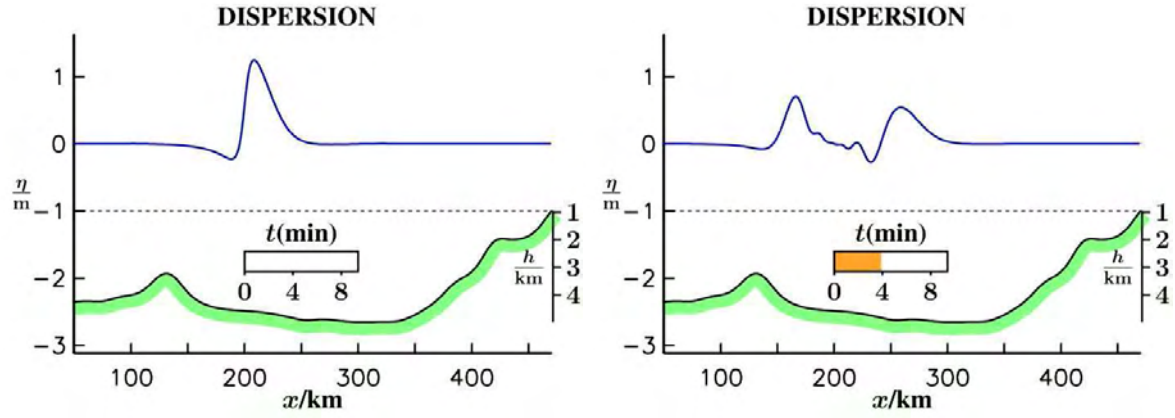

Fig. 5.2.1 Initial phase of the propagation (right) of an impulse-type signal (left) in the deep ocean (linear Boussinesq equations, η surface elevation, h undisturbed water depth, 10.5: PEDpT).

The simulation begins with a prescribed initial distribution (Fig. 5.2.1, left) of the surface elevation that is typical of a tsunami generated by vertical bottom excursion. It was modelled on the basis of the 1969 earthquake off Portugal (earthquake of magnitude 7.9 at 5,000 m depth). The initial disturbance propagates in all directions. Thus, in this simulation, a wave of only half the initial wave height moves towards the coast. The right part of Fig. 5.2.1 (right) shows this kind of separation and the change in surface elevation under the impact of dispersion weakening the initial signal.

In this simulation, the bottom of the deep ocean is relatively flat in the direction away from the continental slope. Transatlantic tsunami may be modified or deflected by submarine ridges and sea mounts. Mofjeld et al. (2000) defined a parameter, on the basis of linear theory, which characterises the relevance of dispersion and reflection by different submarine structures to tsunami.

5.3 Modification on the continental slope

The first transition to shallower water is at the continental slope. Off Sumatra, the continental slope is extremely close to the coastline. With respect to the German North Sea coast, it is a distant and dynamically special feature. On the continental slope, $\sqrt{gh}$ decreases strongly, while the phase velocity $gT_{short}/2\pi$ of short waves is independent of depth. With $gT_{short}/2\pi > \sqrt{gh}$, the short waves may catch up to the long waves (Mirchina et al. 2001), strengthening the leading signal. Under real ocean conditions, however, very short waves are dampened out, and the originally medium-length waves turn into long waves with decreasing depth due to the decreasing h/L quotient. Therefore, dispersion normally will further weaken the leading signal.

In the long-wave dispersion-free part, dominant waves are overtaken by following waves, and superposition then produces a higher signal. In addition, the individual waves are shortened at the shelf edge, with their energy concentrated on a smaller area (shoaling). However, part of the energy potentially available to shoaling is reflected back into the deep ocean at the continental slope.

Linear hydrostatic theory is appropriate for estimating the behaviour of single long waves. It provides simple formulas for changes in wave height, length, and steepness with decreasing depth (Masselink 2005). In the absence of friction, the energy flow $E\sqrt{gh}$ remains constant as the wave enters shallower water. In this hydrostatic case, the energy propagates with velocity $\sqrt{gh}$, and it changes according to $E/E_{deep} = (h_{deep}/h)^{0.5}$. By the same approximation, energy is proportional to wave height squared, and hence $H/H_{deep} = (h_{deep}/h)^{0.25}$. In this approximation, a transition from 4,000 m to 1,000 m thus would lead to an increase in wave height by the factor $\sqrt{2}$. As energy dissipation is entirely neglected, the wave period is also retained in the transition to shallower water. Wave length $L = T_{deep}\sqrt{gh}$ is reduced according to $L/L_{deep} = (h/h_{deep})^{0.5}$, and wave steepness $S = H/L$ increases according to $S/S_{deep} = (h_{deep}/h)^{0.75}$. With the depths shown in Fig. 5.3.1, 4,000 and 1,000 m, wave length would decrease by half and wave steepness would increase three-fold.

However, that applies only to gentle bottom slopes. The continental slope represents a rather abrupt change in depth and, for an impact perpendicular to the slope, H/H_{deep} is estimated better by $H/H_{deep} = 2h_{deep}^{0.5}/\left(h_{deep}^{0.5} + h^{0.5}\right)$ (Camfield 1990). With the above values, H thus would increase by the factor 1.33 (instead of 1.41). Camfield (1990) also provides suitable equations for other bottom profiles and impact angles.

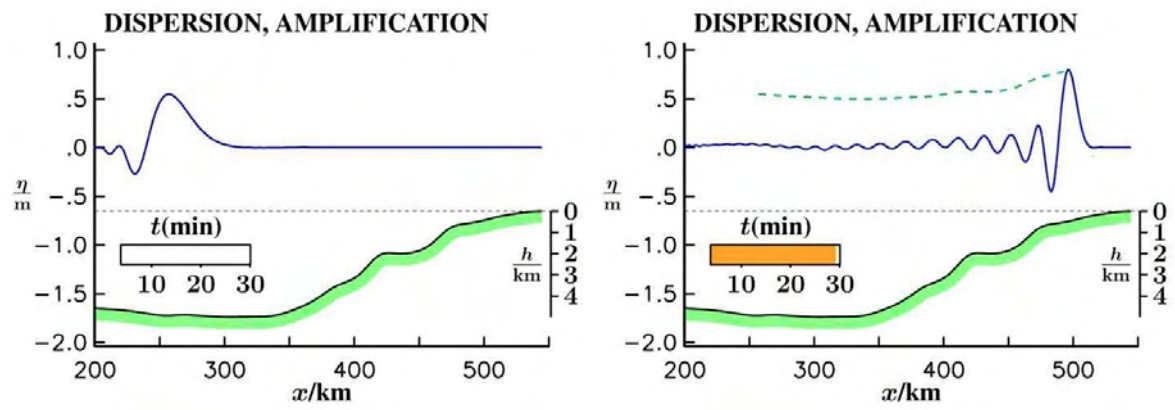

Fig. 5.3.1: Transformation at the continental slope (linear Boussinesq equations, η surface elevation, h undisturbed water depth, 10.5: PEDpT)

In the continued simulation using linear Boussinesq equations (Fig. 5.3.1, 10.5: PEDpT), intensification of the leading signal with decreasing depth (shoaling) prevails over weakening due to dispersion as the tsunami travels into shallower water.

In comparison, consider the two-dimensional barotropic model of the North-East Atlantic in section 7.2. As its analytical basis is hydrostatic non-linear equations, the topographic modification of the propagation velocity is computed according to $\sqrt{gh}$. The model also simulates the reduction of wave length $\sqrt{ghT}$ with decreasing depth. As the model equations include friction terms, T does not remain constant, and the simple linear estimation $L = T_{deep}\sqrt{gh}$ for a single wave is only approximately valid, as in real nature. In the model, the height of the individual waves increases at the continental slope. However, local increases are mainly due to superposition of single waves.

The energy balance in the model regarding reflection, non-linearity, and dissipation was not explicitly considered. It is known, though, that the numerical approximation of analytical equations and of non-linearities, in particular, has an influence on the magnitude of dissipation.

All three approaches – linear hydrostatic equations, linear Boussinesq equations, and non-linear hydrostatic equations in numerical form – are barotropic modelling concepts. In stratified media, tsunami may also cause internal waves, which will also be modified at the continental shelf. Their forcing by tsunami has been studied by Hammack (1974).

5.4 Modification and attenuation on the continental shelf

5.4.1 Modification

On the shelf, barotropic equations provide an adequate description for the transformation and propagation of tsunami because bottom friction in this area causes strong mixing in the water column. In the continuation to the Pedersen simulation (10.5:PEDpT) using linear Boussinesq equations, the change in bottom topography is modelled after the depth distribution off Portugal, where the shelf is narrow, unlike in the North Sea. The depth profile on the entire shelf shows a slope of 500 m per 50 km, i.e. $\Delta h : L_h = 1:100$. On the shelf, nearly all partial waves of the simulated tsunami (Fig. 5.2.1) are long waves ($h/L << 0.05$), and the influence of frequency dispersion is very low. Fig. 5.4.1 shows primarily a further reduction of wave length and an increase in the wave height of the leading signal due to the decrease in undisturbed depth (shoaling).

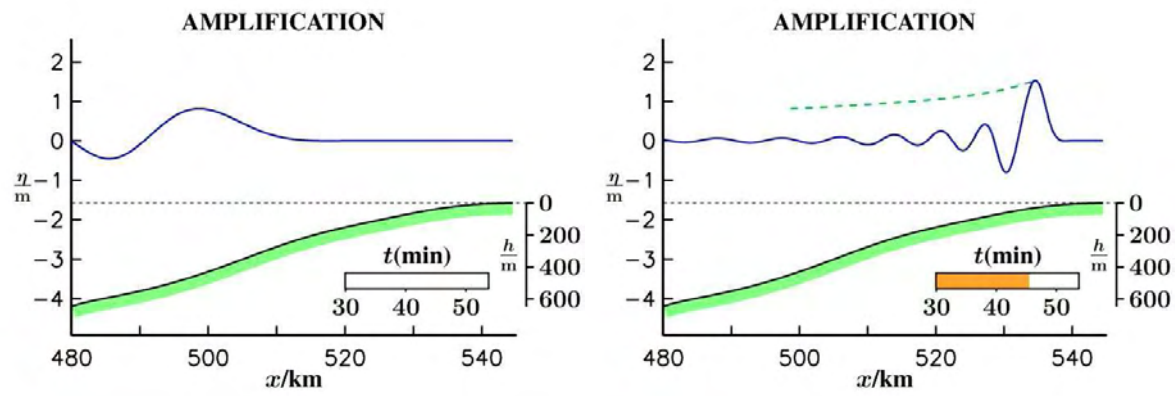

Fig. 5.4.1: Transformation on the shelf (linear Boussinesq equations, η surface elevation, h undisturbed water depth, 10.5:PEDpT)

With respect to the transition from 540 m to 60 m water depth, the result of the simple, linear, dispersion-free estimation in section 5.1 is that the wave height increases further, by the factor 3.0, to $4.3H_{deep}$, that the wavelength decreases by an additional factor of 0.3, and steepness increases by an additional factor of 5.2.

On the shelf, especially on a wide shelf like that of the North Sea, these values are not valid, however, because linear equations lose their validity with increasing steepness and, in particular, because it is no longer justifiable to neglect bottom friction. Also frictionless simulation (Fig. 5.4.1) thus gives only a general picture.

5.4.2 Attenuation

The depth at which sea and swell ($T \approx 10$ s) are strongly affected by the ocean bottom ($h/L > 0.05$) is about 25 m (Holthijsen 1998). For the long-wave proportion of a tsunami (with $T \geq 10$ minutes), the condition $h/L > 0.05$ is met on the entire shelf (cf. Table 5.1.1).

If only large-scale processes are considered, the destructive energy of a tsunami may be assessed without considering the details of wave mechanics. The width of the North European Shelf in the area of the North Sea is 800 km. The average slope angle in this region is 0.014°. Therefore, in the following assessment of energy (Kleine 2005), a tsunami is approximated as a portion of energy travelling at $\sqrt{gh}$.

The starting point is the balance equation for the total spectral energy of a wave train:

$$\frac{\delta E}{\delta t} + \nabla \cdot \left(\vec{c}_g E\right) = Q_E$$

($\vec{c}_g$ the effective propagation velocity of total energy, Q_E net effect of energy sources, non-linear interaction and dissipation, used for deep water waves, Reistad et al. 1998).

Neglecting non-linear effects and concentrating on the long-wave part of the spectrum, the energy balance equation in advective form applies:

$$\frac{\partial E}{\partial t} + \vec{i}\sqrt{gh}\nabla E + (\nabla(\vec{i}\sqrt{gh}))E = -D \qquad (3)$$

($\vec{i}$ the unit vector in the direction of propagation, $\sqrt{gh}$ scalar propagation velocity, $D > 0$ energy dissipation due to bottom friction).

Equation 3 thus describes the temporal change of energy due to advection, shoaling, and dissipation at a particular shelf location. On a flat bottom, only the mechanical energy arriving

at this location due to advection would be available for partial dissipation by bottom friction. On a sloped bottom, more mechanical energy per unit area is available for dissipation because of shoaling. The simple balance equation is limited to gently sloping shelves ($\Delta h/L_h \le h/L$).

With the approach $D = \kappa(E/h)^{1.5}$ for dissipation by bottom friction (κ dissipation coefficient) and a bottom slope assumed to be constant, $-\vec{i}\nabla h = \Delta h/L_h =: \sigma > 0$, a closed solution can be found for equation 3:

$$\frac{1}{h^{0.25}}\left(\frac{1}{E^{0..5}} - \frac{2}{5}\frac{\kappa}{\sigma}\frac{1}{g^{0.5}h}\right) = \frac{1}{h_{deep}^{0.25}}\left(\frac{1}{E_{deep}^{0.5}} - \frac{2}{5}\frac{\kappa}{\sigma}\frac{1}{g^{0.5}h_{deep}}\right)$$

or, expressed by wave height H of a representative shallow water wave, $E = gH^2/8$:

$$H/H_{deep} = h\Bigg/\left(h\frac{h^{0.25}}{h_{deep}^{0.25}} + \frac{\kappa}{5\sqrt{2}\sigma}H_{deep}\left(1 - \frac{h}{h_{deep}}\right)\right),$$

i.e. for $\kappa = 0$ the expression in section 5.3 is regained. In near-shore waters of $h \to 0$ the result shows, as an important property, an asymptotic behaviour of energy, or wave height, according to $\frac{H}{h} \to 5\sqrt{2}\frac{\sigma}{\kappa}$. Table 5.4.2, with $\kappa = 6 \cdot 10^{-3}$, gives the asymptotic behaviour at different bottom slopes.

	Bottom slope	*H (asymptotic)*	*H (asymptotic, h=20 m)*
North Sea	1:4,000	0.27 h	5.4 m
German Bight	1:2,500	0.43 h	8.6 m
Thailand	1:1,000	1.08 h	21.7 m
[Lisbon	1:100	10.83 h	216.6 m]

Table 5.4.2: Asymptotic wave height with different bottom slopes

The above energy balance ceases to be valid at bottom slopes of 1:1,000. However, it provides a good estimate for the North Sea. In addition, all results are limited to relative wave heights of $H / h \le 1$.

There are two important conclusions: firstly, clearly less energy is available for the as yet insufficiently understood near-shore processes on a shallow shelf than on a steep one and, secondly, the asymptotic value for wave height is independent of the initial wave height.

Fig. 5.4.3 shows the amplitude profile for several initial amplitudes on an idealised north-south profile across the North Sea. Fig. 5.4.2 shows profiles on an equally idealised, somewhat steeper section in the German Bight. The amplitude development in Fig. 5.4.2-3 is comparable to the dotted lines in the frictionless simulation (Figs. 5.3.1 and 5.4.1) which mark the amplitude change of the primary signal.

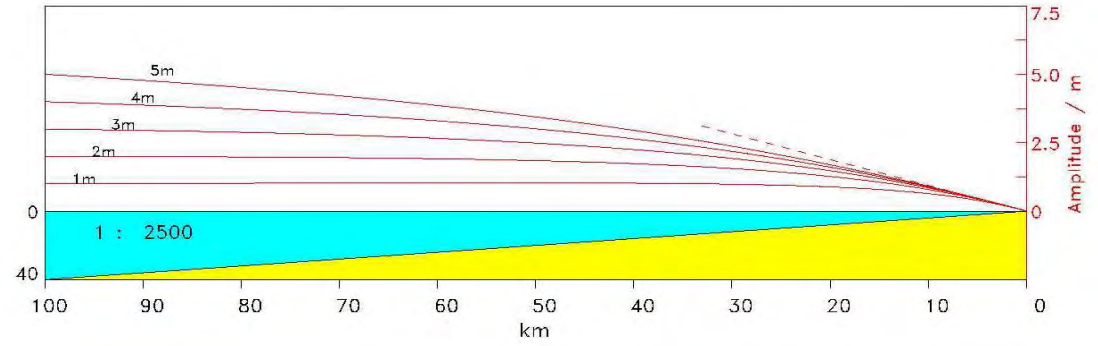

Fig. 5.4.2: Amplitude development on a 1:2,500 shelf slope at a shelf width of 100 km (left scale: depth, "German Bight")

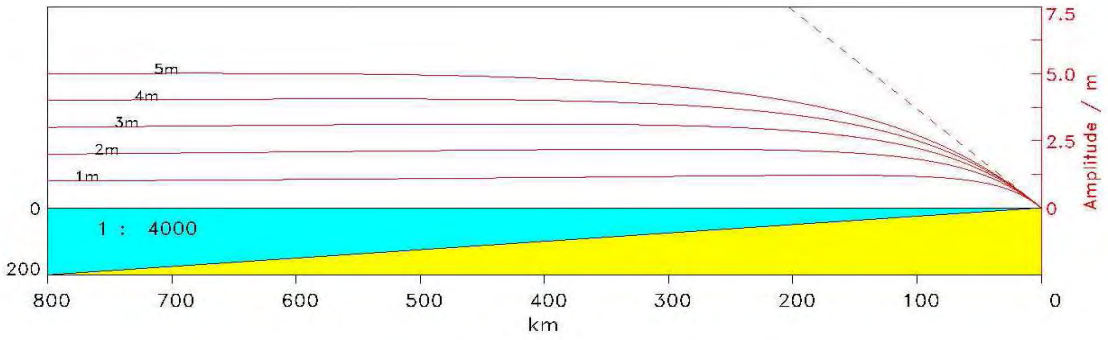

Fig. 5.4.3: Amplitude development on a 1:4,000 shelf slope at a shelf width of 800 km (left scale: depth, "North Sea")Topographic effects

5.4.3 Topographic effects

In the barotropic two-dimensional North Sea models referred to in sections 7.3 to 7.5, the dissipation of energy through internal friction and bottom friction is taken into account in complex form (Dick et al. 2001). Fig. 7.4.9 shows no asymptotic behaviour of wave height, but a limitation. A successive increase in initial wave heights by 1 m leads to an increase of just 0.05 m in wave height for waves arriving near the coast (at Cuxhaven, first signal in Fig. 7.4.9). However, Cuxhaven is not a well-chosen example because at this location even the primary signal is caused exclusively by diffraction (compare section 7.4.2). Fig. 5.4.4 shows peak water levels at selected stations along the North Sea coast. The lines between Wick and Borkum are comparable to those in Fig. 5.4.3. The high values at North Shields and the additional values from Ijmuiden til Hirtshals indicate an influence other than dissipation.

Bottom topography and the shape of the coastline influence the propagation and modification of tsunami-size waves in various ways. Fig. 7.3.1 shows a circular wave in the northwest that has been caused by diffraction. Figs. 7.4.1 to 7.4.6 are examples of the superposition of such secondary waves (interference), which may lead to very high water levels, especially in bays where wave reflection is a contributing factor.

Waves on the shelf are reflected and scattered by topographic features, just like they are in the deep ocean and on the continental slope. Especially pronounced in the North Sea is the influence of topography on the propagation velocity $\sqrt{gh}$ and on changes in the direction of propagation due to refraction (cf. figures in sections 7.3 - 7.5).

Such wave phenomena are understood (e.g. Masselink 2005) and have been discussed with respect to tsunami (Camfield 1990, Mofjeld 2000). To simulate these processes in detail, a good representation of the bottom topography is indispensable.

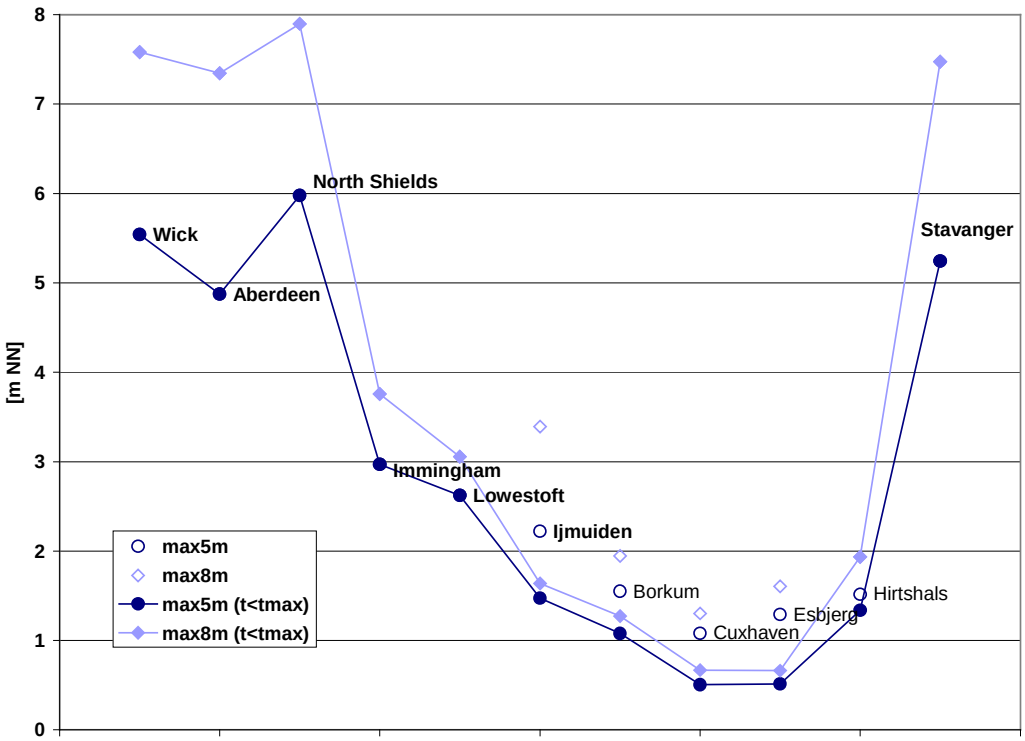

Fig. 5.4.4: Peak water levels at selected sites (input signal: 3 positive signals, T 1800 s, H 5 m (dark blue) and H 8 m (light blue), from the north; model: North Sea 2 km).

5.5 Modification near the coastline

Near the coastline, it is no longer possible to estimate the modification of simple waves by means of analytical solutions to linear equations because this would require the flow of mechanical energy and the wave period to be constant during tsunami propagation and modification. That applies only as long as the influence of friction is low. In the immediate vicinity of the coast, however, mechanical energy is dissipated inhomogeneously and *T* rather is a function of location than of the tsunami generation process (Munk 1962, Sabatier 1986).

Fig. 5.5.1 shows the continuation of frictionless simulation. Close to the coast, the wave height is of the same order as undisturbed water depth. The propagation velocity thus is described more precisely by $\sqrt{g(h+\eta)}$. In this way, the signal height not only increases with decreasing depth, but its front also becomes steeper.

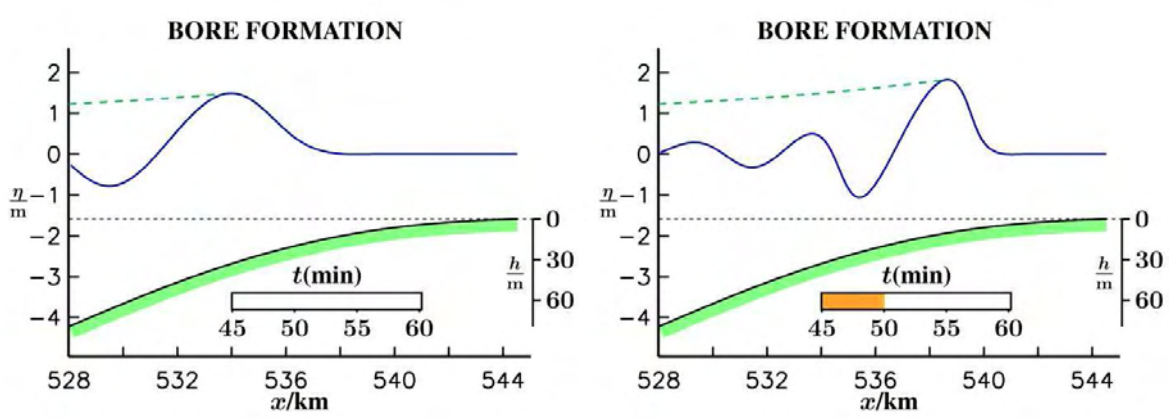

Fig. 5.5.1: Change in signal shape near the coast (linear Boussinesq equations, η surface elevation, h undisturbed water depth, 10.5: PEDpT).

Non-linear effects would finally cause the wave to break and form a bore. Since the breaking of a tsunami involves considerable dissipation of energy, shoaling does not lead to a further increase in the wave height of the bore despite decreasing water depth, but wave height even decreases again (Fig. 5.5.2, right). Bore formation has been parameterised in the course of the exemplary simulation of (10.5:PEDpT).

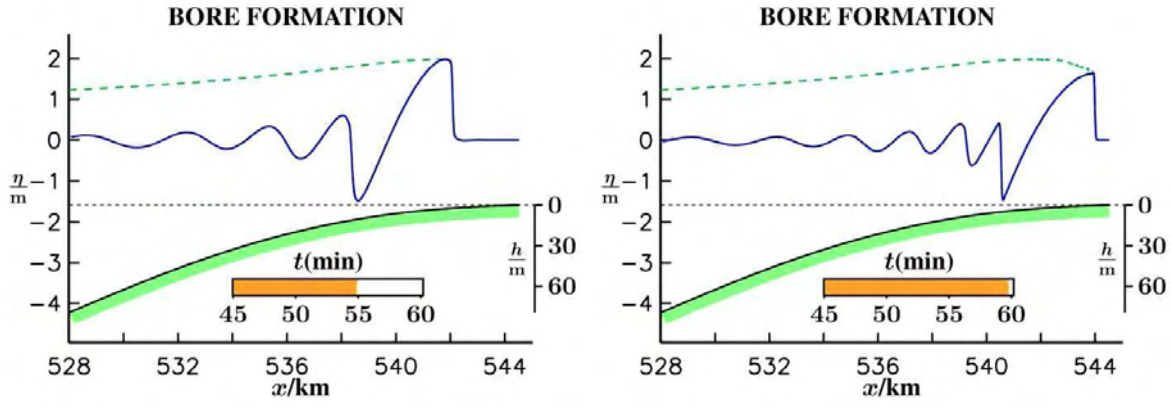

Fig. 5.5.2: Bore formation (linear Boussinesq equations, η surface elevation, h undisturbed water depth, 10.5: PEDpT).

A tsunami turning into a bore does so along the entire shore. Tidal waves in estuaries form bores mainly under the influence of a change in cross section. In some funnel-shaped river estuaries narrowing toward upstream, the height increase of the tidal wave is so sudden that it takes the shape of a surf wave (Dietrich et al. 1975, Figs. 8.45 and 10.6: CAR04). Also tsunami travelling into estuaries may develop into this type of bore.

The numerical simulation of processes close to the coastline and the propagation of tsunami on land are still subject to intensive research (Geist et al. 2006).

6 Model concept

Tsunami forecast models for the Pacific Ocean and the Mediterranean Sea have existed for a long time. Models have also been developed for the North Atlantic Ocean and the Norwegian Sea, and have been used in relevant studies. Of course, work on this subject has intensified after the tsunami event of December 2004 (Geist et al. 2006). Even with respect to the German coast, the question has been raised: what are the capabilities of existing models, especially those used for water level predictions at the BSH, and what would be the best concept for modelling water levels on the German North Sea coast, including hypothetical tsunami?

The most commonly used method of tsunami prediction is MOST (Method of Splitting Tsunami, Titov et al. 1997). It uses different models for the three tsunami phases: generation, propagation, and modification close to the coastline. Also hindcasts of tsunami in the Atlantic Ocean (Gjevik et al. 1997, Fine et al. 2005) and Norwegian Sea (Harbitz 1992, Bondevik et al. 2005) are based on this principle.

The modelling requirements for a simulation of the tsunami impact on the German North Sea coast are slightly more differentiated:

- Generation of an initial distribution of the surface elevation (6.1.1)
- Propagation and modification in the near field (6.1.2)
- Propagation in the deep ocean (6.1.3)
- Modification on the continental slope (6.1.4)
- Propagation and modification on the shelf (6.1.5)
- Propagation and modification near the coast (water depth smaller than 20-10 m) and in estuaries (6.1.7)
- Run-up and inundation (6.1.8)

6.1 Concepts of existing models and their relevance to BSH models

6.1.1 Generation of an initial distribution of the surface elevation

From the seismic data of an earthquake-generated tsunami, fault parameters are derived and used to construct surface elevations (Okada 1985, Titov 1997, Smallman 2006). The computations have been satisfactory in general, but secondary faulting and other causes may lead to major errors (Shuto 2003, Geist et al. 2006). Basic studies were also carried out with a temporally variable bottom topography (Androsov et al. 2005). Other mechanisms of tsunami generation are understood less clearly. Models of submarine slides have been described by Rubino (1998), Harbitz (1992), Fine et al. (2005), and Ward (2001). More complicated simulations are those involving landslides, during which large volumes of material slip into the water from great heights, and tsunami triggered by meteoritic impacts (Gisler et al. 2003, Glimsdal 2007, Weiß 2006). The models used are physically and numerically highly demanding. However, after a relatively short time, a status is reached which is also accessible to simpler, continuous model equations.

It does not appear necessary to have models of the generation phase available at the BSH. An initial distribution of water levels and boundary conditions for more precise, exemplary studies should be computed in collaboration with other institutions using their models. For a realistic warning situation, boundary values for the North-East Atlantic model and/or the North Sea/Baltic Sea model would have to be constructed from observations (e.g. real-time gauge station data).

6.1.2 Propagation and modification in the near field

To simulate the modification and propagation of a tsunami in the near field, the non-hydrostatic equations for viscous media have to be solved in order to reproduce the

dispersion and subsequent dissipation of the short-wave components of the signal and the resultant weakening of the leading signal. The difference between hydrostatic and non-hydrostatic computations may be less problematic in three-dimensional simulations of pointlike initial distributions (10.5: PEDpT) or slow bottom changes (Androsov et al. 2005) than in simulations of long faults or impulse-type bottom changes.

The influence of advection in the horizontal momentum equation and in the surface boundary conditions is low, like that of turbulent, horizontal momentum exchange. Nevertheless, both may significantly change the shape of a tsunami propagating in the deep ocean. Therefore, it is advisable to use the full non-hydrostatic, non-linear equations in this area. However, this is done only in research simulations.

In section 3, causes of possible North Sea tsunami have been compiled. The near field of such tsunami would be located outside the North Sea. Adequate simulation of the tsunami near-field in the North-East Atlantic would require major changes to the BSH model concept. However, the BSH is not planning to carry out such near field studies.

6.1.3 Deep ocean propagation

As a tsunami travels across the deep ocean, dispersion only plays a major role if an equilibrium signal (e.g. a soliton) of short and long waves has formed in the near field. Otherwise the short waves have dissipated, and propagation of the remaining long-period signal is simulated well with the hydrostatic assumption. In MOST (Titov et al. 1997), a hydrostatic model is used both for the simulation of near-field and deep-ocean propagation. However, dispersion is deliberately re-introduced in this case via the numerical method chosen. Gjevik et al., 1997, in a tsunami simulation, studied numerical dispersion caused by finite differences using an Arakawa-C-grid, a grid which is also used in the BSH models. They found that numerical dispersion did not always behave in a way that was consistent with physical law. The results of hydrostatic models are nevertheless useful (Horrillo et al. 2006). Good knowledge of the bottom topography is essential for modelling the propagation of long waves. In particular, a good approximation to travel times is obtained by integration of the distance covered at local speed $\sqrt{gh}$ (Annunziato et al. 2005). Such computations are very fast and, provided that a suitable resolution of topography covering also the coastal waters is available, they give reasonable results, especially if corrections are made to include diffraction on islands and coastal spits. The authors, Annunziato et al. (2005), announced that their model would be extended to provide an equally fast estimation of energy. Following a comparison of such computations with exemplary simulations using more complex models, and by including the bottom topography of the BSH models, an adaptation of this type of model might lead to the development of a suitable warning instrument for the North Sea. The report (Buch et al. 2005) of the Danish Meteorological Institute (DMI) on tsunami risks includes this type of travel time computations for the starting points Cape Farvel (Greenland), Faeroe Islands, and Hanstholm (Denmark). Nirupama et al. (2006) computed travel times for 118 starting points around the Atlantic Ocean. The bottom topography used was ETOPO2 (available at 10.4: GFDL), which has a resolution of 2 minutes of arc, i.e. about 3.3 km near the equator and about 2 km in the North Sea region.

6.1.4 Modification on the continental slope

A tsunami undergoes a substantial modification on the continental slope. Here, not only a good resolution is needed but also a non-hydrostatic simulation (Rubino 1998). Although the North-East Atlantic model of the BSH, in its new resolution of about 10 km, in fact shows expected alterations of wave height and length in this area (cf. section 7.2), this mainly reflects the influence of bottom topography on $\sqrt{gh}$. The influence of non-linear effects is low, dispersion only takes place as numerical dispersion, and the explicit turbulent momentum exchange has a lower boundary due to the numerical scheme used. To arrive at

a better understanding of tsunami modifications on the continental slope, some reference computations using baroclinic, three-dimensional, non-hydrostatic models would be useful.

6.1.5 Propagation and modification on the shelf

Wave propagation and modification on the shelf excluding near-shore waters are simulated adequately by non-linear hydrostatic models like those used at the BSH provided that a suitable grid resolution is available which accurately represents the topography and coastline.

Figure 6.1.1 shows water levels at Helgoland comparing hydrostatic (black) and non-hydrostatic (red) computations of the Federal Waterways Engineering and Research Institute (BAW) using the MARTIN model (Milbradt 2002). The model uses a finite element method with a higher resolution close to the coast. According to the estimations in section 5.1, there are only minor differences between the hydrostatic and non-hydrostatic simulations at this location.

However, a definite improvement of the simulation results is achieved by reducing grid spacing in the entire gridded area from 9 km to 2.5 km maximum grid length (Fig. 6.1.2).

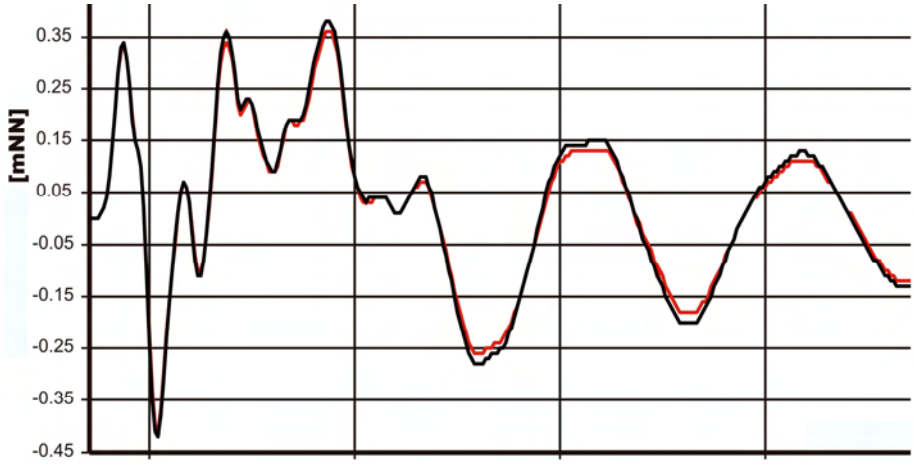

Fig. 6.1.1: Water level curves at Helgoland in a hydrostatic (black) and a non-hydrostatic (red) simulation during a 12 h period (input signal: 1 positive signal, period 1800 s, wave height 3m at the northern boundary of the North Sea, MARTIN model, Plüß 2005, personal communication)

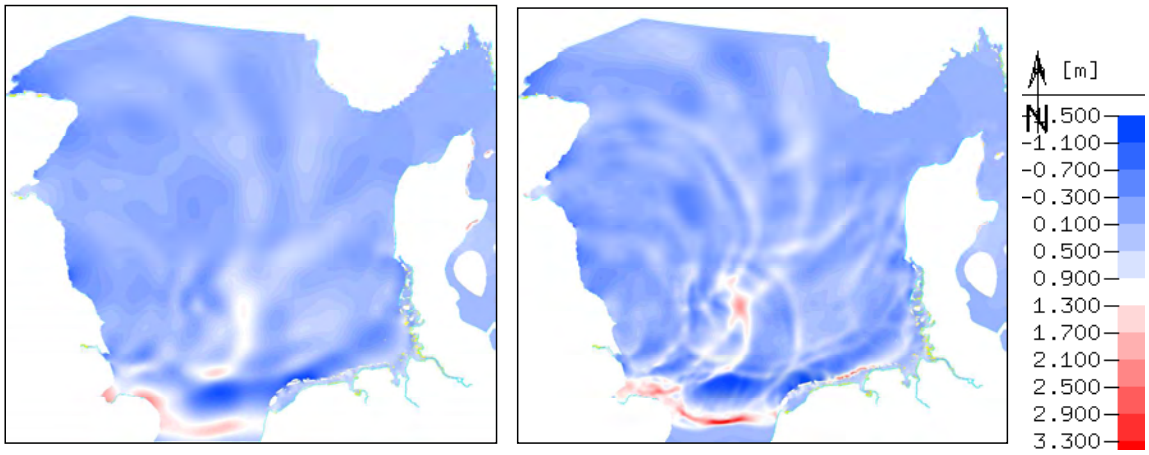

Fig. 6.1.2: Water level distribution 13 hours after simulation start (input signal: 1 positive signal, period 1800 s, wave height 3 m at the northern boundary of the North Sea, MARTIN model), coarse grid max. 9 km grid length (left), fine grid max. 2.5 km (right) (Lehfeldt et al. 2007).

The BSH models use a finite difference method and nested grids with constant grid spacing in the individual grids. Fig. 6.1.3 shows the effect of a grid spacing reduced from about 10 km to 2 km in simulations with two different two-dimensional, barotropic model versions (see sections 7.5 and 7.4). As the two models cover slightly different areas and the simulations were not started at exactly the same time, the time axis in Figs. 6.1.4 and 6.1.5 was shifted in such a way that the signals arrived at Wick simultaneously. The input signal (three positive signals, period 30 minutes, wave height 5 m) in the coarse-resolution model (Fig. 6.1.4, green) hardly shows any modification at Wick and is higher in the first two signals than in the fine-resolution grid (Fig. 6.1.4, red). In both models, Cuxhaven is reached first by extensions of the input signal that has been attenuated on the shelf, followed by a higher signal caused by diffraction (cf. sections 7.4 and 7.5). However, the simulations differ in two important aspects. In the coarse-resolution simulation (Fig. 6.1.5, green), the primary signal is higher, and the secondary signal lower, than in the simulation using the finer grid (Fig. 6.1.5, red). Besides, in the coarse-resolution model the primary signal reaches Cuxhaven about two hours later; the secondary maximum occurs about one hour later. Since not only a refined grid but also an improved bottom topography was used in the North Sea model with the 2-km resolution, any conclusions as to the dependence of propagation velocity on the grid resolution would be premature.

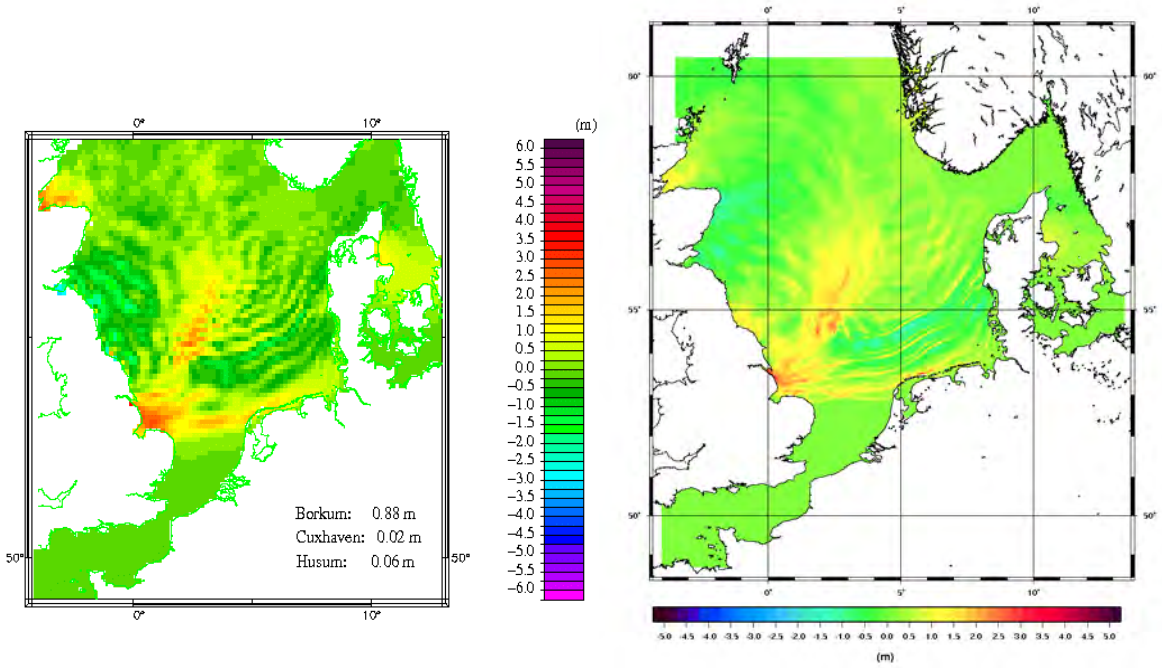

Fig. 6.1.3: Water level distribution with equal input signals (3 positive single signals, period 1800 s, wave height 5 m) and different models. Left: North Sea model 10 km resolution (after 8 hours), right: North Sea model 2 km resolution (after 9 hours).

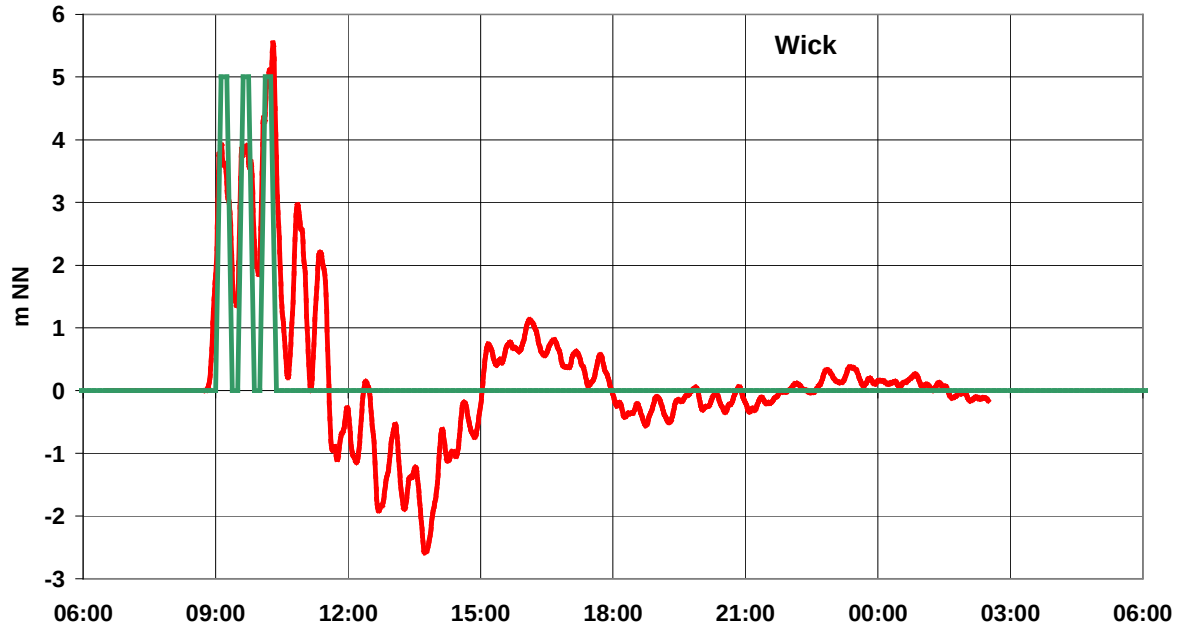

Fig. 6.1.4: Temporal evolution of water levels at Wick in two models (North Sea model 10 km (green), North Sea model 2 km (red) with equal input signal (3 positive single signals, period 1800 s, wave height 5 m).

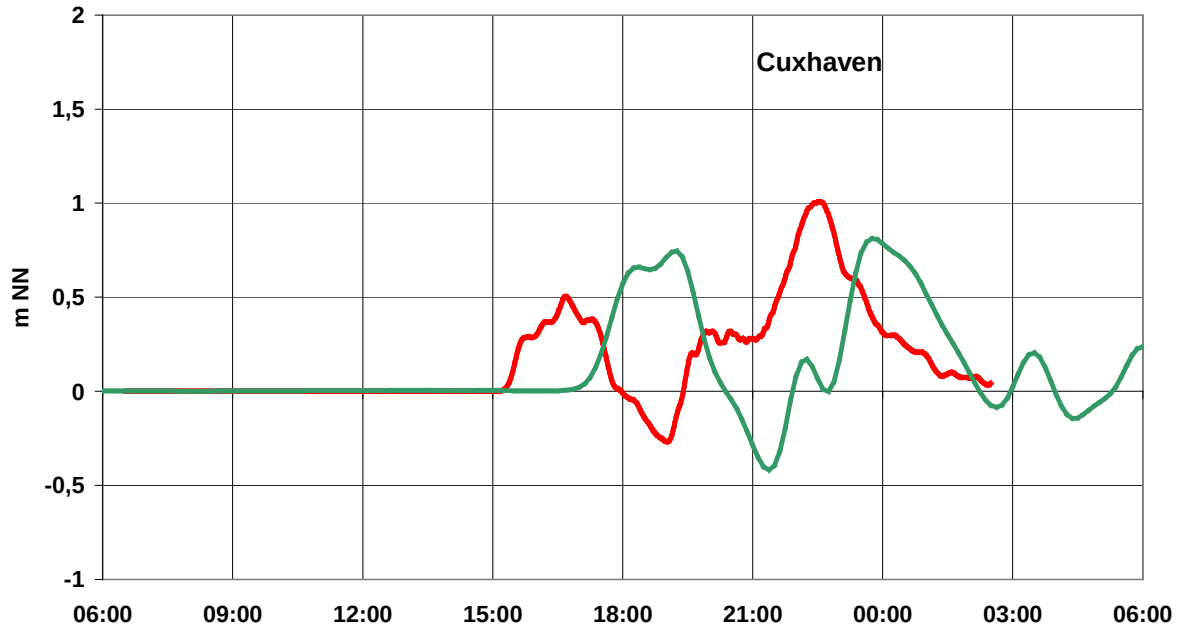

Fig. 6.1.5: *Temporal evolution of water levels at Cuxhaven in two models (North Sea model 10 km (green), North Sea model 2 km (red) with equal input signal (3 positive single signals, period 1800 s, wave height 5 m).*

Up to now, it has not been taken into account that a tsunami entering the North Sea does not encounter calm water but currents and water levels that have been influenced by tides and winds. The periods of the main components of tides and tsunami are relatively far apart, so

that strong interactions are not to be expected. Nevertheless, simple addition of both influences is not adequate to deal with the problem. That applies similarly to the simultaneous occurrence of a storm surge and a tsunami. The following figure gives an impression of the mutual interactions of a tide (Fig. 6.1.6 top, black) and the Helgoland signal from Fig. 6.1.1 (Fig. 6.1.1, bottom, blue). Mutual interactions are weak but the residual signal (Fig. 6.1.6 bottom, green) differs clearly from the signal that is unaffected by the tidal wave (Fig. 6.1.6 bottom, blue).

An example of a coinciding tide, storm surge, and standard signal entering the North Sea from the north (3 positive single signals, period 1800 s, wave height 5 m) is described in section 7.5.

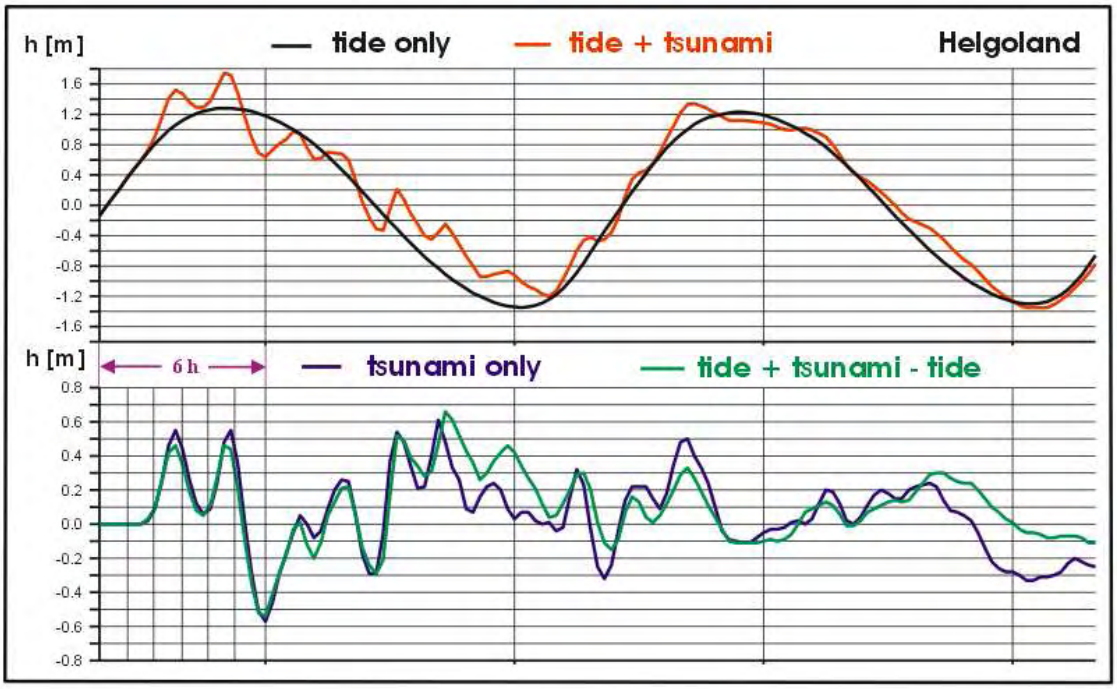

Fig. 6.1.6: Superposition of tide and input signal (1 positive signal, period 1800 s, wave height 3 m, at the northern boundary of the North Sea, MARTIN model, Lehfeldt et al. 2007).

6.1.6 Boundary conditions

If the tsunami generation process itself has not been modelled, a way to include it is by prescribing initial conditions for the surface elevation (Buch et al. 2005 and Kerridge 2005, run H). If the source of the tsunami is outside the model area, the tsunami has to be defined as a signal entering the model area. This involves two types of problem. The signal must be physically plausible, i.e. it must adequately represent the signal arriving from a potential source region, and developments at the boundary must be modelled in a numerically adequate way.

In simulations of hypothetical tsunami different kind of boundary conditions have been cohosen. The BAW simulations (MARTIN model, 2D, finite elements) in section 6.1.5 are based on a positive analytical signal entering the North Sea. In the simulations described in the DMI report (Buch et al. 2005, model MOG2D, finite element method), the problem has been solved with respect to the North Sea by locally using a finer grid resolution. Winter (Winter 2005) used the simulation of a tsunami triggered by the Storegga slide (Bondevik et al. 2005) to obtain boundary values for computations of wave propagation into the North Sea. Similarly, in the UK report (Kerridge 2005), a tsunami simulation assuming a potential submarine slide (run H) using the fine grid (N10, 2D, horizontal resolution 3.5 km) is driven by boundary values from a coarser model run (NEA, 2D, horizontal resolution 35 km). In further simulations, a wave from southerly direction is prescribed at the boundary of NEA,

and the quantities computed in NEA are then transferred to N10 as boundary values. Both a positive and a negative initial signal were used, each with a one-hour period. In a second report (Smallman 2006) NEA is replaced by an extended form of the British operational storm surge model CS23 (Flather 2000, 2D, horizontal resolution 12 km) and the simulations are started from known initial conditions. Boundary conditions are then transferred to a model with variable grid spacing (TELEMAC-2D, finite elements, horizontal resolution 12 km down to 1 km).

In its operational applications, the BSH's model system also uses nested models. For the simulations in section 7.2, three positive signals with a half-hour period were prescribed for the North-East Atlantic model (North-East Atlantic model, 2D, horizontal resolution 10 km). However, the signal modification toward the North Sea was not considered fully reliable (cf. section 7.1), and analytical signals were used as boundary conditions for the North Sea model (North Sea model, 2 km, 2D, horizontal resolution 2 km) as well.

It is remarkable that in all simulations using an analytical boundary the signal comes from a single direction and enters perpendicular to the open boundary. This is attributable to the fact that the mathematical and numerical treatment of open (non-physical) boundaries in numerical models is problematic (e.g. Durran 1998, Blayo et al. 2005). The numerical problem involves the requirement to have an unfalsified incoming signal and an unhindered outward transportation of a signal from the interior, both in arbitrary directions with respect to the boundary. Furthermore, on short time scales, the transported outward signal should be saved and allowed to be transported back if required. The first two aspects are explained on the basis of a one-dimensional example (cf. Kowalik 2003 and Flather and Davis 1975).

For flat bottom and initial conditions $u = 0$ and $\eta_0 = 2\eta_0^- f(x)$ for $x < 0$, $\eta_0 = 2\eta_0^+ f(x)$ for $x > 0$, the linear, hydrostatic, one-dimensional shallow water equations $\partial u/\partial t = -g\,\partial\eta/\partial x$ and $\partial\eta/\partial t = -h\,\partial u/\partial x$ provide the solutions (e.g. Gill 1982):

$$\eta = \eta^- + \eta^+ = \eta_0^- f\left(x + \sqrt{gh}t\right) + \eta_0^+ f\left(x - \sqrt{gh}t\right),$$

$$u = u^- + u^+ = -\sqrt{g/h}\eta_0^- f\left(x + \sqrt{gh}t\right) + \sqrt{g/h}\eta_0^+ f\left(x - \sqrt{gh}t\right).$$

Fig. 6.1.7 shows the temporal evolution of the simple initial condition, $2\eta_0^- = 2\eta_0^+$, $f(x) = 1$ for $|x| < L$ and $f(x) = 0$ otherwise.

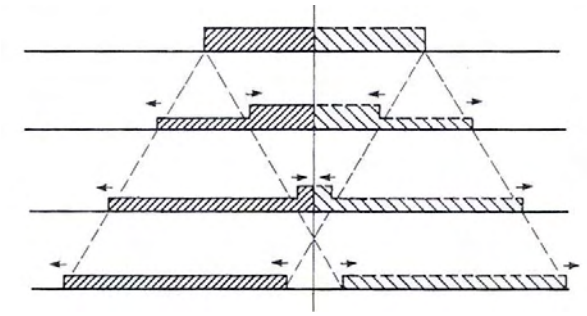

Fig. 6.1.7: Solution of one-dimensional shallow water equations for an initially constant elevation confined to a finite region (Gill 1982, Fig. 5.9 b).

The solution thus is an additive superposition of two signals propagating in opposite directions. Vice versa, the two partial solutions can be represented by the total solution:

$\eta^+ = 0.5(\eta + u\,h/\sqrt{gh})$ and $u^+ = 0.5(\eta\sqrt{gh}/h + u)$,

$\eta^- = 0.5(\eta - u\,h/\sqrt{gh})$ and $u^- = 0.5(\eta\sqrt{gh}/h - u)$.

Owing to the linearity of the equations, also the partial solutions satisfy the shallow water equations. Likewise, solutions for different initial conditions are additive. Consider an initial condition consisting of two spatially separate signals.

Let η_{ext}, u_{ext} and η_{int}, u_{int} each be solutions for one of the spatially separate initial conditions. Like the total solution, they consist of partial solutions running in separate directions. At any arbitrary point, the total solution can also be composed of these solutions to form

$\eta = \eta_{ext}^{+} + \eta_{ext}^{-} + \eta_{\mathrm{int}}^{+} + \eta_{\mathrm{int}}^{-}$ and $u = u_{ext}^{+} + u_{ext}^{-} + u_{\mathrm{int}}^{+} + u_{\mathrm{int}}^{-}$.

Let the external initial condition in space be to the left of the internal condition. Then the area between the two initial signals is first reached only by the external partial solution running in positive direction and by the internal partial solution running in negative direction because the other partial solutions are moving away from this area. In an infinitely extended area, it also remains like that. In the area between the two initial signals, the composed solution in this case reduces to

$\eta_b = \eta_{ext}^{+} + \eta_{\mathrm{int}}^{-}$ and $u_b = u_{ext}^{+} + u_{\mathrm{int}}^{-}$, which implies $\eta_{ext}^{-} = 0$ and $\eta_{\mathrm{int}}^{+} = 0$.

For the partial solutions η^{+}, η^{-} of the total solution η,

$\eta_b^{+} = \eta_{ext}^{+}$, $\eta_b^{-} = \eta_{\mathrm{int}}^{-}$ and $u_b^{+} = u_{ext}^{+}$, $u_b^{-} = u_{\mathrm{int}}^{-}$ applies in this area.

Expressed by the external and the internal total solution, the following is true for η_b in the area between the assumed initial conditions in a one-dimensional, infinitely extended area:

$\eta_b = 0.5(\eta_{ext} + u_{ext}\sqrt{h/g}) + 0.5(\eta_{\mathrm{int}} - u_{\mathrm{int}}\sqrt{h/g})$ or equivalently

$0 = 0.5(\eta_{ext} - u_{ext}\, h/\sqrt{gh})$ and $0 = 0.5(\eta_{\mathrm{int}} + u_{\mathrm{int}}\, h/\sqrt{gh})$. The solution for u_b is:

$u_b = 0.5(\eta_{ext}\sqrt{g/h} + u_{ext}) + 0.5(\eta_{\mathrm{int}}\sqrt{g/h} - u_{\mathrm{int}})$.

In case the external initial condition in space is to the right of the internal initial condition

$\eta_b^{-} = \eta_{ext}^{-}$, $\eta_b^{+} = \eta_{\mathrm{int}}^{+}$ and $u_b^{-} = u_{ext}^{-}$, $u_b^{+} = u_{\mathrm{int}}^{+}$ is valid respectively.

At open boundaries, especially in case of a variable topography, such simple approaches quickly cease to be valid. Nevertheless, the boundary conditions formulated by Flather (Flather et al. 1975) on that basis have been used with some success in water level predictions.

To allow a smooth transition from known external values to a computed internal solution left of the external solution, often the condition $\eta_{\mathrm{int}}^{+} = \eta_{ext}^{+}$ is enforced. Then, to satisfy continuity, either the computed η_{int} is used to derive u_{int} from $\eta_{\mathrm{int}}^{+} = \eta_{ext}^{+}$ (e.g. Jones et al. 2003) or η_{int} is derived using computed u_{int} (Kowalik 2003).

The purpose of the BSH's North-East Atlantic model is to simulate atmospherically forced water level changes entering the North Sea as external surges. It is assumed at its open boundary (Atlantic, Norwegian Sea) that no signal enters from the Atlantic Ocean and Norwegian Sea, i.e. $\eta_{ext}, u_{ext} = 0$. The incoming signal used for the simulations in section 7.2 is a prescribed u_{ext}, and η_{ext} is described by $\eta_{ext}^{-} = 0$ at the western and southern boundaries and by $\eta_{ext}^{+} = 0$ at the northern boundary. As the signal is assumed to enter an ocean at rest, η_{int}, $u_{\mathrm{int}} = 0$ is used in the initial stage of the simulation.

In contrast, in routine operational use of the North Sea models, it is primarily a water level signal (tide, external surge) that is to be transported across the open boundary into the North Sea region. Therefore, η_{ext} in this case is prescribed. For the simulations shown in sections 7.3 and 7.4, u_{ext} at the North Sea boundary was prescribed as in the North-East Atlantic model, and η_{ext} was determined by $\eta_{ext}^{+} = 0$ at the northern boundary and by $\eta_{ext}^{-} = 0$ at the western boundary. In the computations in section 7.5, however, the originally used formulation of the boundary condition was retained and, like tidal waves and external surges, the external signal at the North Sea boundary was prescribed by η_{ext}.

6.1.7 Propagation and modification in near-shore areas and estuaries

The propagation of tsunami in near-shore areas was studied in various model simulations (10.5: BEN04). Pedersen (2004) considers dispersion important in this test case, and the inclusion of non-linearity less important. The decisive aspect in numerical simulations is the grid resolution. Chubarov et al. (2003) reproduced water level rise in the wave shadow of an island and obtained good results with a hydrostatic model, though with a grid spacing of 50 m. Besides, comparative computations (Pedersen 2004) showed that hydrostatic models adequately simulate water levels but underestimate the velocity of water particles.

The tsunami of December 2004 has led to an intensification of research in the modelling of nearshore processes in the Indian Ocean, also in Germany. The Center for Marine and Atmospheric Sciences (ZMAW, Zentrum für Marine und Atmosphärische Wissenschaften), the Institute for Coastal Research at GKSS-Research Center (GKSS, GKSS-Forschungszentrum) and other German institutions have taken up the subject (e.g. Androsov et al. 2005). As part of a BMBF project, GKSS uses the MIKE21 BW model based on Boussinesq equations (10.4: MIK21, Günther et al. 2005). Simulations of German coastal areas might benefit from these studies. Processes on the German coasts are expected to be similar but, referring to section 5.4.2, are likely to involve less energy than the Sumatra event.

Bore modelling requires Lagrangian models or parametric representation. Tsunami travelling into estuaries become shorter, higher, and steeper in their leading part under the influence of bottom friction and funnelling, comparable to tidal waves. They may finally form a bore. Fig. 6.1.1 shows the evolution of water levels from Cuxhaven to Geesthacht during the propagation of a shelf-modified input signal of an original height of 3 m, simulated by the MARTIN model of BAW (Millbradt 2002). The BSH model system is not capable of modelling tsunami wave propagation into river estuaries.

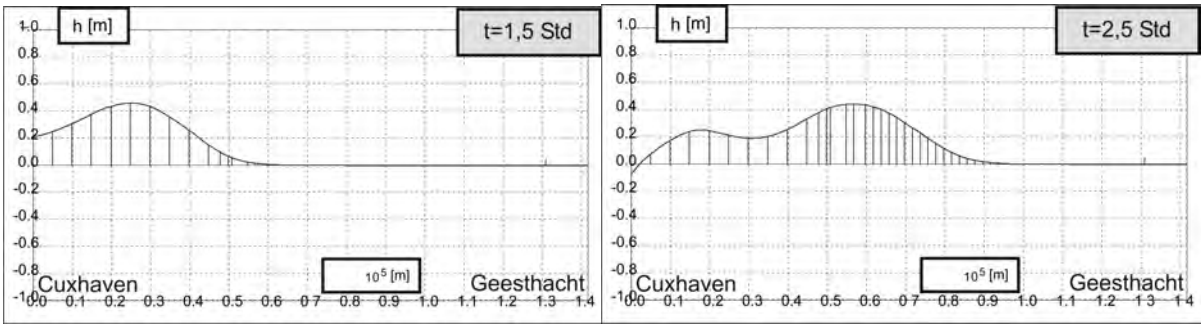

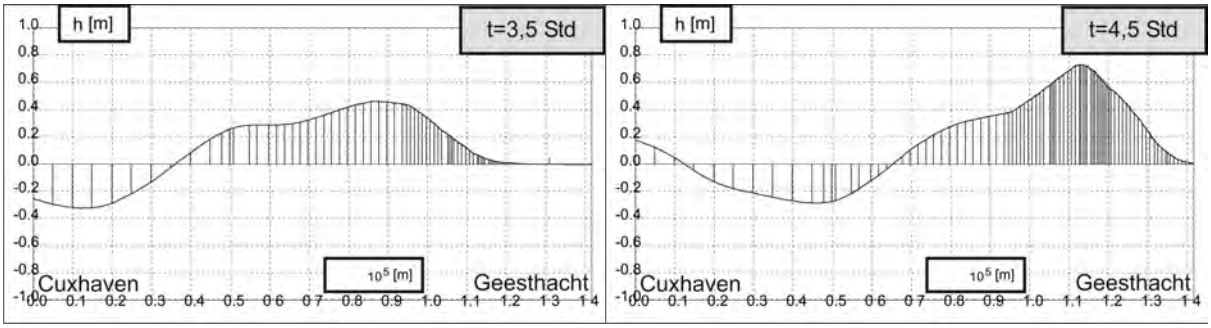

Fig. 6.1.8: Propagation of modified North Sea input signal between Cuxhaven and Geesthacht (distance in 100 km, 1 positive signal, period 1800 s, wave height 3m from the north, MARTIN model, Plüß 2005, personal communication)

6.1.8 Run-up and inundation

Run-up onto dry land was not taken into account by operational tsunami warning models prior to the tsunami of December 2004. Since then, both the MOST model and the Japanese Tsunami-N2 model (Imamura et al. 2006) have successfully integrated the simulation of land inundation and reproduced historical tsunami (Geist et al. 2006). A recent comparison of the performance of different models in simulating run-up during the tsunami of December 2004 is given by Horrilio et al. (2006).

The BSH models easily simulate flood and ebb tides in the North German tidal flats, including their exposure at low water, but are not capable of simulating the inundation of higher land and sea dikes.

In case a real tsunami should flood the North German marshes, it would have to be taken into account that grassland would not dissipate much of the energy of the arriving bore, and that a tsunami would propagate faster in narrow channels, where water is deeper, than on land.

However, it appears hardly reasonable to model inundation caused by a hypothetical tsunami before achieving a satisfactory simulation of the near-shore processes.

6.2 Outlook for dispersion modelling in BSH models

An important reason for the limited suitability of the BSH's models for the simulation of tsunami is the hydrostatic assumption implied, and hence the complete neglect of frequency dispersion. Non-hydrostatic model computations still are very time-consuming. Boussinesq models are non-hydrostatic to the first order and are often used in wave simulations as a compromise between high computational demands and the incorporation of modifications due to dispersion. (For a comparison with regard to the tsunami of December 2004 see Horrillo et al. 2006.) The following section deals with a possible way of including dispersion effects in the BSH's models in order to achieve the level of accuracy that Boussinesq models have. For that purpose, the important approximations of analytical wave theory have been formulated for primitive equations.

In the analytical wave theories referred to in section 5.1, terms in the equations of motion and their boundary conditions are not simply disregarded. Rather, the dependent variables are expanded according to a characteristic parameter, and higher-order terms in the equations are expressed by lower-order quantities. Finally, terms are neglected from a certain order upwards. In this way, a closed system of equations for lower-order quantities is created (e.g. Peregine 1972, Liu et al. 2002). Such systems include the different types of Boussinesq equations (e.g. Boussinesq 1871, Voit 1987, Madsen et al. 1991, Madsen et al. 1992), mostly two-dimensional approximations to describe long waves taking into account dispersion ($h^2/L^2 \neq 0$) and non-linear effects ($0.5H/h \neq 0$, but mostly $h^2/L^2 \cdot 0.5H/h \approx 0$).

In contrast, numerical models like the BSH models (Dick et al. 2001) are based on so-called primitive equations. "Primitive" implies that the equations are solved for the complete quantities. In general, however, statistically averaged equations are solved in which correlations resulting from the non-linear terms of the equation are expressed by averaged quantities. An additional approximation in numerical models is the parameterisation of processes with length scales below the model's grid resolution (in the BSH models, this also includes sea and swell).

The starting point for the following discussion is equations 1 (section 5.1), the non-averaged, three-dimensional mass and momentum balance equations in co-ordinate-free form (Pichler 1984). The approximations, which in their simplest form were already given in section 5.1.1, are now presented using the so-called p-equation, which is derived as divergence of the impulse equation, solved to obtain $\nabla^2 p$:

$$\nabla^2 p = -\frac{\partial}{\partial t}(\nabla \cdot \rho\vec{v}) - \nabla \cdot \nabla\rho\vec{v}\vec{v} + \nabla \cdot \vec{F} - \nabla \cdot \rho\nabla(\phi + \phi_G) - \nabla \cdot (2\vec{\Omega} \times \rho\vec{v})$$

From conservation of mass, it follows:

$$\nabla^2 p = +\frac{\partial^2 \rho}{\partial t^2} - \nabla \cdot \nabla\rho\vec{v}\vec{v} + \nabla \cdot \vec{F} - \nabla \cdot \rho\nabla(\phi + \phi_G) - \nabla \cdot (2\vec{\Omega} \times \rho\vec{v}).$$

With $\rho = \rho(p)$, a prognostic equation for p is obtained. The compressibility of water has to be taken into account only in special cases, though, e.g. in simulations of meteoritic impacts (e.g. Mader 2004), volcanic eruptions involving ash admixture, or gas admixture in the course of slope failure.

In most cases, tsunami can be simulated using the Boussinesq approximation, which considers water incompressible, $\nabla \cdot \vec{v} = 0$, and density differences are only considered in connection with gravity impacts. (This is not the approximation used to deduce the Boussinesq equations.) Besides, with $\nabla \cdot \nabla(\phi + \phi_G) = 0$ according to the general rules of vector calculation, the p-equation in the Boussinesq approximation takes the form:

$$\nabla^2 p = -\rho_0 \nabla \cdot \nabla\vec{v}\vec{v} + \nabla \cdot \vec{F} - \nabla\rho \cdot \nabla(\phi + \phi_G) - \nabla \cdot (2\vec{\Omega} \times \rho_0\vec{v}).$$

Although the tidal potential ϕ_G is taken into account in the BSH's models (Müller-Navarra 2002), the influence of tides in the North Sea is determined primarily by the lateral boundary conditions. The vertical component of $\nabla\phi_G$ is generally neglected. From the p-equation it vanishes if density differences are considered strictly in connection with $\nabla\phi$.

In analytical discussions, earth rotation is often neglected and flow is assumed to be irrotational, i.e. $\nabla \times \vec{v} = 0$, which simplifies the first term on the right side of the equation to $\rho_0 0.5\nabla^2(v^2)$. Furthermore, the vector $\vec{v}$, which in general can be represented as a sum of a scalar and a vector potential, in that case can be expressed by a scalar potential alone. With respect to the North Sea, the assumption of irrotationality is not reasonable, though, because bottom friction, wind forcing and the influence of its variable topography are not negligible. Therefore, no potentials are introduced here.

Also the neglect of earth rotation is not justifiable in simulations of tsunami impacts in the North Sea. As tsunami periods are smaller than the inertial period, there is no formation of Kelvin waves, as in the case of long external surges, but earth rotation may influence phase velocity (Gill 1982, Akylas 1994). Besides, a tsunami does not enter a North Sea at rest but interacts with tidal and wind-forced currents, both of which are influenced by earth rotation. Although strong interaction is not to be expected because of different periods, tsunami may undergo refraction due to such currents. Neglecting the horizontal component of $\vec{\Omega}$, however, is rather common use.

Using $\vec{\Omega} = (0,0,\Omega_v)$ together with $\nabla\phi = (0,0,\nabla_v\phi)$ the p-equation is dimensionally uncoupled in the last two terms:

$$\nabla^2 p = -\rho_0 \nabla\cdot\nabla\vec{v}\vec{v} + \nabla\cdot\vec{F} - \nabla_v \rho \nabla_v \phi - \nabla_h \cdot (2\vec{\Omega}\times\rho_0\vec{v})_h . \qquad (4)$$

Now, to explain different approximations, a "transport velocity" $\tilde{\vec{v}}$ with $\nabla\cdot\tilde{\vec{v}} = 0$ is introduced and the time derivative of the divergence is retained:

$$\nabla^2 p = -\rho_0 \frac{\partial}{\partial t}\nabla\cdot\vec{v} - \rho_0 \nabla\cdot\nabla\tilde{\vec{v}}\vec{v} + \nabla\cdot\vec{F} - \nabla_v \rho\cdot\nabla_v\phi_v - \nabla_h\cdot(2\vec{\Omega}\times\rho_0\vec{v})_h . \qquad (5)$$

The individual approximation is then (after introducing some sort of co-ordinate system with vertical axis r) determined by the definitions of $\vec{v}$, $\tilde{\vec{v}}$ and $\vec{F}$:

$\vec{v} = (\vec{v}_h, v_v)$	$\tilde{\vec{v}} = (\vec{v}_h, v_v)$	$\vec{F} = (\vec{F}_h, F_v)$	non-hydrostatic, non-linear
$\vec{v} = (\vec{v}_h, v_v)$	$\tilde{\vec{v}} = (0,0,0)$	$\vec{F} = (0,0,0)$	non-hydrostatic, linear
$\vec{v} = (\vec{v}_h, v_v)$	$\tilde{\vec{v}} = (0,0,0)$	$\vec{F} = (0,0,0)$	hydrostatic, linear
$\vec{v} = (\vec{v}_h, v_v)$	$\tilde{\vec{v}} = (\vec{v}_h, -\int_{-h}^{r} \nabla_h\cdot\vec{v}_h dr)$	$\vec{F} = (\vec{F}_h, 0)$	hydrostatic, non-linear
$\vec{v} = (\vec{v}_h, -\int_{-h}^{r} \nabla_h\cdot\vec{v}_h dr)$	$\tilde{\vec{v}} = (\vec{v}_h, -\int_{-h}^{r} \nabla_h\cdot\vec{v}_h dr)$	$\vec{F} = (\vec{F}_h, 0)$	Boussinesq, non-linear
$\vec{v} = (\vec{v}_h, -\int_{-h}^{r} \nabla_h\cdot\vec{v}_h dr)$	$\tilde{\vec{v}} = (0,0,0)$	$\vec{F} = (0,0,0)$	Boussinesq, linear.

The first non-hydrostatic case is just a reformulation without any additional assumptions. In both non-hydrostatic approximations and for the Boussinesq equations, $\nabla\cdot\vec{v} = 0$, which removes the first term from equation 5, regaining equation 4. In the hydrostatic cases, $\frac{dv_v}{dt} = 0$ is assumed. Thus the first term in equation 5 takes the form of $-\rho_0 \frac{\partial}{\partial t}\nabla_h\cdot\vec{v}_h$ and the horizontal part of the p-equation is completely uncoupled from the vertical.

The hydrostatic formulation and the Boussinesq equations have in common that the vertical velocity component is computed diagnostically from the mass balance equation, and p is determined by integration of the third momentum equation:

$$p_{hs} = p_\eta + \int_r^\eta \rho\nabla_v\phi\, dr$$

$$p_B = p_\eta + \rho_0 \int_r^\eta \frac{\partial}{\partial t}\int_{-h}^{r'} \nabla_h\cdot\vec{v}_h dr'' dr' + \rho_0 \int_r^\eta (\nabla\tilde{\vec{v}}\vec{v})_v dr + \int_r^\eta \rho\nabla_v\phi dr .$$

In the equation for p_B, as compared to hydrostatic pressure, the first additional term is the most important one because it allows dispersion (frequency dispersion). The second additional term is neglected also in non-linear Boussinesq equations.

Therefore, it may be relatively easy to integrate dispersion effects with the same accuracy that Boussinesq models have into models such as those used at the BSH, just by storing $\nabla_h\cdot\vec{v}_h$ at different time levels. By contrast, in the non-hydrostatic case, the third momentum equation would have to be solved in prognostic form, as well as the Poisson equation 4 with suitable boundary conditions (Marshall et al. 1997a,b).

7 Model simulations as part of the project

The BSH model system comprises three models. A two-dimensional, barotropic model of the North-East Atlantic Ocean computes the boundary conditions for a three-dimensional baroclinic model of the North and Baltic Seas, especially to account for the occurrence of external surges. A higher-resolution model of the German Bight and western Baltic Sea is interactively nested into the latter model (Dick et al. 2001). Additionally, a two-dimensional barotropic model of the North Sea (North Sea 10 km) is available for fast forecasts of storm surges (Müller-Navarra et al. 2003). These models solve hydrostatic non-linear shallow water equations taking into account variable bottom topography and bottom friction.

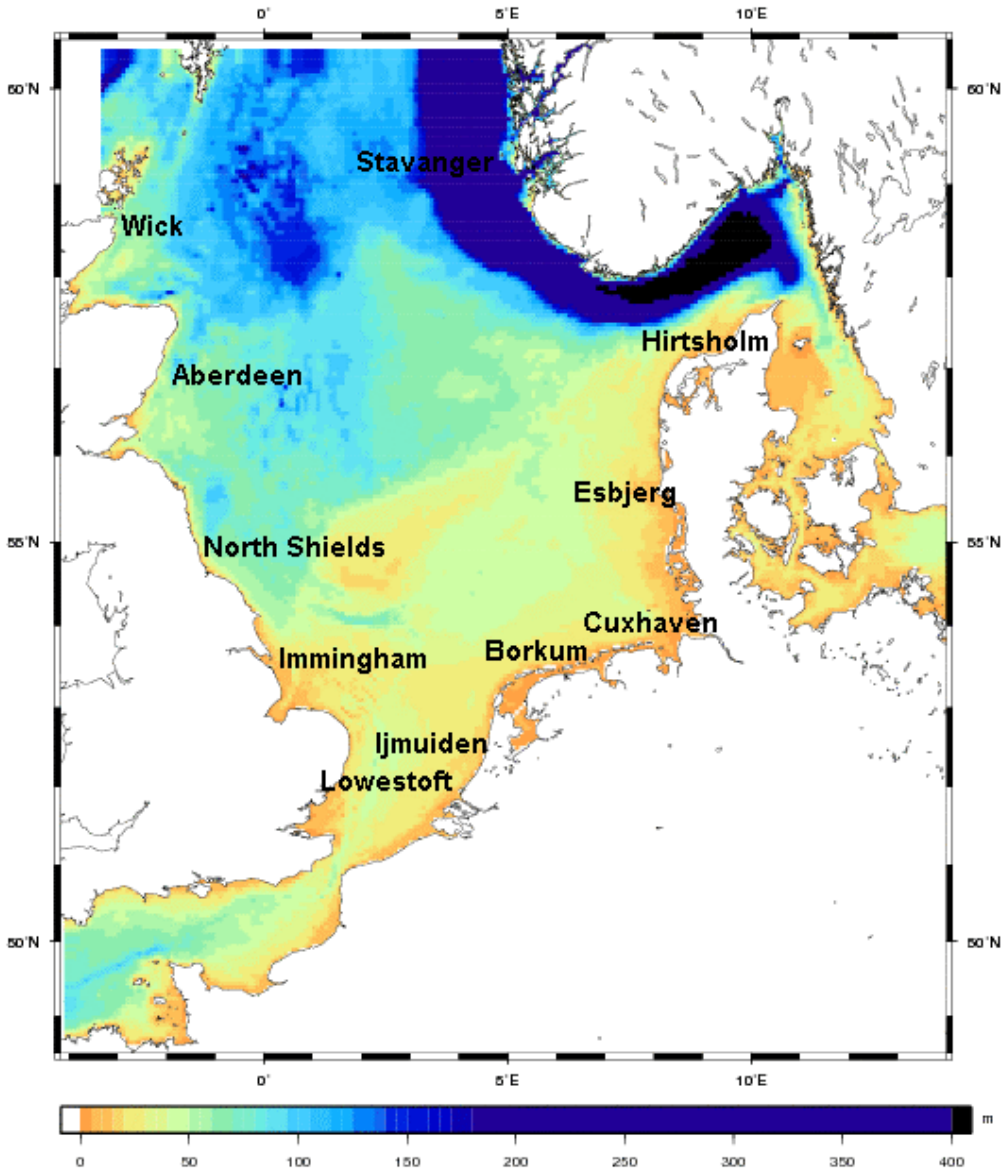

Fig. 7.0.1: Bathymetry of the BSH's "North Sea 2 km" model.

As has been pointed out under 5 above, the model equations of the North and Baltic Sea model are suitable, in principle, for modelling the propagation and modification of tsunami on the shelf. In contrast, the North-East Atlantic model has only limited suitability for computing tsunami propagation in the deep ocean and its modification on the continental slope. Adequate simulation of tsunami in the North Sea, therefore, first of all requires a profound

physical knowledge of the boundary conditions for the North Sea area. Another weakness is the numerical formulation of these boundary conditions, a problem which is far from being solved, in spite of interesting attempts (e.g. van Joolen et al. 2005). In all of these models, the grid spacing has to be fitted to the shorter wave lengths.

Fundamental changes in model physics, as proposed in section 6.2, have not been made for the model simulations discussed in this section. Analytical waves are prescribed at the model boundary. For the North Sea, the input wave height (5 m) was chosen to reflect the Storegga slope failure. The boundary condition for the North-East Atlantic model is rather arbitrary. Wave height (3 m) is chosen in such a way that potential boundary conditions for the North Sea model (Fig. 7.2.6) have about the same height as the wave prescribed as analytical boundary condition of the North Sea model. The boundary conditions were slightly modified numerically (cf. section 6.1.6), and problems were reduced by allowing signals to enter the model areas only perpendicular to the boundary.

A major adjustment, compared to the operational models, has been made in the horizontal resolution. The simulations discussed in the following were run using a higher resolution of about 10 km in the North-East Atlantic model (future version of the BSH using topographic data from the DMI version, 10.4: DMImo). The North Sea simulations were made using a high-resolution (about 2 km) two-dimensional, barotropic version of the BSH model for the North and Baltic Seas. This version (North Sea 2 km) also covers an area extending somewhat farther to the north. The topography, especially that of the German Bight, was reconstructed completely using data from numerous sources (Fig. 7.01).

With the fitted models, a coarse impression of the behaviour of a hypothetical tsunami with periods of 30 minutes or longer in the North-East Atlantic is obtained. On the shelf, using a realistic bottom topography, it is possible to adequately simulate the propagation of a tsunami with comparable periods up to the near-shore area (36 grid points/wave length at 500 m depth, 20 at 50 m, and 9 at 10 m). Hydrostatic non-linear models like those used at the BSH reproduce the modification of incoming signals by diffraction on coastline features, reflection in bays, reflection and refraction by bottom topography, shoaling of individual waves, and rear waves catching up with leading waves due to decreasing depth. (For a brief explanation of such processes, cf. e.g. section 5 and Masselink 2005). In particular, realistic travel times can be given for the shelf. However, non-linear hydrostatic equations overestimate increases in energy density per area unit for a wave train in shallow water because they neglect dispersion. For a wide, shallow shelf sea like the North Sea, it is important that the models adequately simulate dissipation by bottom friction. In this way, the signals for the simulation of potentially devastating processes in the immediate near-shore area of the German Bight contain less energy than signals travelling across a narrow continental shelf before they reach the coast. However, numerical methods almost always lead to an additional, artificial dissipation of energy. The BSH models, and similar models of this type, cease to be valid near the coast, where wave lengths become so short that dispersion effects become relevant again. The applicability of the model assumptions (including the Boussinesq equations) is restricted more severely by the breaking criterion ($H/h < 0.78$ as $h/L < 0.1$). The water level elevations given for the individual coastal stations, therefore, have to be interpreted with caution.

The following simulations were carried out:

- North-East Atlantic: wave train from the north (*H* 3 m, *T* 1800 s, Fig. 7.2.1, 7.2.4-6)
- North-East Atlantic: wave train from the south (*H* 3 m, *T* 1800 s, Fig. 7.2.2, 7.2.4-6)
- North-East Atlantic: wave train from the west (*H* 3 m, *T* 1800 s, Fig. 7.2.3, 7.2.4-6)

- North Sea 2 km: wave train from the west (*H* 5 m, *T* 1800 s, Fig. 7.3.1-6)
- North Sea 2 km: wave train from the north (*H* 5 m, *T* 1800 s, left Fig. 7.4.1-6, 7.4.7-9)
- North Sea 2 km (*h*=500 m): wave train from the north (*H* 5 m, *T* 600 s, right Fig. 7.4.1-6)
- North Sea 2 km: wave train from the north (*H* 6, 7 and 8 m, *T* 1800 s, Fig. 7.4.8-9)

- North Sea 10 km: wave train from the north (*H* 5 m, *T* 1800 s, Fig. 7.5.1, Fig. 6.1.3-5)
- North Sea 10 km: wave train from the north (*H* 5 m, *T* 1800 s) interacting with tide and extreme storm surge (Fig. 7.5.1-7.5.4)

7.1 Boundary conditions and input signals

Each of the wave trains entering the model areas consisted of three successive positive single waves. In the computations in sections 7.2 to 7.4, they have been prescribed at the appropriate boundary via velocity u_{ext} (cf. section 6.1.6). With respect to the North-East Atlantic model, Fig. 7.1.1 (left) shows the temporal evolution of the velocity (light blue curve) for a water depth of 2000 m, the selected period of 1800 s, and a wave height of 3 m. That corresponds to a positive surface elevation input signal that is independent of depth (Fig. 7.1.1, right). This is not a realistic formulation, but it allows a straightforward interpretation of the propagation and modification of the boundary signal as it travels across the North-East Atlantic.

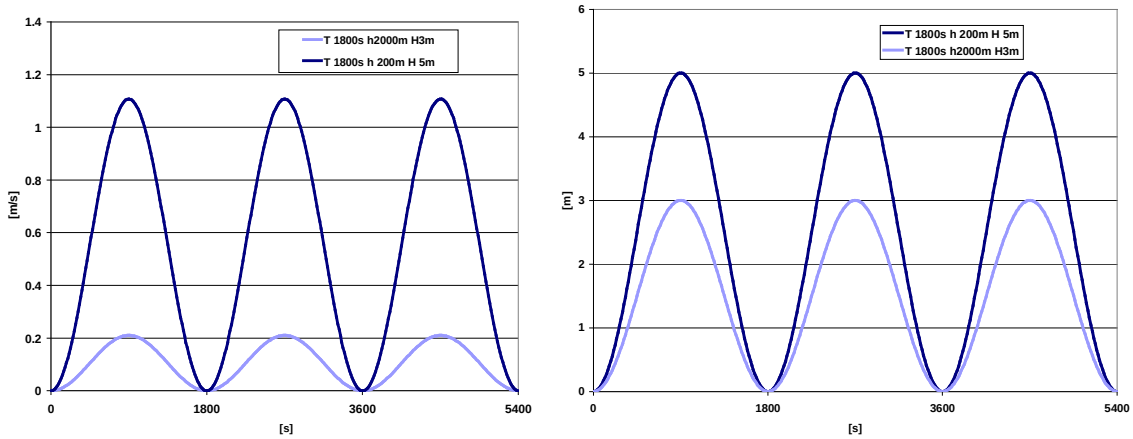

Fig. 7.1.1: Input signal North Atlantic and North Sea. Left: $u = H\sqrt{gh}/h\sin^2(2T/2\pi\, t)$. *right:* $\eta = uh/\sqrt{gh}$.

Because of the arbitrarily chosen boundary condition for the North-East Atlantic model and its inability to reproduce all features modifying a tsunami in deep water and at the continental slope, results from this model were not used as boundary condition for the North Sea model.

Therefore, an input signal defined in the same manner as that in the North-East Atlantic model was prescribed for the North Sea but generally with a standard wave height of 5 m (Fig. 7.1.1 in 200 m of water, dark blue curve). In comparative computations, the wave height of the input signal was increased to 6 m, 7 m, and 8 m, with an identical period. Fig. 7.1.2 shows the water level evolution at a point close to the boundary (Bergen), with the time related to first entry of the signal into the model area, i.e. Bergen was reached after just a few minutes.

Although higher water levels in the Storegga event were reconstructed for the Shetland Islands (Fig. 3.3.2), 5 m appears to be an adequate wave height for the boundary signal because such high water levels are not unlikely to result from secondary processes. Using the standard signal, water levels exceeding 10 m were simulated, e.g. in Lerwick (Fig. 7.1.3).

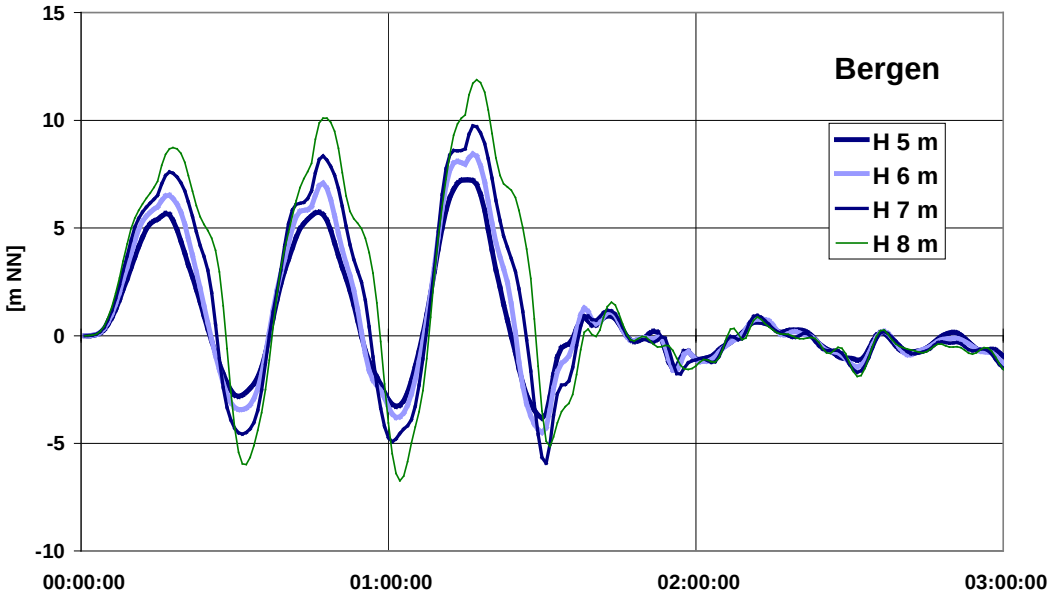

Fig. 7.1.2: Water level evolution in Bergen using different wave height input signals (3 positive single waves, period 1800 s, North Sea model 2 km).

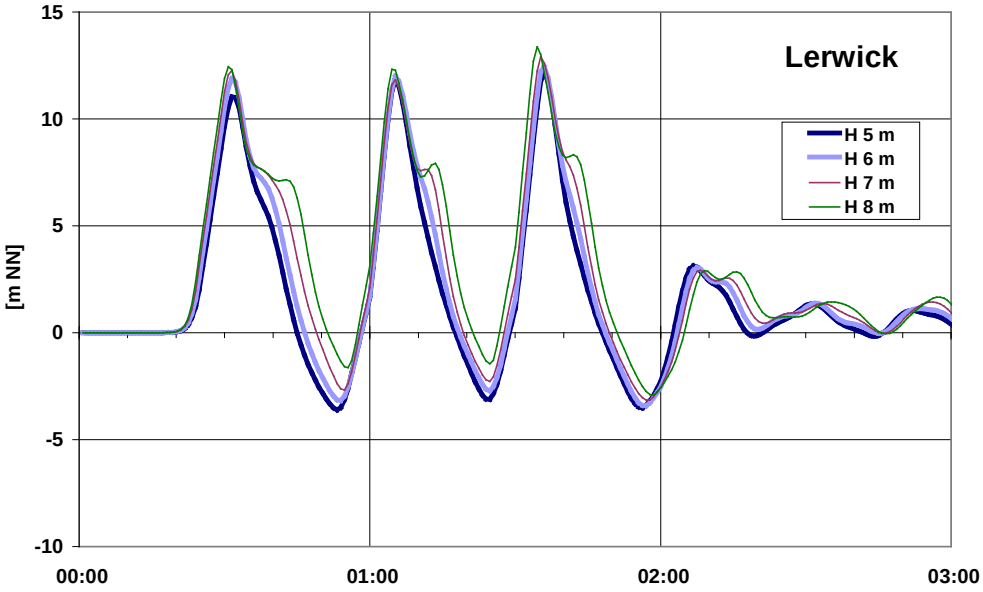

Fig. 7.1.3: *Water level evolution in Lerwick using different wave height input signals (3 positive single waves, period 1800 s, North Sea model 2 km)*

7.2 North-East Atlantic Ocean

The simulations run on the North-East Atlantic model show the evolution of relatively well resolved signals, 35 grid points per single signal at 4,000 m depth, and still about 15 grid points per single signal at 1,000 m depth. The area covered by the model (Fig. 7.2.0) includes the continental slope and the shelf. In both areas, tsunami are subject to strong modification.

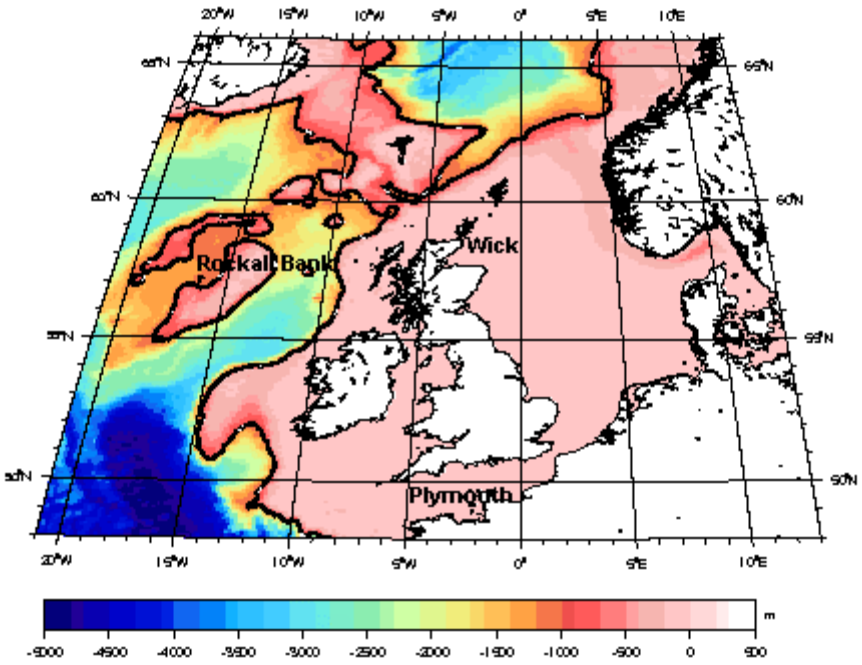

Fig. 7.2.0: Bathymetry of the BSH's North-East Atlantic model 10 km.

7.2.1 Propagation

The propagation velocity of tsunami, i.e. of energy, is very high in deep water (about 200 m s^{-1} in 4,000 m of water as compared to 20 m s^{-1} in 40 m of water). With the numerical method chosen for the model, also the numerical energy dissipation is higher than is to be expected form physical laws. An increase of single signals due to shoaling occurs at a few locations in Fig. 7.2.1-3 and is also seen in Fig. 7.2.6, but local increases more often result from superposition of the three single signals. The essential modifications during propagation in the deep ocean and across the continental shelf all reflect the influence of changing $\sqrt{gh}$ with depth (cf. section 5.3). This, e.g., causes the individual signals to be compressed and shortened at the shelf edge. The way turbulent momentum exchange is modelled (Dick et al. 2001) allows the three initial signals to be clearly distinguished even on the shelf, where wavelength has become very small. Dispersion is not included in the analytical formulation of the model. With the chosen boundary condition – all single signals have the same period – this should not matter theoretically. Approximation by finite differences, however, destroys this property and the signal is modified due to numerical dispersion. Despite all restrictions, the simulation shows that propagation of a tsunami towards the North Sea is complex and highly variable in space.

The leading input signal in all simulations propagated during a 12-hour period. Figs. 7.2.1-3 all include a state where all three single signals have entered the model area. Then their evolution until reaching the northern boundary of the North Sea or the Channel entrance is shown. In Fig. 7.2.3, three identical signals entering the area at the boundary at equal time intervals have changed their distances after 1.5 hours. By the time they reach the transition to shallower water, i.e. when they cross the depicted 1,000 m depth contour, the back waves have caught up with the front waves. This effect is especially pronounced at Rockall. When the waves reach the deep water of the Norwegian Sea, their distance has increased again.

A signal from the northern model boundary reaches the North Sea after nearly 2.5 hours (Fig. 7.2.1). The signal prescribed at the southern boundary reaches northern Scotland after 5 hours (Fig. 7.2.2) and, as a weak signal, the northern North Sea after 7 hours. Owing to its shallower depth, the Channel entrance is reached hardly earlier, and signal propagation within the Channel is very slow (cf. section 7.3). The signal from the west reaches Scotland after 3.5 hours (Fig. 7.2.3). Deflected to shallower water, it enters the North sea nearly from the north (Fig. 7.2.3).

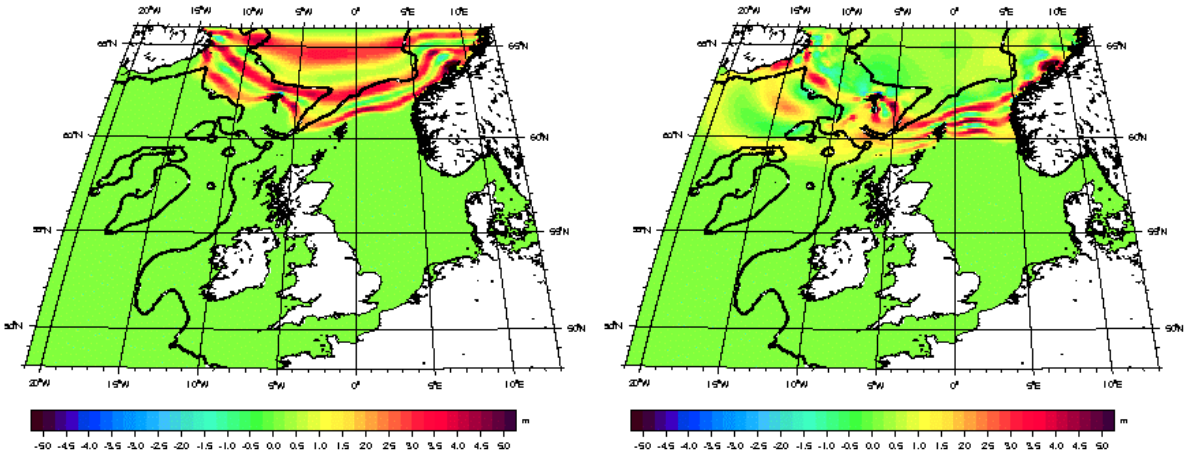

Fig. 7.2.1: Water level distribution after 1.5 hours (left) and 2.5 hours (right) (input signal: 3 positive single signals from N, T 1800 s, H 3 m, North-East Atlantic model 10 km)

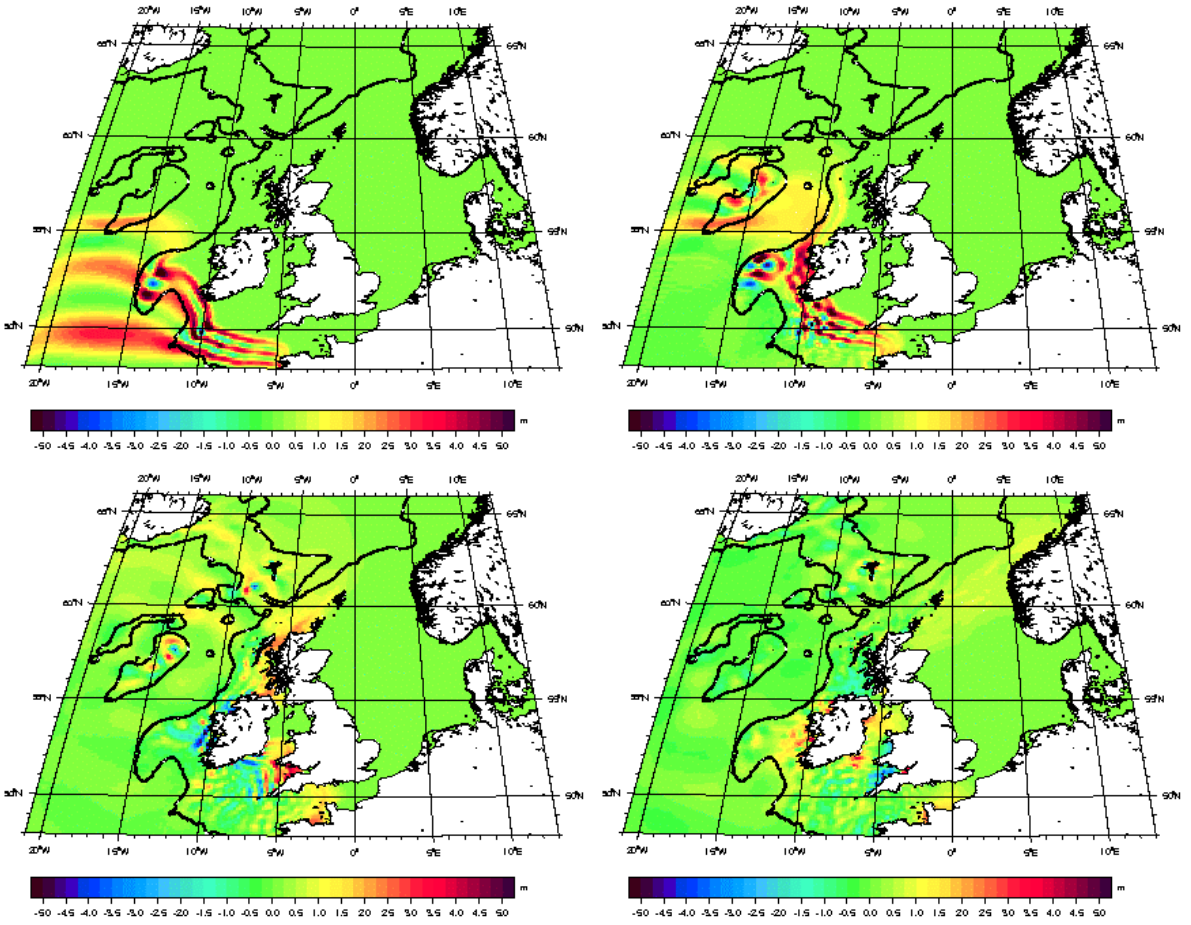

Fig. 7.2.2: Water level distribution after 1.5 hours (top left), 2.5 hours (top right), 5 hours (bottom left), and 7 hours (bottom right) (input signal: 3 positive single signals from S, T 1800 s, H 3 m, North-East Atlantic model 10 km)

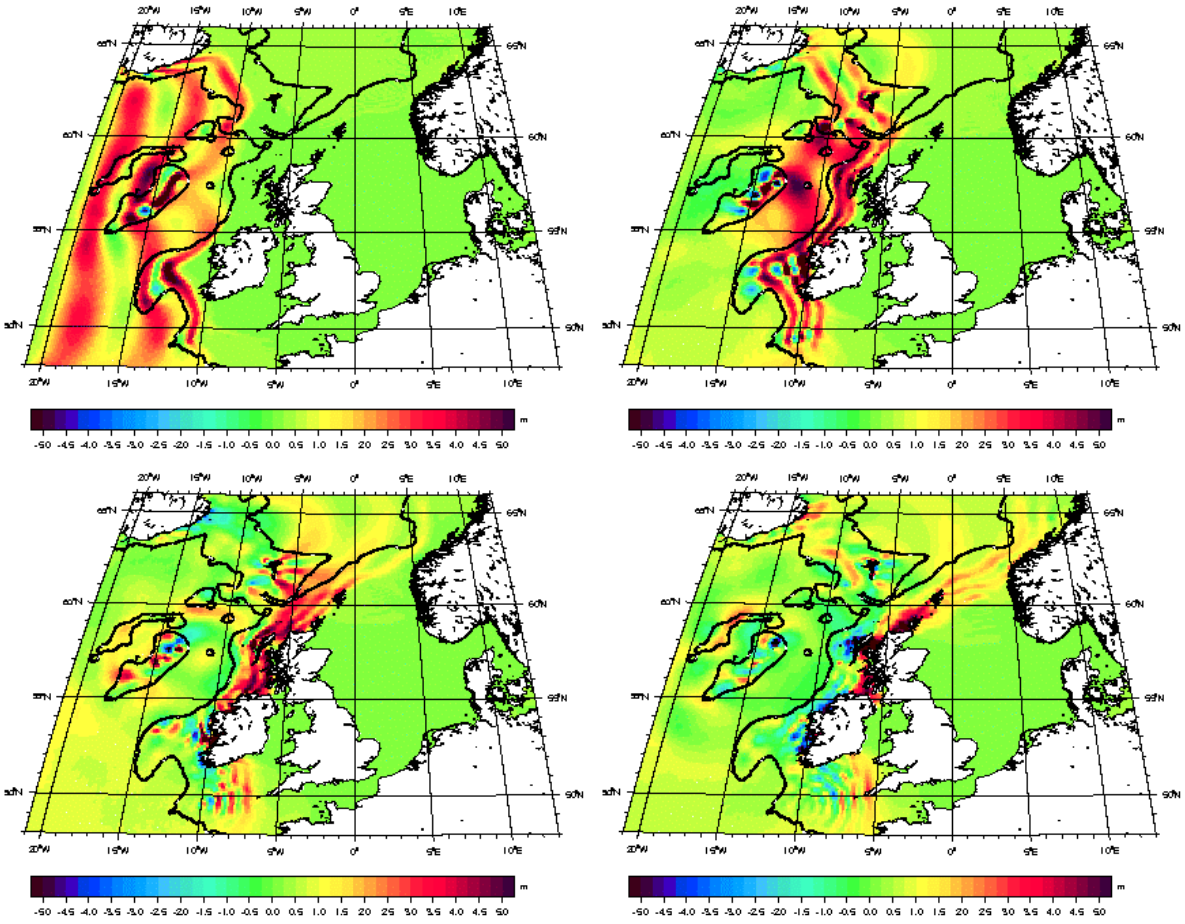

Fig. 7.2.3: Water level distribution after 1.5 hours (top left), 2.5 hours (top right), 3.5 hours (bottom left), and 4.5 hours (bottom right) (input signal: 3 positive single signals from W, T 1800 s, H 3 m, North-East Atlantic model 10 km)

7.2.2 Travel times and water levels

Travel times are read more accurately from local water level time series. At Plymouth (Fig. 7.2.4), the first maximum of the signal coming from the south arrives after about 3 hours. The signal coming from the western boundary takes about twice as long and is evidently weakened, as compared to the initial signal.

A signal from the northern boundary reaches Wick (Fig. 7.2.5) after a considerably longer time than it takes to reach the open North Sea near Shetland (Fig. 7.2.6). It arrives at Wick almost after the same time as the signal from the western boundary. However, the two signals differ significantly in shape. The signal from the south arrives 2 hours later than the northern and western signals. In all three cases, the maximum water level is lower than the initial wave height.

In contrast, in Fig. 7.2.6, the signal from the northern boundary has clearly increased to 5 m wave height due to shoaling. The signal from the west has the same height as that arriving in Wick. The latter two signals have different shapes. Near Shetland, the western signal has preserved its initial shape (3 single waves, T=1800 s), while in Wick the water level for the western signal reaches values of up to 2 m which last for more than 4 hours.

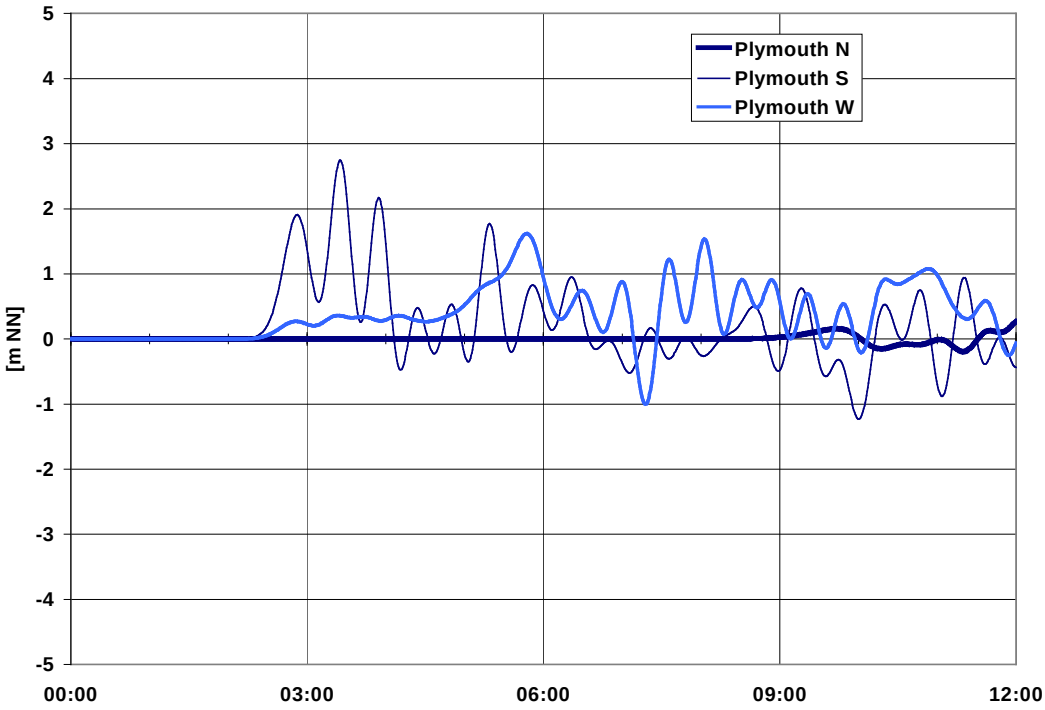

Fig. 7.2.4: Water level evolution at Plymouth (input signal: 3 positive single signals, T 1800 s, wave height 3 m, from the north N, from the south S and from the west W, North-East Atlantic model 10 km)

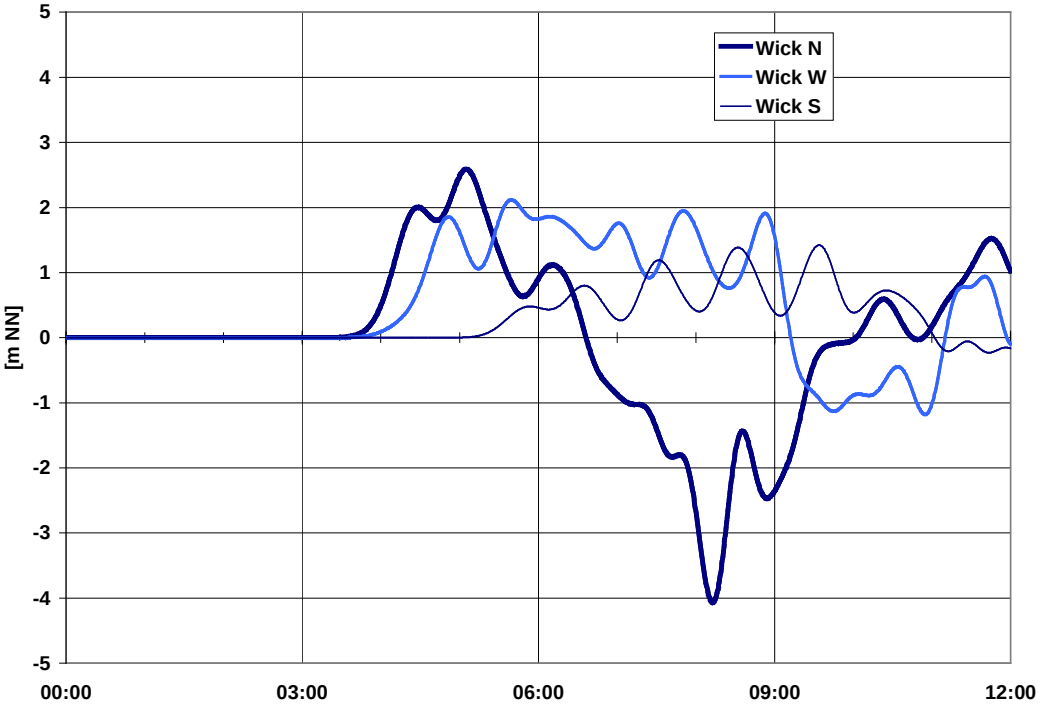

Fig. 7.2.5: Water level evolution at Wick (input signal: 3 positive single signals, T 1800 s, wave height 3 m, from the north N, from the south S and from the west W, North-East Atlantic model 10 km)

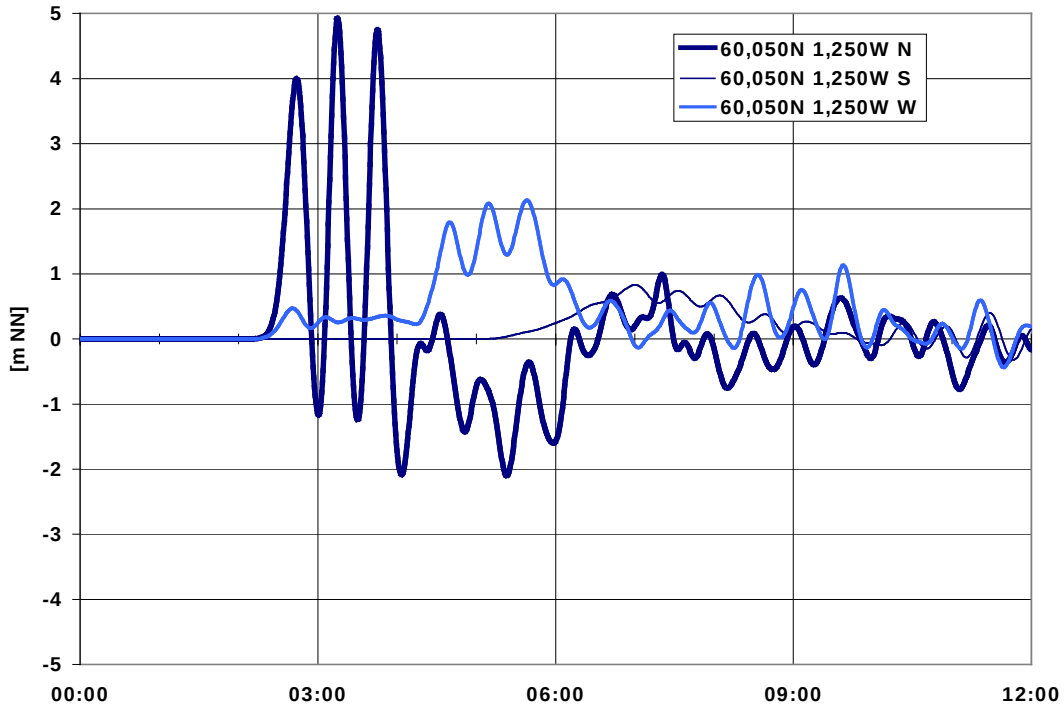

Fig. 7.2.6: Water level evolution near Shetland (input signal: 3 positive single signals, T 1800 s, wave height 3 m, from the north N, from the south S and from the west W, North-East Atlantic model 10 km)

7.3 North Sea signal from the west

As has been explained in section 7.1, the simulations run on the North Sea model (grid spacing 2 km) were not carried out using boundary values from the North-East Atlantic model as input signal but an analytical standard wave train (3 positive single waves, period 1800 s, wave height 5 m). First, a boundary signal from the west was prescribed. The signal is identical in the western part of the Channel and off Scotland, where it starts at the same time (t=0). This specific kind of boundary condition is not to be expected from the results of section 7.2. The initial phase of the simulation should rather be considered the simultaneous representation of two theoretical types of boundary conditions.

7.3.1 Propagation

The input signal initially leads to very high local water levels, both in the north and in the Channel (Fig. 7.3.1). In Plymouth, for example, about 8 m is reached. In the north, propagation of the single waves is circular (Fig. 7.3.2), with subsequent superposition with a diffraction pattern caused by the Norwegian coast (Fig. 7.3.3). In general, this signal is weaker in the North Sea than a comparable signal entering from the north (cf. section 7.4). This is mainly because there is less energy available right from the start (incoming signals travel across a shorter section of the boundary). The wave front then widens due to circular propagation, whereas in subsequent simulations (sections 7.4 and 7.5) the wave front initially maintains a relatively constant length.

Signal propagation in the Channel is slow, but the high resolution allows the propagation to be modelled along the continental coastline into the North Sea (Figs. 7.3.3 and 7.3.4). Finally, the signals from the Channel and from the north superimpose (Figs. 7.3.5 and 7.3.2).

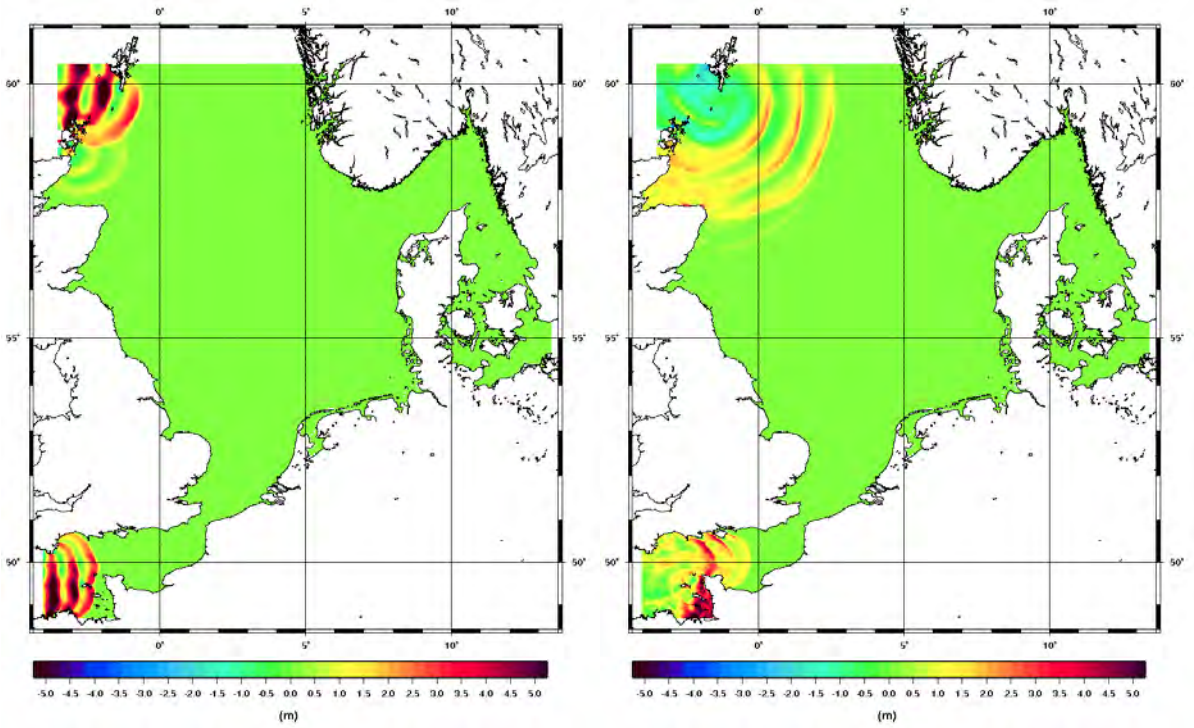

Fig. 7.3.1 (left): Water level distribution after 1.5 h (input signal: 3 positive single signals, period 1800 s, wave height 5 m, from the west, North Sea 2 km)

Fig. 7.3.2 (right): Water level distribution after 3 h (input signal: 3 positive single signals, period 1800 s, wave height 5 m, from the west, North Sea 2 km)

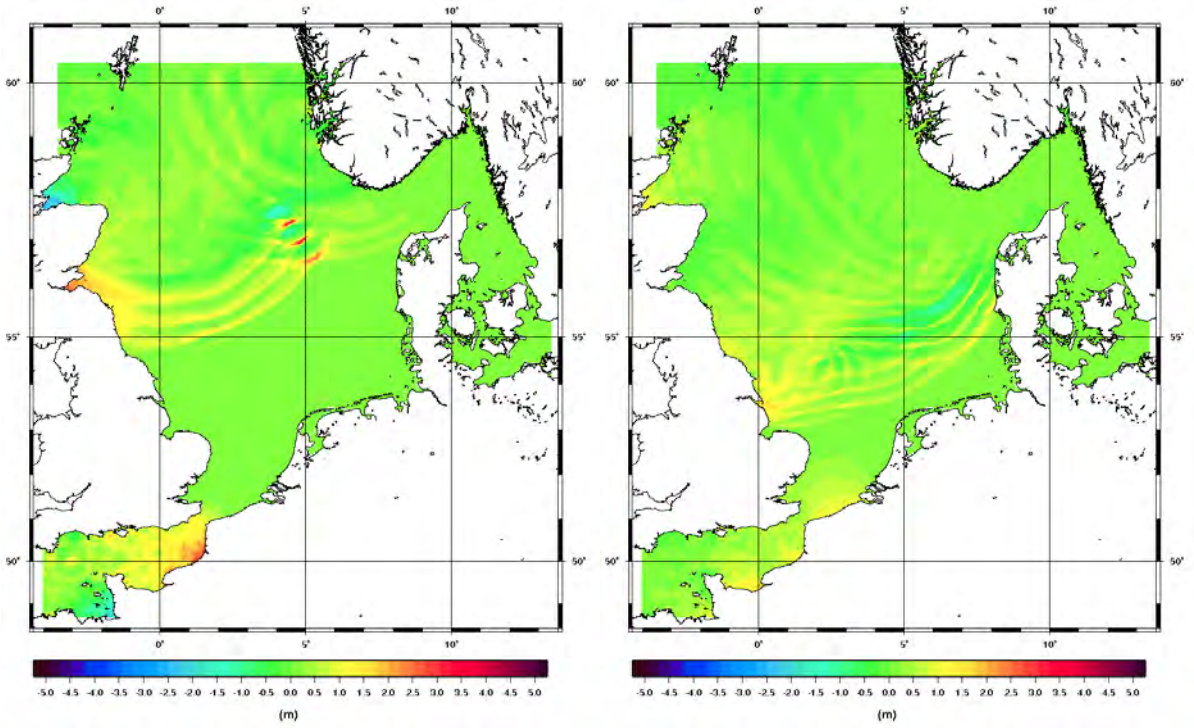

Fig. 7.3.3 (left): Water level distribution after 6 h (input signal: 3 positive single signals, period 1800 s, wave height 5 m, from the west, North Sea 2 km)

Fig. 7.3.4 (right): Water level distribution after 9 h (input signal: 3 positive single signals, period 1800 s, wave height 5 m, from the west, North Sea 2 km)

7.3.2 Travel times and water levels

When a signal propagates from the western model boundary (North Sea 2 km), the signal component starting north of Scotland is the first to arrive on the German coast. The waves proper reach their maximum at Cuxhaven 12 hours after having entered the model area from the north-west. A secondary maximum occurs about 3 hours later (Fig. 7.3.5). The continued water level rise thereafter results from a highly unrealistic superposition of the signals arriving from the north-west and from the Channel (Fig. 7.3.6).

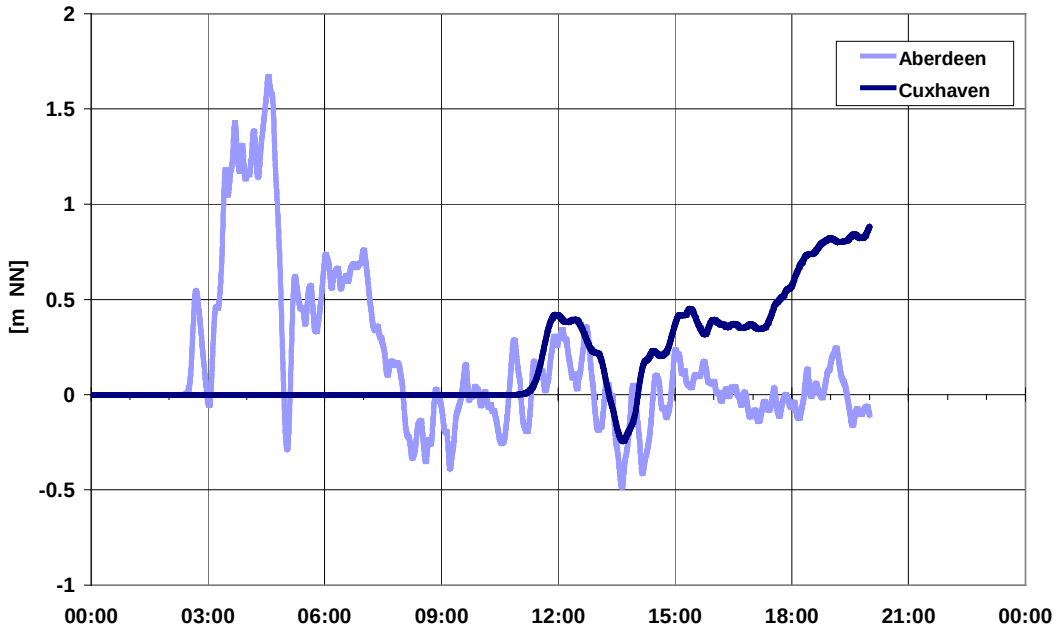

Fig. 7.3.5: Water level evolution at Aberdeen and Cuxhaven (input signal: 3 positive single signals, period 1800 s, wave height 5 m, from the west, North Sea 2 km)

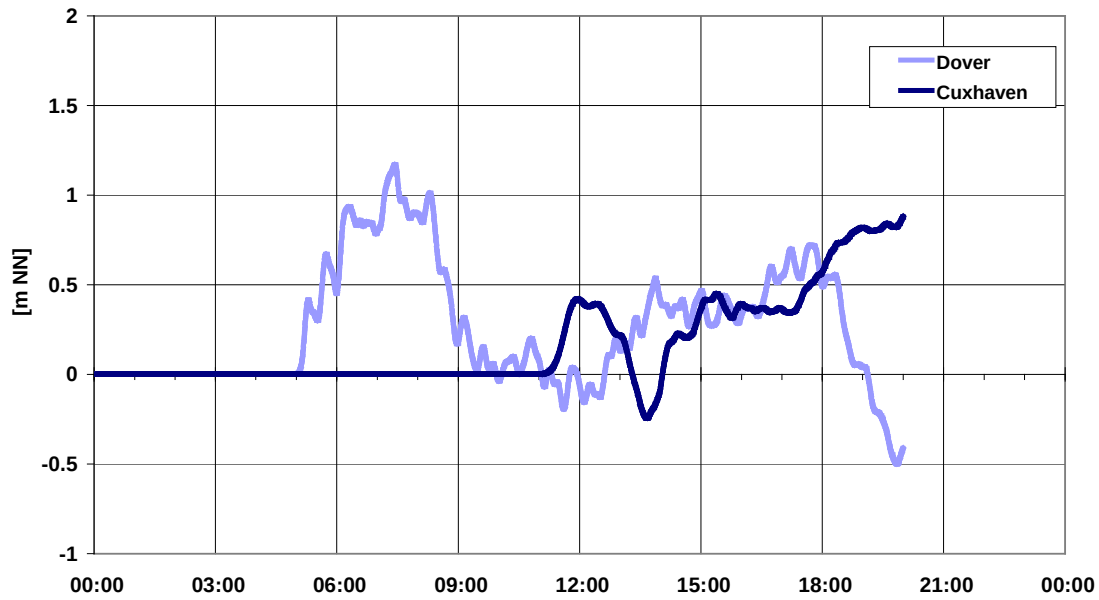

Fig. 7.3.6: Water level evolution at Dover and Cuxhaven (input signal: 3 positive single signals, period 1800 s, wave height 5 m, from the west, North Sea 2 km))

7.4 North Sea signal from the north

Figs. 7.4.1-6 show, in their left part, the propagation of the boundary signal described in section 7.1 (three positive signals, *T* 1800 s, *H* 5 m). For better physical understanding, computations were additionally carried out with a constant water depth of 500 m in the entire North Sea. In these simulations, the same kind of boundary signals were used, but a period of 600 s.

7.4.1 Propagation

The influence of realistic bottom topography is obvious from the faster propagation in deep water, in this case the Norwegian Trench. In the north, the simulation shows major local water level maxima (Figs. 7.4.1 and 7.4.2, left figures). They are caused by directional changes and subsequent superposition among the single signals due to an inhomogeneous depth gradient (refraction). These maxima do not occur in the comparative computations with a flat bottom (right figures).

Diffraction and reflection produce locally very high water levels in bays and estuaries, and near islands (e.g. Lerwick station, Fig. 7.1.3). Such processes are governed by the shape of the coastline and the location of islands. They may, however, be subject to modification by variable bottom topography, which influences the direction and velocity of propagation, cf. Figs. 7.4.2 and 7.4.3, left figures.

The German coast is located in the wave shadow of Norway. It is reached first by extensions of the input signal that has weakened on the shelf (Fig. 7.4.4). Later, a secondary signal generated by superposition of a diffraction pattern also arrives at the coast (Fig. 7.4.6). It is generated mainly by diffraction and reflection on the British coast. It is better visible in the flat-bottom simulations but also constitutes a significant signal in model time series using a realistic topography.

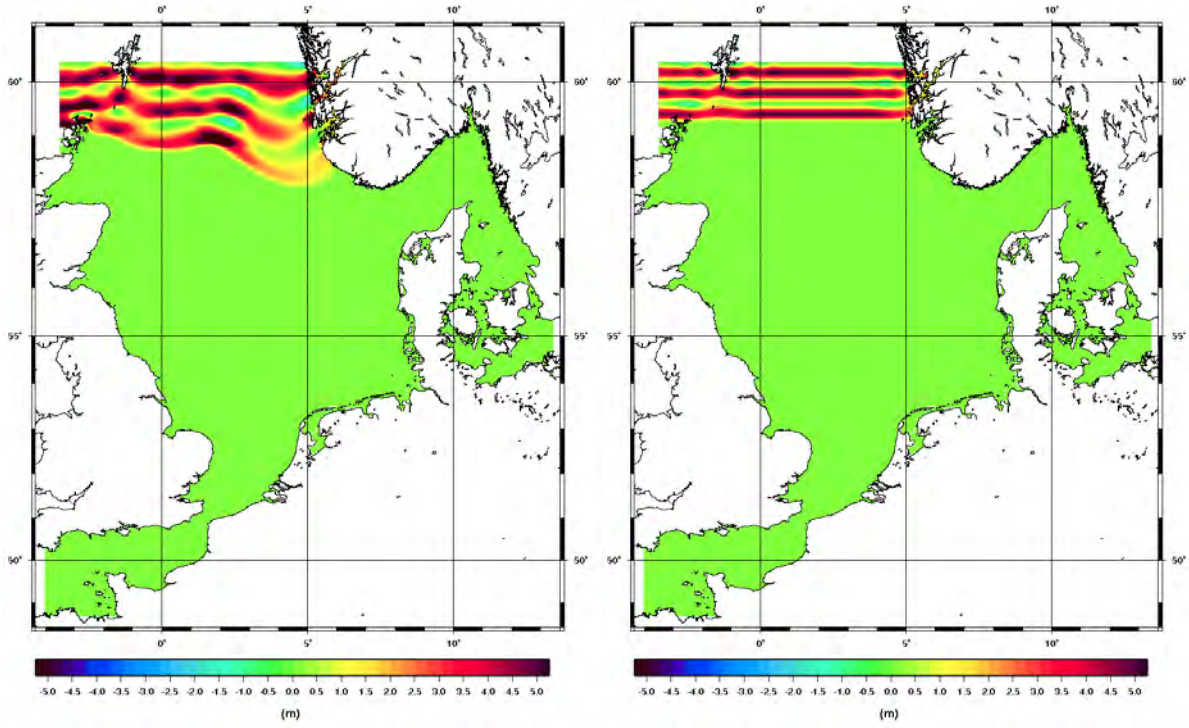

Fig. 7.4.1: Water level distribution (input signal: 3 positive single signals, wave height 5 m, from the north, North Sea 2 km)
Left: after 1.5 hours with realistic depth distribution (T 1800 s)
Right: after 0.5 hour with constant water depth (h 500 m, T 600 s)

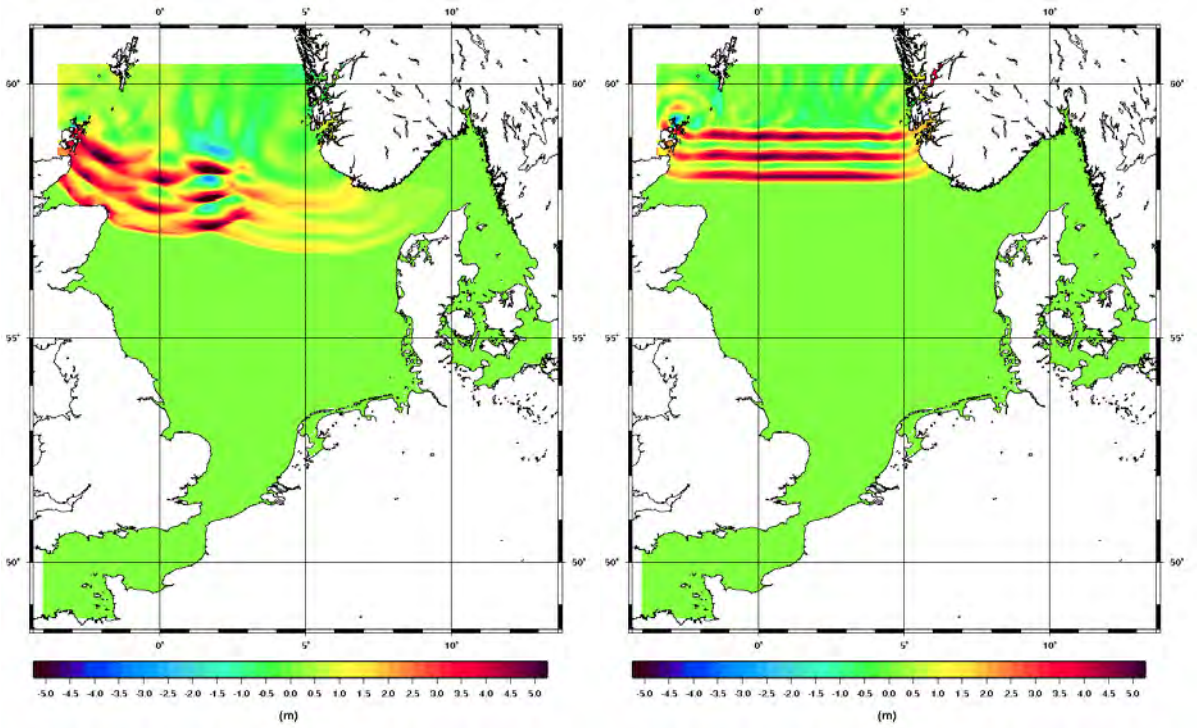

Fig. 7.4.2: Water level distribution (input signal: 3 positive single signals, wave height 5 m, from the north, North Sea 2 km)
Left: after 3 hours with realistic depth distribution (T 1800 s)
Right: after 1 hour with constant water depth (h 500 m, T 600 s)

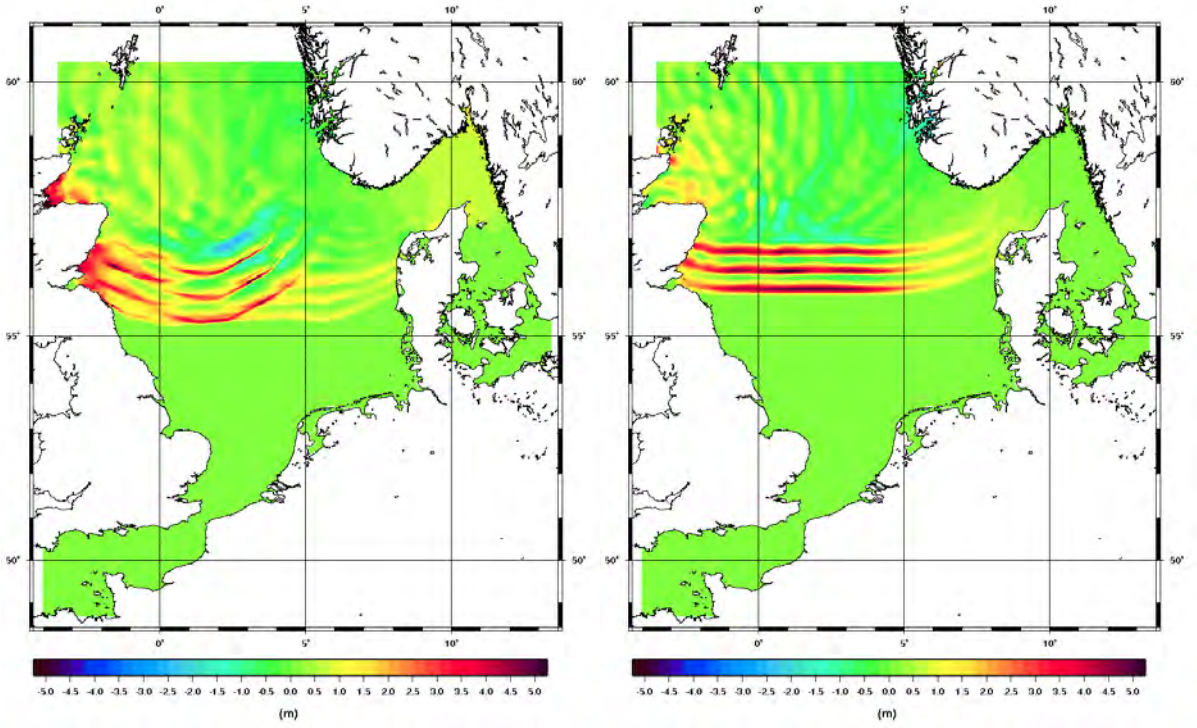

Fig. 7.4.3: Water level distribution (input signal: 3 positive single signals, wave height 5 m, from the north, North Sea 2 km)
Left: after 5 hours with realistic depth distribution (T 1800 s)
Right: after 2 hours with constant water depth (h 500 m, T 600 s)

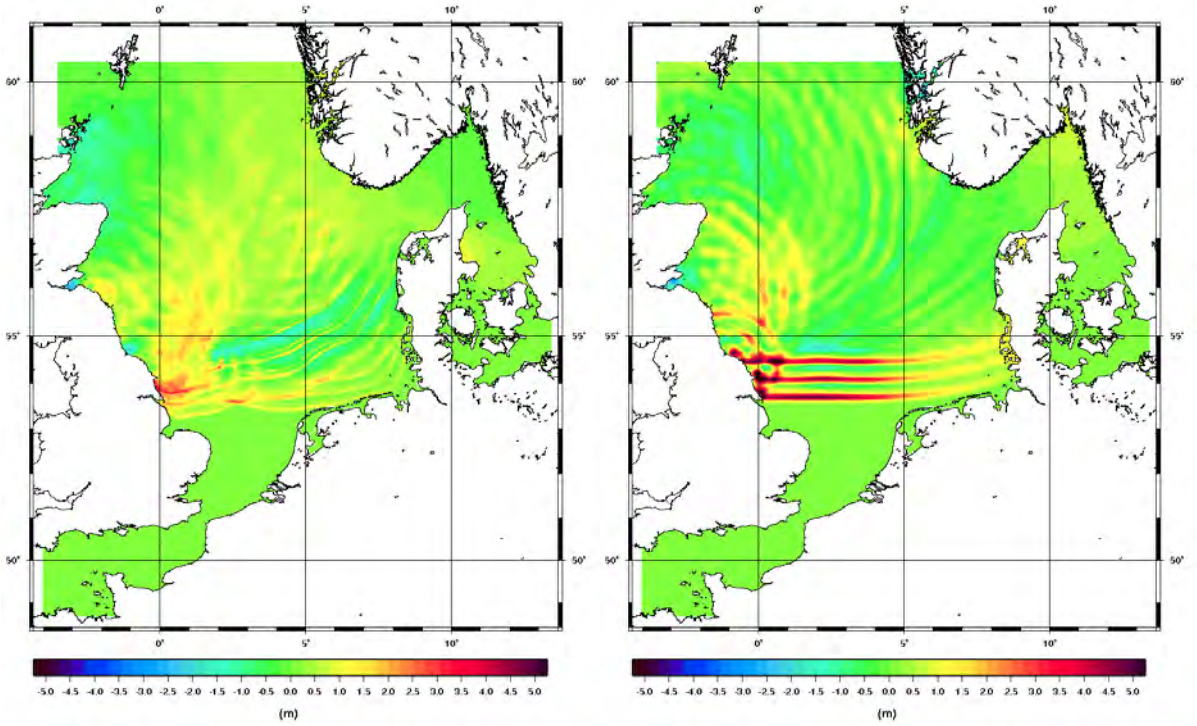

Fig. 7.4.4: Water level distribution (input signal: 3 positive single signals, wave height 5 m, from the north, North Sea 2 km)
Left: after 8 hours with realistic depth distribution (T 1800 s)
Right: after 3 hours with constant water depth (h 500 m, T 600 s)

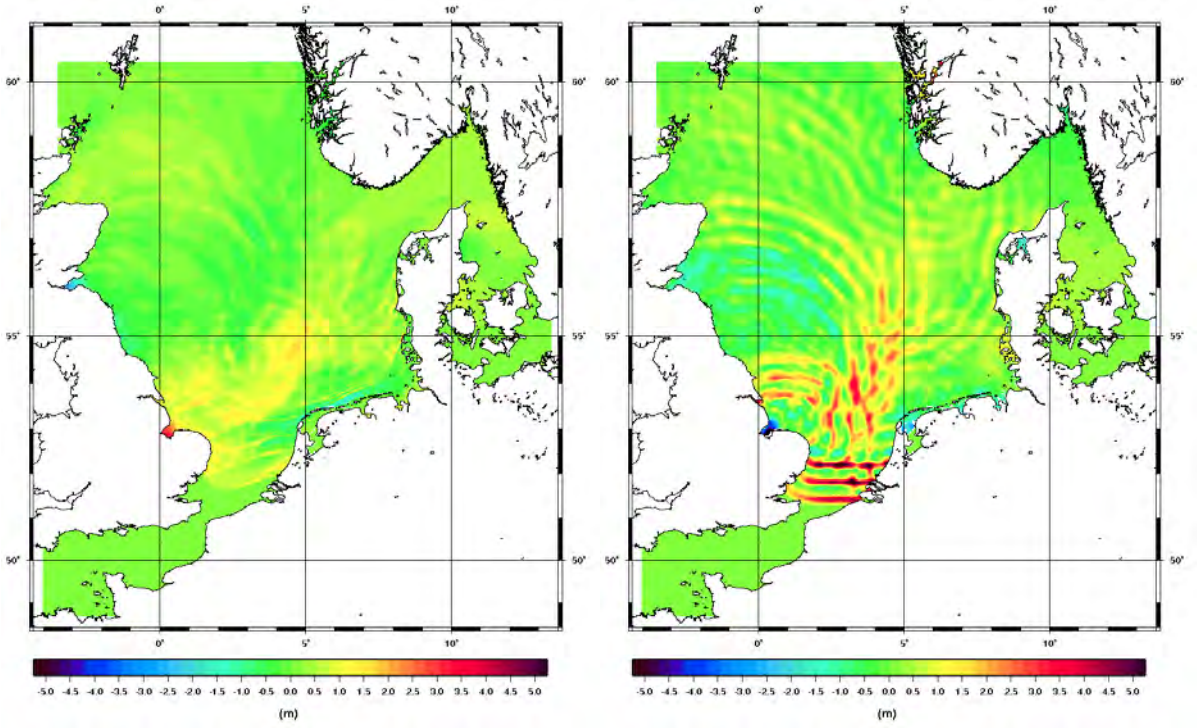

Fig. 7.4.5: Water level distribution (input signal: 3 positive single signals, wave height 5 m, from the north, North Sea 2 km)
Left: after 11 hours with realistic depth distribution (T 1800 s)
Right: after 4 hours with constant water depth (h 500 m, T 600 s)

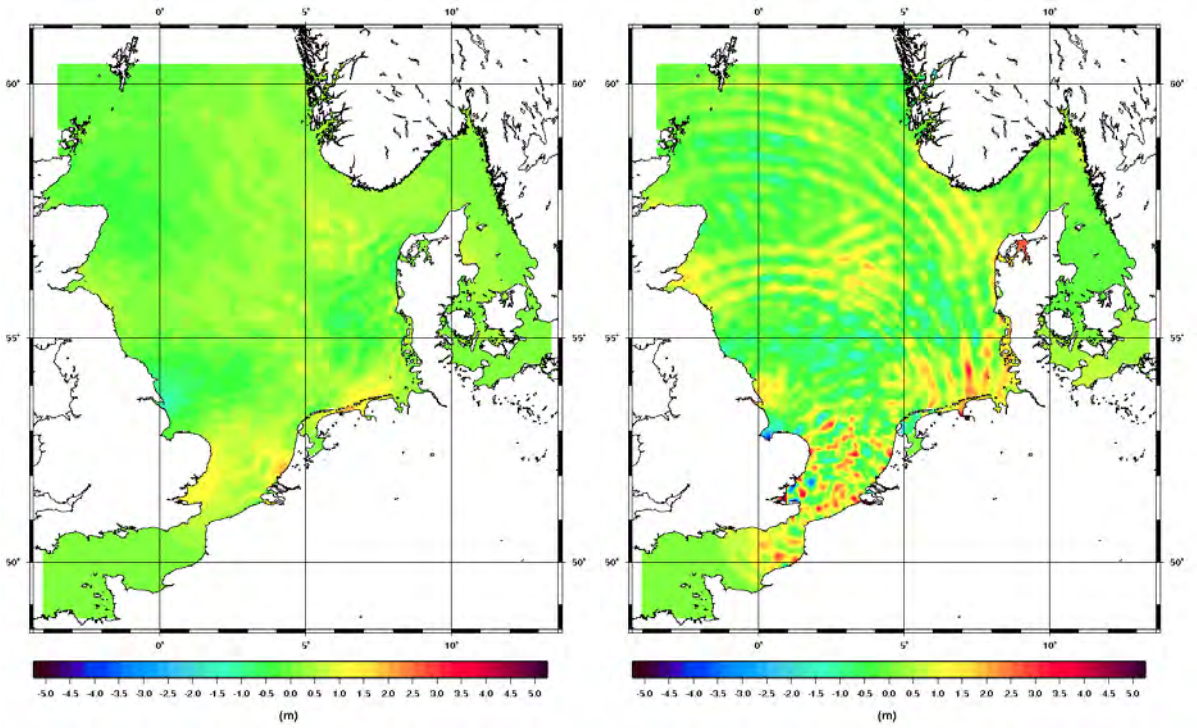

Fig. 7.4.6: Water level distribution (input signal: 3 positive single signals, wave height 5 m, from the north, North Sea 2 km)
Left: after 14 hours with realistic depth distribution (T 1800 s)
Right: after 5 hours with constant water depth (h 500 m, T 600 s)

7.4.2 Local water level evolution

Fig. 7.4.7 shows the water level evolution at stations on the western coast (Wick, Aberdeen, North Shield, Immingham, Lowestoft) and on the eastern and southern coast (Stavanger, Hirtshals, Esbjerg, Borkum, Ijmuiden) of the North Sea. The times indicated relate to the start of the input signal at the northern model boundary.

Besides the initial signal, a secondary signal resulting from diffraction and interference patterns or from reflection is visible at all locations. The stations were chosen in such a way that the primary signal arrived about simultaneously in the west and east, i.e. the stations have about the same geographical latitude. For example, both the primary and secondary wave signals reach Borkum earlier than Ijmuiden. As in the spatial representations in section 7.4.1, also Fig. 7.4.7 shows a higher primary signal in the west and north, while the secondary signal is more pronounced in Ijmuiden, Borkum, Esbjerg (Fig 7.4.7) and Cuxhaven (Fig. 7.4.9), i.e. in the south-eastern North Sea.

The primary signal east of about 5^{o} E is low because it reaches the wave shadow of Norway only by diffraction. By contrast, the western coasts are exposed to the full initial signal which is, however, weakened by dissipation (see Fig. 5.4.4).

Figs. 7.4.8 and 7.4.9 (as well as Figs. 7.1.2 and 7.1.3) also show the influence of a higher input signal on the local evolution of water levels. In contrast to Aberdeen (Fig. 7.4.8), that influence is low at the German coast. At Cuxhaven (Fig. 7.4.9), the secondary component increases more strongly than the primary component.

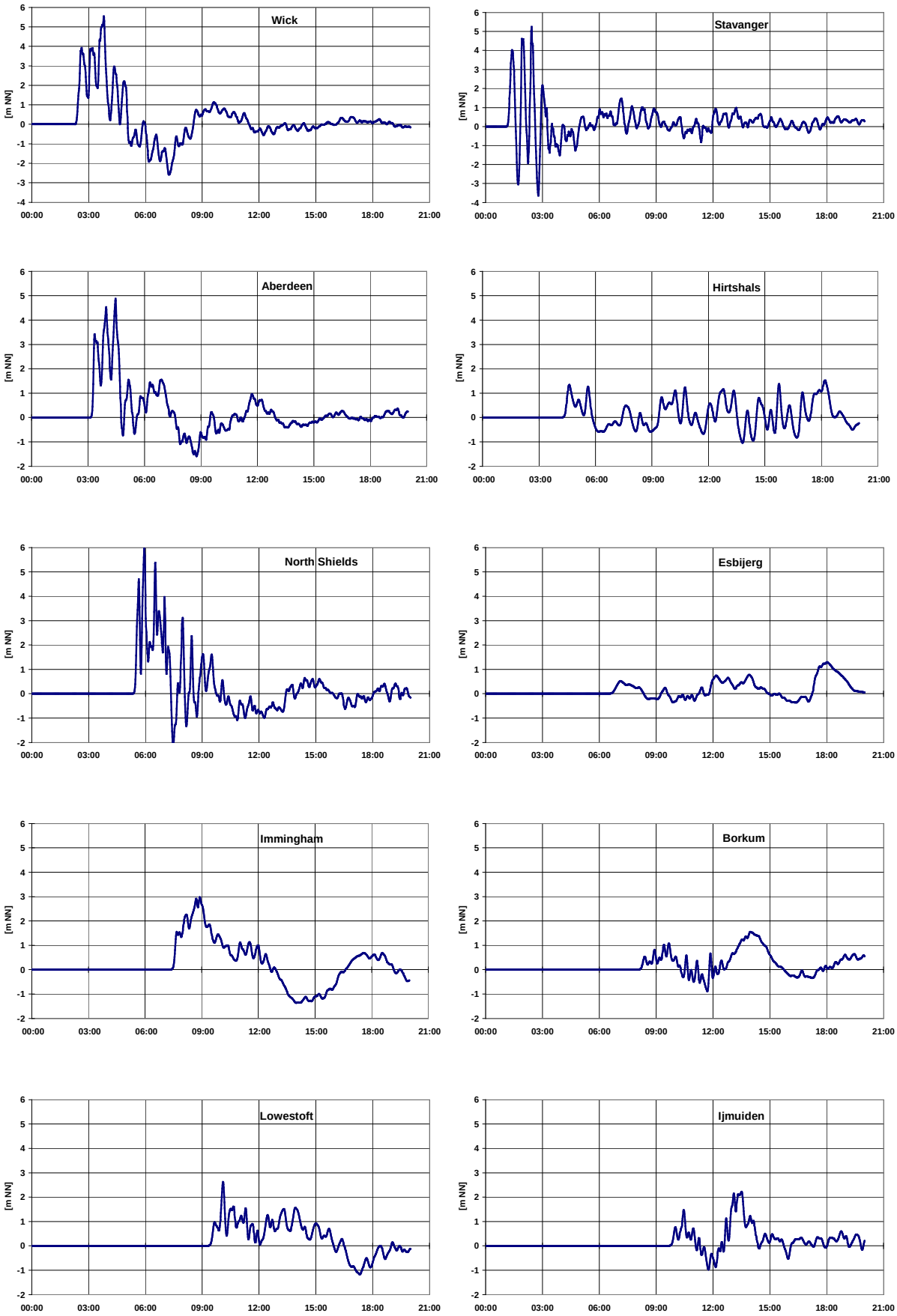

Fig. 7.4.7: Water levels at selected sites at the west and east coasts of the North Sea (input signal: 3 positive single signals, T 1800 s, H 5 m, from the north, North Sea 2 km)

7.4.3 Travel Times

With a group velocity of $c_{g0} = \sqrt{gh_0}$ and a constant depth of 70 m (average depth of the North Sea), travel times of 10.6 hours, 5.3 hours, and 1.1 hours are computed for distances of 1,000 km, 500 km, and 100 km, respectively.

The travel time from the northern boundary of the North Sea to Borkum, about 8 hours for the primary signal, fits well with this simple estimation. In this simulation, Cuxhaven is reached after about 9 hours by the wave train starting at the latitude of the Shetland Islands (Fig. 7.4.9). From Aberdeen, the signal travels about 6 hours (Fig. 7.4.8). The good fit between the simple estimation at the beginning of this section and the model simulation is attributable to the hydrostatic assumption made in the model. It is not possible, however, to predict the entry time of the secondary signal by such simple estimation. It reaches its maximum at Cuxhaven about 7 hours after the lower primary maximum (Fig. 7.4.9).

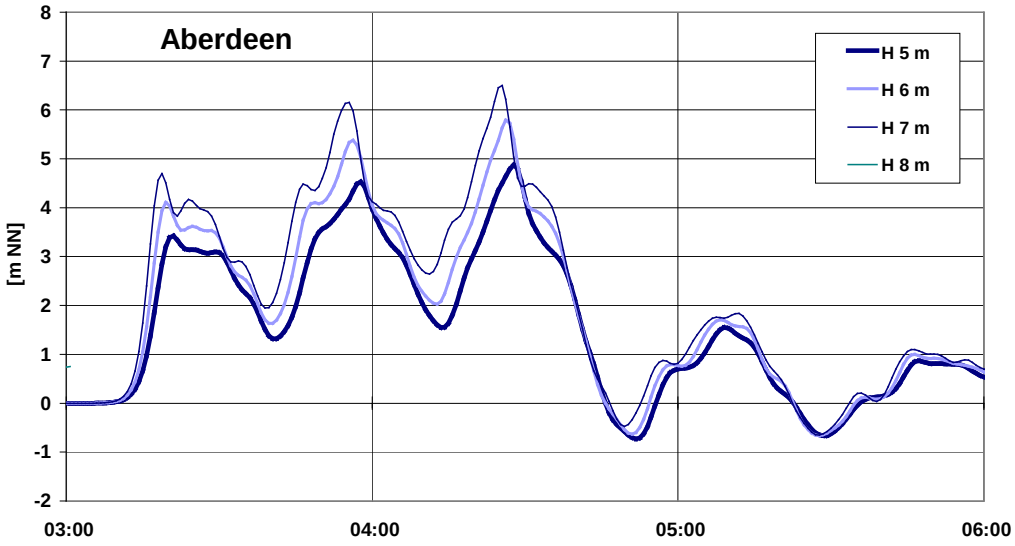

Fig. 7.4.8: Water levels at Aberdeen (input signal: 3 positive single signals, T 1800 s, H 5 m, from the north, North Sea 2 km)

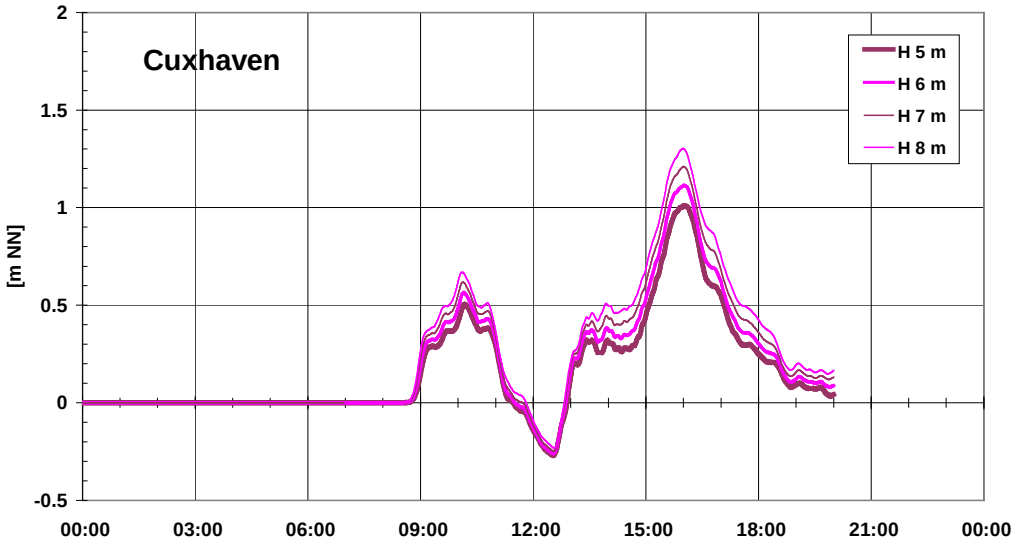

Fig. 7.4.9: Water levels at Cuxhaven (input signal: 3 positive single signals, T 1800 s, H 5 m, from the north, North Sea 2 km)

7.5 Signal from the north simultaneous with extreme storm surge (including tide and external surge)

Severe storm surges are a familiar phenomenon to the population living on the North Sea coast. That raises the question what would happen if a tsunami hit the German coast at the same time as a storm surge. As the meteorological forcing had not been fitted to the new version (North Sea 2 km) when the model computations discussed here were made, an older two-dimensional barotropic model of the North Sea and western Baltic (Müller-Navarra et al. 2003), which has a horizontal resolution of about 10 km (North Sea 10 km), was used to obtain a rough idea of the interactions between medium-length waves, tides, and a storm surge event.

At first, the simulations using a realistic topography as described in section 7.4 were repeated using the same input signal (Fig. 7.5.1), neglecting tidal and wind forcing. Although the results differ with respect to the propagation velocity and signal height at Cuxhaven (cf. section 6.1.5), they are similar enough to demonstrate the interactions between storm surge, external surge, tide, and a hypothetical tsunami using the North Sea 10 km model.

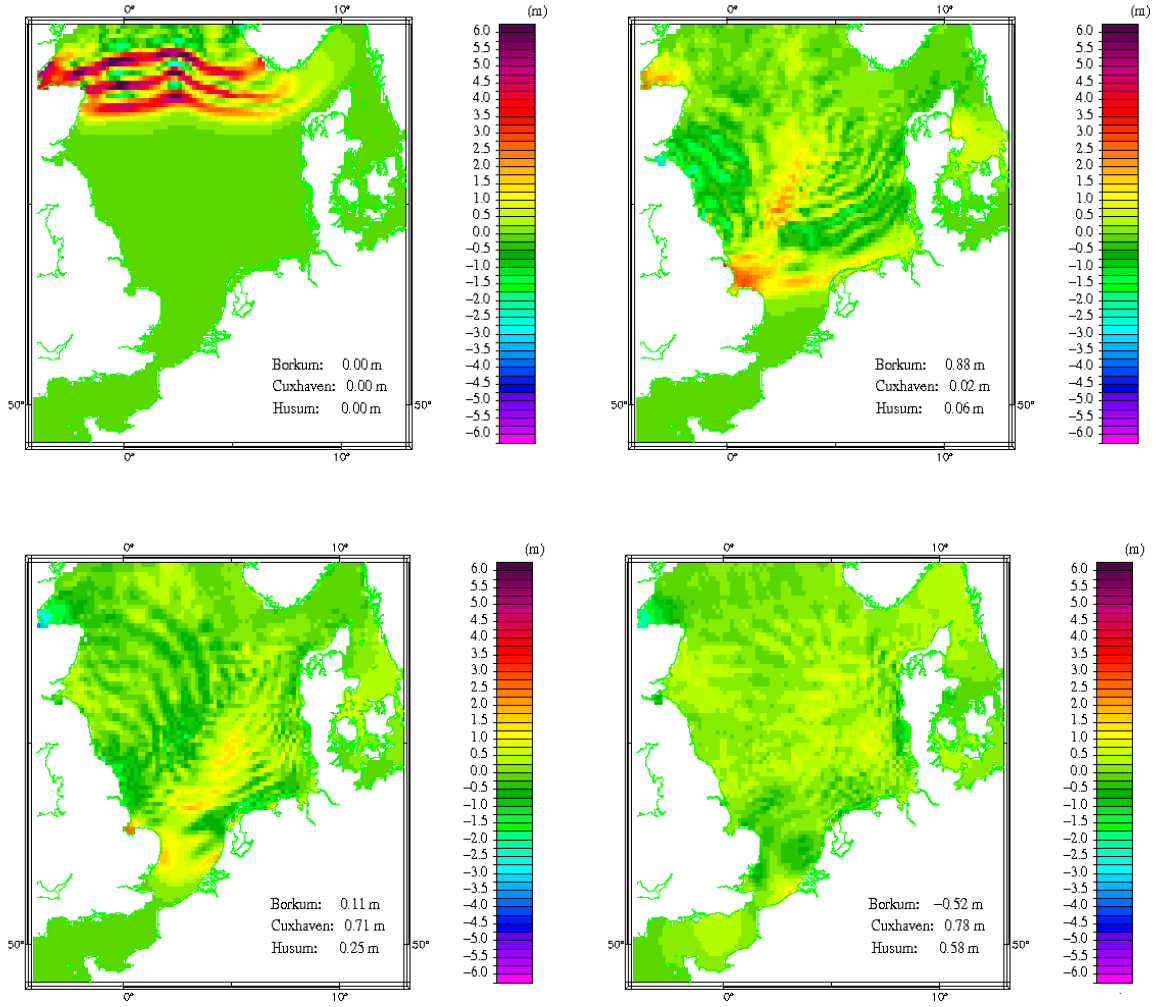

Fig. 7.5.1: Water level distribution after 2, 8, 10, and 15 hours (input signal: 3 positive single waves, T 1800 s, H 5 m, North Sea 10 km)

To carry out the simulation, the external surge of an extreme storm surge event (Jensen et al. 2007) was superimposed with the pure tsunami signal at the northern boundary in such a way that the second maximum of the simulation excluding the storm surge signal (Figs. 7.5.3 and 7.5.4, thin lower curve) arrives at Cuxhaven at the same time as the peak of the pure storm surge signal (Figs. 7.5.3 and 7.5.4, thin upper curve). In addition, unlike the

simulations described earlier, this simulation was carried out taking into account the meteorological forcing (atmospheric pressure and wind stress) of the extreme storm surge and the tide.

At Wick, close to the northern model boundary, there is an almost linear superposition of the tsunami signal and the storm surge signal (Fig. 7.5.2). The increase of the peak water levels at Cuxhaven is lower than the simple signal (Fig. 7.5.3). At Borkum, however, the simulated peak water level almost corresponds to linear superposition (Fig. 7.5.4).

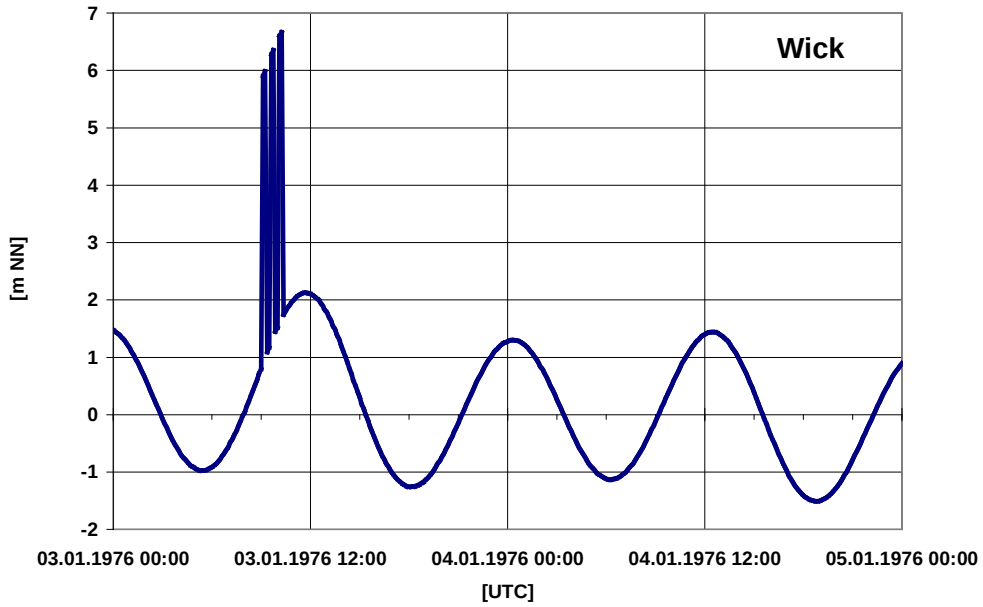

Fig. 7.5.2: "Tsunami signal", extreme storm surge, and tide. Water levels at Wick (North Sea 10 km)

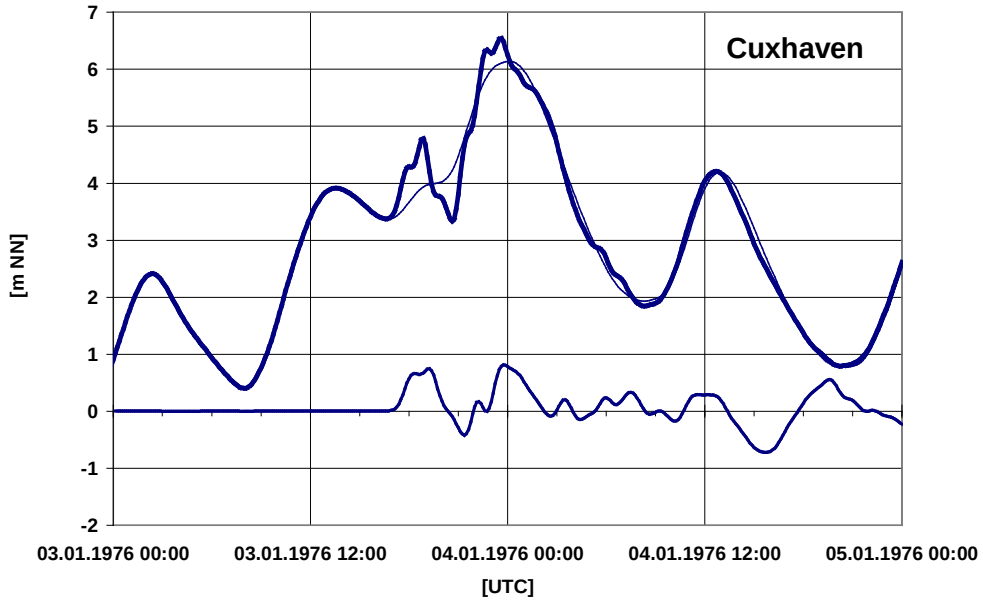

Fig. 7.5.3: "Tsunami signal", extreme storm surge, and tide. Water levels at Cuxhaven (thick lines, North Sea 10 km). Pure storm surge signal (thin line) and pure "tsunami signal" (medium-thick line below).

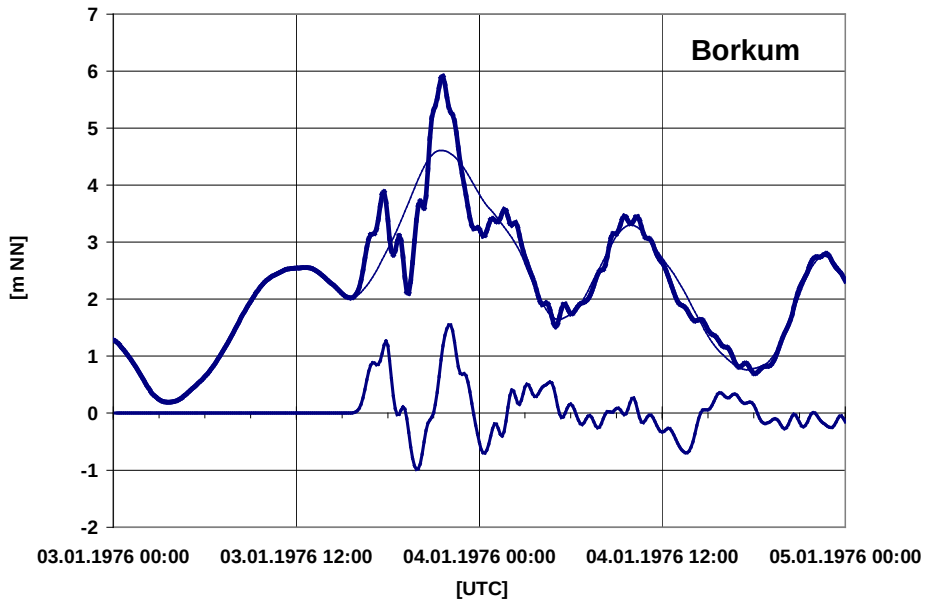

Fig. 7.5.4: "Tsunami signal", extreme storm surge, and tide. Water levels at Borkum (thick lines, North Sea 10 km). Pure storm surge signal (thin line) and pure "tsunami signal" (medium-thick line below).

8 Conclusions

The population living on the German North Sea coast is familiar with the changing tides and the occurrence of storm surges with high water levels (4-5 m above NN, German ordnance datum). Observing the weather, they know when to expect a storm surge. External surges generated outside the North Sea are either insignificant or, in the majority of cases, they are part of a storm surge event. Storm surges can be predicted with high accuracy. The phenomenon of waves "coming out of the blue", like the tsunami of December 2004, has raised concerns among the German population. The BSH, as the authority issuing the official German water level predictions, felt compelled to investigate the occurrence of historical tsunami in the North Atlantic Ocean, and to study the special characteristics of tsunami propagating in wide, shallow shelf seas like the North Sea.

Different events might conceivably cause a tsunami in the North Sea. The risk of a volcanic eruption and its consequences is low or non-existent in the North Sea. Meteoritic impacts in the North Sea are relatively unlikely. Tsunami research has seriously considered the consequences of minor meteoritic impacts in the North-East Atlantic. Near-earth asteroids are subject to continuous monitoring, however, and are planned to be either deflected or destroyed if they pose a real threat.

There exists historical and geological evidence for the impacts of an earthquake off Lisbon and of a slope failure at Storegga off the Norwegian coast. Tsunami whose primary cause is an earthquake pose only a low threat to the German North Sea coast. A more realistic scenario is an earthquake of low magnitude triggering a major slope failure in the North-East Atlantic. It is not possible to estimate the probability of occurrence of slope failures attributable either to this or to another cause. The most recent slope failure that had an impact on the North Sea was an event off Newfoundland in 1929. However, no evidence for a tsunami has been found in historical records of water levels at Cuxhaven.

The BSH is operating a model system consisting of non-linear, hydrostatic models. It comprises two three-dimensional baroclinic models and one two-dimensional barotropic model for the North and Baltic Seas, as well as a two-dimensional barotropic model for the North-East Atlantic Ocean. The question as to whether this modelling system, which is used operationally for storm surge predictions at the BSH, is suitable for simulating waves comparable to a tsunami has been discussed. Tsunami have frequencies and wave lengths ranging between those of sea/swell and tides/storm surges. There is no model that is equally suited to all uses, but each model is based on reasonable assumptions for the particular process to be simulated. Wave models and tide/storm surge models differ fundamentally in this respect. Neither of these models is suitable for tsunami simulation without prior modification. Nevertheless, only minor modifications were made to existing models at the BSH and other institutions before running simulations of the propagation of tsunami-type signals in the North-East Atlantic and North Sea. Two-dimensional barotropic models were used almost exclusively. The North Sea model (North Sea 2 km) used for the simulations in section 7 is a barotropic non-linear hydrostatic model and is thus suitable for computing the propagation, modification, and attenuation of tsunami with periods of 1800 s or more on the shelf. The North-East Atlantic model of the BSH was found to have limited suitability for simulating the propagation of medium-length waves in the deep ocean and their modification on the continental shelf. The BSH models in their current configuration are not suitable to simulate near-shore processes.

According to the model simulations, the prescribed signal travels about seven hours from the northern boundary of the North Sea (e.g. Shetland Islands) to Esbjerg, and about nine hours to Cuxhaven. A secondary signal that forms in the North Sea, mainly due to diffraction and reflection on coastal features, is higher in Cuxhaven than the primary signal and arrives a few hours later.

The standard signal used in the simulations (3 positive single waves, T 1,800 s, H 5 m, from the north) leads to a water level of 0.5 m in Cuxhaven for the primary signal, and 1 m for the

secondary signal. A successive increase in the input signal in steps of 1 m increases the secondary signal at Cuxhaven only by 0.1 m each.

Although there may be objections to the numerical simulations performed, it still appears justified to conclude that the German Bight will be protected from the catastrophic impacts of a hypothetical tsunami by its location in the wave shadow of Norway and at the end of a wide, shallow shelf and by the narrow British Channel.

9 Literature

Airy, G. B.: Tides and Waves. Encyclopaedia metropolitana (1841), Art. 192, 241-396 (Dated according to Craik 2004)

Androsov, A., Rubino, A.: Tsunami Propagation on Complex Bathymetric Features: Numerical Studies. Presented at Workshop „Tsunami – eine Gefahr für unsere Küste?“, Hamburg (2005)

Annunziato, A., Best, C.: The Tsunami Event – Analyses and Models. (2005, 10.4: ANN05)

Akylas, T. R.: Three-dimensional Long Water-Wave Phenomena. Annual Reviews of Fluid Mechanics 26 (1994) 191-210

Beringhausen, W. H.: Tsunamis and seismic seiches reported from the eastern Atlantic south of the Bay of Biscay. Bulletin of the Seismological Society of America 54, 1 (1964) 430-442

De Blasio, F.V., Issler, D.D., Elverhøi, A., Harbitz, C. B., Ilstad, T., Bryn, P., Lien, R., Løvholt, F.: Dynamics, Velocity and Run-out of the Giant Storegga Slide. In: Locat, J., Meinert, J. (Ed.): Submarine Mass Movements and Their Consequences. Kluwer Academic Publishers (2003) 223-230

Blayo, E., Debreu, L.: Revisiting open boundary conditions from the point of view of characteristic variables. Ocean Modelling 9 (2005) 231-252

Bondevik, S., Løvholt, F., Harbitz, C., Mangerud, J., Dawson, A., Svendsen, J. I.: The Storegga Slide tsunami – comparing field observations with numerical simulations. Marine and Petroleum Geology 22 (2005) 195-208

Boussinesq, J.: Théorie de l’intumescence liquide appelée onde solitaire ou de translation se propageant dans un canal rectangulaire. Comptes Rendus des Séances de l’Académie des Sciences 72 (1871) 755-759

Brunelli, J. C.: Dispersionless limit of integrable models. Brazilian Journal of Physics 30, 2 (2000) 455-468

Bryant, E.: Tsunami. The Underrated Hazard. Cambridge University Press (2001) 320 p.

Buch, E., Batholdy, J., Gregersen, S., Grauert, M., Hansen, A. W., Højerslev, N., Laustrup, C., Lomholt, S., Kliem, N., Nielsen, J. W., Pedersen, G. K., Risbo, T., Tscherning, C. C.: TSUNAMI Risikovurdering for danske, færøske og grønlandske farvande. DMI – Teknisk Rapport no. 05-08, Danish Meteorological Institute, Kopenhagen (2005, 10.1: DMI05) 44 p.

Burgers, J. M.: The nonlinear diffusion equation: asymptotic solution and statistical problems. Reidel, Dordrecht (1974) 173 p.

Camfield, F. E.: Tsunami. In: Herbich, J. B. (Ed.): Handbook of Coastal and Ocean Engineering, 1 (1990) 591-634

CD of the workshop of 21.6.2005: available from B. Brügge, BSH

Chubarov, L. B., Fedotova Z. I.: A method for mathematical modelling of tsunami runup on a shore. In: Yalçiner, A. C. et al. (Ed.): Submarine Landslides and Tsunamis. Kluver Academic Publishers, Dordrecht (2003), Nato Science Series, Serie IV, 21, 203-216

Couper, A. (Ed.): The Times Atlas of the Oceans. Times Books, London (1983) 58-59

Cox, D. C.: Status of Tsunami Knowledge. Proceedings of the Tsunami Meetings associated with the Tenth Pacific Science Congress, University of Hawaii, Honolulu Hawaii Aug. –Sept. 1961, 1-6

Craik, A. D. D.: The origins of water wave theory. Annual Review of Fluid Mechanics 36 (2004) 1-28

Derbyshire, D., Highfield, R.: Tsunami turned Britain into an island overnight. TsuInfo Alert 5,2 (2003) 7

Dick, S., Kleine, E., Müller-Navarra, S. H., Komo, H.: The operational circulation model of BSH (BSHcmod) – Model description and validation. Berichte des Bundesamtes für Seeschifffahrt und Hydrographie 29 (2001) 48 p.

Dietrich, G., Kalle K., Krauss W., Siedler G.: Allgemeine Meereskunde. Gebrüder Borntraeger Berlin (1975, 3. Aufl.) 593 p.

Durran, D. R.: Numerical Methods for Wave Equations in Geophysical Fluid Dynamics. Springer-Verlag, New York (1999) 465 p.

Fine, I. V., Rabinovich, A. B., Thomson, R. E., Kulikov, E. A.: Numerical Modeling of Tsunami Generation by Submarine and Subaerial Landslides. In: Yalçiner, A. C. et al. (Ed.): Submarine Landslides and Tsunamis. Kluver Academic Publishers, Dordrecht (2003), Nato Science Series, Serie IV, 21,69-88

Fine, I. V., Rabinovich, A. B., Bornhold, B. D., Thomson, R. E., Kulikov, E. A.: The Grand Banks landslide-generated tsunami of November 18, 1929: preliminary analysis and numerical modeling. Marine Geology 215 (2005) 45-57

Flather, R. A.: Existing operational oceanography. Coastal Engineering 41 (2000) 13-40

Flather, R. A., Davies, A. M.: The Application of Numerical Models to Storm Surge Prediction. Institute of Oceanographic Sciences 16 (1975) 23 p., 11 Abb.

Fröhle, P., Kohlhase, S., Weiss, D.: Seegang und Brandung. Die Küste 65 (2002) 34-142

Froude, W.: On the rolling of ships. Transactions of the Royal Institution of Naval Architects 3 (1862) 45-62

Geist, E. L., Titov, V., Synolakis, C. E.: Lehren aus der Monsterwelle. Spektrum der Wissenschaft April (2006) 74-82

Gerstner, F.: Theorie der Wellen. Abhandlungen der Königlichen Böhmischen Gesellschaft der Wissenschaften, Prag (1802) 16 und 18 p. und 1 Tafel

Gill, A. E.: Atmosphere – Ocean Dynamics. International Geophysics Series 30, Academic Press, New York (1982) 662 p.

Gisler, G., Weaver, R., Mader, C., Gittings, M.: Two- and three-dimensional simulations of asteroid ocean impacts. Science of Tsunami Hazards 21, 2 (2003) 119-133

Gjevik, B., Pedersen, G., Dybesland, E., Harbitz, C. B., Miranda, P. M. A., Baptista, M. A., Mendes-Victor, L., Heinrich, P., Roche, R., Guesmia, M.: Modeling tsunamis from earthquake sources near Gorringe Bank southwest of Portugal. Journal of Geophysical Research 102, C13 (1997) 27,931-27,949

Glimsdal, S., Pedersen, G., Dypvik, H., Langtangen, H. P., Shuvalov, V.: Tsunami generation and propagation from the Mjølnir asteroid impact. Meteoritics and Planetary Science (2007) in press

Grindlay, N. R., Hearne, M., Mann, P.: High risk of tsunami in the Northern Caribbean. EOS 86, 12 (2005), 121, 126.

Günther, H., Gayer, G.: Tsunamis und Küste. Presented at Workshop „Tsunami – eine Gefahr für unsere Küste?“, Hamburg (2005)

Hammack, J. L.: Tsunamis in a stratified ocean. Tsunami Research Symposium 15 (1974) 225-239

Harbitz, C. B.: Model simulations of tsunamis generated by the Storegga Slides. Marine Geology 105 (1992) 1-21

Henry, R. F., Murty, T. S.: Model studies of the effects of the Storegga slide tsunami. Science of Tsunami Hazards 1, 1 (1992) 51-62

Horrillo, J., Kowalik, Z., Shigihara, Y.: Wave Dispersion Study in the Indian Ocean - Tsunami of December 26, 2004. Marine Geodesy 29, 3 (2006) 149-166

Holthuijsen L.: Waves in shallow water. In: Guide to wave analysis and forecasting. WMO-No. 702 (1998 2. Auflage) 81-88

Housley, J. G., Taylor, D. C.: Application of the solitary wave theory to shoaling oscillatory waves. Transactions of the American Geophysical Union 38 (1957) 56-61

Imamura, F., Yalçiner, A. C., Ozyurt, G.: Tsunami Modelling Manual. (2006, 10.4: TN106) Draft

Imsland, P.: Study Models for Volcanic Hazards in Iceland. In: Latter, J. H.: Volcanic Hazards. Springer Verlag, Berlin (1989) 36-56

Jensen, J., Mudersbach, C., Müller-Navarra, S. H., Bork, I., Koziar, C., Renner, V.: Modellgestützte Untersuchungen zu Sturmfluten mit sehr geringen Eintrittswahrscheinlichkeiten an der Deutschen Nordseeküste. Die Küste 71 (2007) in press

Jones, J. E., Davies, A. M.: Processes Influencing Storm-Induced Currents in the Irish Sea. Journal of Physical Oceanography 33 (2003) 88-104

Van Joolen, V. J., Neta, B., Givoli, D.: High-order Higdon-like boundary conditions for exterior transient wave problems. International Journal for Numerical Methods in Engineering 63, 7 (2005) 1041-1068

Keller, J. B.: The solitary wave and periodic waves in shallow water. Comm. Appl. Math. 1, 4 (1948) 323-329

Kerridge, D. (Ed): The Threat Posed by Tsunami to the UK. Report to Defra, the Department for Environment, Food and Rural Affairs (2005, 10.3: UKB05)

Kleine, E.: Tsunamis in der Nordsee? – Versuch einer Skizze. Presented at Workshop „Tsunami – eine Gefahr für unsere Küste?“, Hamburg (2005)

Kodomtsev, B. B., Petviashvili, V. I.: On the stability of solitary waves in weakly dispersing media. Soviet Phys. Dokl. 15 (1970) 539-541

Komar, P. D.: Beach Processes and Sedimentation. Prentice-Hall, INC., Englewood Cliffs, New Jersey (1976) 429 p.

Korteweg, D. J., de Vries, G.: On the change of form of long waves advancing in a rectangular canal, and on a new type of long stationary waves. Phil. Magazine, series 5, 39 (1895) 422-443

Kowalik, Z.: Basic Relations between Tsunamis calculation and their Physics – II. Science of Tsunami Hazards 21, 3 (2003) 154-173

Laplace, P. S.: Recherches sur quelques points du système du monde. Mémoires de l'Académie des Sciences. (1776), Oeuvres Complètes, 9, Nr. 88, 187 p.

Latter, J. H.: Tsunamis of volcanic origins: Summary of causes, with particular reference to Krakatau, 1883. Bulletin Volcanologique 44 (1981) 467-490

Lehfeldt, R., Milbradt, P., Plüß, A., Schüttrumpf, H.: Ausbreitung einer Tsunamiwelle in die Nordsee. Die Küste 72 (2007) in press

Liu, P. L.-F., Losada, I. J.: Wave propagation modeling in coastal engineering. Journal of Hydraulic Research 40, 3 (2002) 229-240

Liu, P. L.-F., Yeh, H., Synolakis, C. (Ed.): Advanced numerical models for simulating tsunami waves and runup. Advances in Coastal and Ocean Engineering 10 (2007) in press

Lomdahl, P. S.: What is a Soliton? Los Alamos Science 10 (1984) 27-31

Long, D., Smith, D. E., Dawson, A. G.: A Holocene tsunami deposit in eastern Scotland. Journal of Quaternary Sciences, 4 (1989) 61-66

Mader, Ch. L.: Numerical Modeling of Water Waves. CRC Press, Boca Raton (2004, 2. Aufl.) 274 p.

Madsen, P. A., Murray, R., Sørensen, O. R.: A new form of the Boussinesq equations with improved linear dispersion characteristics. Coastal Engineering 15 (1991) 371-388

Madsen, P. A., Sørensen, O. R.: A new form of the Boussinesq equations with improved linear dispersion characteristics. Part 2. A slowly-varying bathymetry. Coastal Engineering 18 (1992) 183-204

Maramai, A., Graziani, L., Tinti, S.: Updating and revision of the European tsunami catalogue. In: Yalçiner, A. C. et al. (Ed.): Submarine Landslides and Tsunamis. Kluver Academic Publishers, Dordrecht (2003), Nato Science Series, Serie IV, 21,25-32

Marshall, J., Hill, C., Perelman, L., Adcroft, A.: Hydrostatic, quasi-hydrostatic, and nonhydrostatic ocean. Journal of Geophysical Research 102, C3 (1997) 5733-5752

Marshall, J., Adcroft, A., Hill, C., Perelman, L., Heisey, C.: A finite-volume, incompressible Navier Stokes model for studies of the ocean on parallel computers. Journal of Geophysical Research 102, C3 (1997) 5753-5766

Masselink, G.: Waves. In: Schwartz, M.L. (Ed.): Encyclopedia of Coastal Science, Springer Verlag, Dordrecht (2005) 1069-1074

McCowan, J.: On the solitary wave. Phil. Magazine, series 5, 32 (1891) 45-58

McNeil, C.: Tsunamis. Encylopedia of Ocean Sciences 7 (2001) 3056-3051

Miche, R.: Undulatory movements of the sea in constant and decreasing depth. Ann. de Ponts et Chaussées, May-June, July-August (1944) 25-78, 131-164.270-292, 369-406

Milbradt, P.: A stabilized finite element method for systems of instationary advection-dominated equations in multi-dimensional domains. Proceedings of 5th World Congress on Computational Mechanics, WCCM V, Vienna, Austria 2002, Ed. Mang, Rammerstorfer, Eberhardsteiner. (Model available under 10.4: MAR06)

Mirchina, N., Pelinovsky, E.: Dispersive intensification of tsunami waves. IST Proceedings 7, 7-10 (2001) 789-794

Mofjeld, H. O., Titov, F. I., González F. I., Newman J. C.: Analytic Theory of Tsunami Wave Scattering in the Open Ocean with Application to the North Pacific. NOAA Technical Memorandum OAR PMEL-166 (2000) 37 p.

Müller-Navarra, S. H.: Implementation of the equilibrium tide in a shelf sea model. Environmental and Chemical Physics 24 (2002) 127–132

Müller-Navarra, S. H., Lange, W., Dick, S. Soetje, K. C.: Über Verfahren der Wasserstands- und Sturmflutvorhersage: Hydrodynamisch-numerische Modelle der Nord- und Ostsee und ein empirisch-statistisches Verfahren für die Deutsche Bucht. promet 29, 1-4 (2003) 117-124

Munk, W. H.: The Solitary Wave Theory and its Application to Surf Problems. Annals of the New York Academy of Sciences 51 (1949) 376-424

Munk, W. H.: Long Ocean Waves. In: The Sea: Ideas and Observations in Progress in Study of the Sea, Interscience, New York (1962) 647-663

Nirupama, N., Nistor, I., Ponnambalam, K., Murty, T. S.: Tsunami Travel Time Atlas for the Atlantic Ocean. Marine Geodesy 29, 3 (2006) 179-199

Okada, Y.: Surface deformation due to shear and tensile faults in a half-space. Bulletin of the Seismological Society of America 75 (1985) 1135-1154

Paralaktuna, M.: Natural gas hydrates as a cause of underwater landslides: A review. In: Yalçiner, A. C. et al. (Ed.): Submarine Landslides and Tsunamis. Kluver Academic Publishers, Dordrecht (2003), Nato Science Series, Serie IV, 21, 163-169

Pedersen, G.: Benchmark problem 1. The third international workshop on long-wave runup models. Catalina Island (2004, 10.5: PEDup)

Peregrine, D. H.: Equations for Water Waves and the Approximation behind Them. In: Meyer, R. E. (Ed.): Waves on Beaches and Resulting Sediment Transport. Academic Press New York (1972) 95-121

Pichler, H.: Dynamik der Atmosphäre. Bibliographisches Institut A.G., Zürich (1984) 456 p.

Press, F., Siever, R.: Allgemeine Geologie: eine Einführung. Spektrum Akademischer Verlag, Heidelberg (1995) 602 p.

Rankine, W. J. M.: On the exact form of waves near the surface of deep water. Phil. Trans. Roy. Soc., London (1863) 127-138

Rayleigh, L.: On waves. Phil. Magazine, series 5, 1 (1876) 257-79

Rayleigh, L.: On progressive waves. Proceedings London Math. Soc., 9 (1877) 21-26

Reistad M., Magnusson A. K.: Introduction to numerical wave modelling. In: Guide to wave analysis and forecasting. WMO-No. 702 (1998 2. Auflage) 57-66

Resolutions of the Tenth Pacific Science Congress Concerning Tsunamis. Proceedings of the Tsunami Meetings associated with the Tenth Pacific Science Congress, University of Hawaii, Honolulu Hawaii Aug. –Sept. 1961, 263

Rubino, A., Pierini, S., Backhaus, J.: Dispersive mudslide-induced tsunamis. Nonlinear Processes in Geophysics (1998) 127-136

Ruffman, A.: Comment on: Tsunamis and tsunami-like waves of the eastern United States by Patricia A. Lockridge, Lowell S. Whiteside and James F. Lander with respect to the November 18, 1929 earthquake and its tsunami. Science of Tsunami Hazards 23, 3 (2005) 52-59

Russell, J. S.: Report on waves. 14th Meeting Brit. Assoc. Advanc. Sci. (1844) 311-390

Sabatier, P. C.: Formation of wave by ground motion. In: Encyclopedia of fluid mechanics, Gulf Publishing Company, Houston (1986) 723-759

Shuto, N.: Tsunamis of Seismic Origin. In: Yalçiner, A. C. et al. (Ed.): Submarine Landslides and Tsunamis. Kluver Academic Publishers, Dordrecht (2003), Nato Science Series, Serie IV, 21, 1-8

Smallman, J. (Ed): Tsunami – Assessing the Hazards for the UK an the Irish Coasts. Report to Defra, the Department for Environment, Food and Rural Affairs (2006, 10.3: UKI06)

Smelror, M., Kelly, S. R. A., Dypvik, H., Mork, A., Nagy, J., Tsikalas, F.: Mjolnir (Barents Sea) meteorite impact ejecta offers a Volgian-Ryazanian boundary marker. Newsletters on Stratigraphy 38, 2/3 (2001) 129-140

Stewart S. A., Allen, P. J.: A 20-km-diameter multi-ringed impact structure in the North Sea. Nature 418 (2002) 520-523

Streif, H.: Die Nordsee im Wandel vom Eiszeitalter bis zur Neuzeit. In: Lozán, J. L. et al.: Warnsignale aus Nordsee & Wattenmeer. Wissenschaftliche Auswertungen, Hamburg (2003) 19-28

Stokes, G. G.: On the theory of oscillatory waves. Trans. Cambridge Phil. Soc. 8 (1847) 441-455

Titov, V. V., Gonzalesz, F. I.: Implementation and Testing of the Method of Splitting Tsunami (MOST) Model. NOAA Technical Memorandum ERL PMEL-112 (1997, 10.3: NOAA) 11 p.

Ursell, F.: The Long – Wave Paradox in the Theory of Gravity Waves. Proceedings of the Cambridge Philosophical Society 49 (1953) 685-694

Voit, S. S.: Tsunamis. Annual Reviews of Fluid Mechanics 19 (1987) 217-236

Ward, S. N.: Landslide Tsunami. Journal o Geophysical Research 106, B6 (2001) 11201-11215

Ward, S. N.: Tsunamis. In: Meyers, R. A. (Ed.): Encyclopedia of Physical Science and Technology (3. Aufl.). Elsevier Academic Press (2002) 175-191

Ward, S. N., Day, S.: Cumbre Vieja Volcano – Potential collapse and tsunami at La Palma, Canary Islands. Geophysical Research Letters 28, 17 (2001) 3397-3400

Ward, S. N., Asphaug, E.: Asteroid impact tsunami of 2880 March 16. Geophysical Journal International 153 (2003) F6-F10

Weiß, R., Wünnemann, K., Bahlburg, H.: Numerical modeling of generation, propagation and run-up of tsunamis caused by oceanic impacts.- Geophysical Journal International 167,1 (2006) 77-88

Whitham, G. B.: Linear and Nonlinear Waves. John Wiley & Sons, INC. New York (1999, 2nd edition) 636 p.

Winter, C.: Simulation der Ausbreitung von Tsunami-Wellen in der Nordsee. Presented at Workshop „Tsunami – eine Gefahr für unsere Küste?“, Hamburg (2005, 10.4: WIN05)

Wynn, R. B., Masson, D. G.: Canary Islands landslides and tsunami generation: Can we use turbidite deposits to interpret landslide processes? Submarine Mass Movements and Their Consequences. Advances in Natural and Technological Hazards Research 19 (2003) 325-332

Yalçiner, A. C., Pelinovsky, E. N., Okal, E., Synolakis, C. E.: (Ed.): Submarine Landslides and Tsunamis. Kluver Academic Publishers, Dordrecht (2003), Nato Science Series, Serie IV, 21, 352 p.

Ziegler, P. A.: Geological Atlas of Western an Central Europe. Shell International Petroleum Maatschappij BV, (1990) second edition 1. Europe. Geology

10 Selected web pages

More than 97 million links are returned (on 3 April 2006) for the keyword “tsunami(s)”. Therefore, the following selection can only be arbitrary. Many sites contain their own selection of pages. The sites were last checked on 9 September 2006.

http://library.lanl.gov/tsunami/
STH82: Journal “Science of Tsunami Hazards“

http://www.sthjournal.org/
STH06: Current issues of journal “Science of Tsunami Hazards“

http://www.lib.berkeley.edu/WRCA/pdfs/wiegel_tsunamibib.pdf
Tsunami **information survey**. R. L. Wiegel 2005.

http://www.dnr.wa.gov/geology/tsuinfo/
TsuInfo Alert: Recent information on Tsunami. Washington Department of Natural Resources, Division of Geology and Earth Resources, started in January 1999.

10.1 Reports and risk assessments

http://www.defra.gov.uk/environ/fcd/studies/tsunami/default.htm
Tsunami Threat to UK, **Defra Report**, June 2005/06

http://www.defra.gov.uk/environ/fcd/studies/tsunami/tsurpmn.pdf
UKB05: UK report: The threat posed by tsunamis to the UK, Kerridge 2005
http://www.defra.gov.uk/environ/fcd/studies/tsunami/tsurp06.pdf
UKI06: UK report: Tsunamis – assessing the hazard for the UK and Irish coasts. Smallman 2006

http://www.dmi.dk/dmi/tr05-08.pdf
DMI05: Risk assessment, report DMI, Buch et al. 2005

http://www.nerc-bas.ac.uk/tsunami-risks/html/HSE1.htm
Results from the project **Tsunami Risks** containing background information, references, links and a special report **Tsunami Risk in the North-East Atlantic Region** by A. G. Dawson 2000

http://www.hydro.com/ormenlange/library/attachments/OTC.pdf
Storegga slide risk assessment. P. Bryn et al. 2004 (Hydro Oil & energy)

http://www.lapalma-tsunami.com/tudelft.html
TUD06: Research concerning the La Palma problem. Technical University Delft, Netherlands 2006

www.olympus.net/IAPSO/tsunami97.html
Report of the IUGG Tsunami Commission Business Meeting and Symposium, Melbourne, Australia, July 2-4, 1997

http://www.oecd.org/dataoecd/39/40/2503992.pdf
Risk due to **near earth objects**. Report OECD 2003

http://www4.tpgi.com.au/users/tps-seti/bioastr2002.pdf
Frequency of cosmic impacts, Paine, M., Peiser, B., 2002

http://www.sthjournal.org./233/concept.pdf
Warning Systems: **Differences between the Pacific, Atlantic and Arctic**. Murty, T. S., Nirupama, N., Nistor, I., Rao, A. D., Science of Tsunami Hazards, 23, 3, 39-51, 2005

http://www.strategic-road.com/confid/risk/earthquakes.htm
Links to **essential open sources** concerning earthquakes, volcanoes and tsunami including **index according to countries**. Stratedic-road.com, March 2006

10.2 Databases and catalogues

http://www.ngdc.noaa.gov/seg/hazard/tsevsrch_idb.shtml
NGDC: Tsunami – Database. National Geophysical Data Centre (NGDC)

http://omzg.sscc.ru/tsulab/
Tsunami – Catalogue, e.g. **Tsunami in the Atlantic –60 to 2003**. Tsunami Laboratory, Russian Academy of Sciences, February 2003

http://tsun.sscc.ru/htdbatl/
HTA03: Tsunami in the Atlantic –60 to 2003. Tsunami Laboratory, Russian Academy of Sciences, February 2003

http://dbh.nsd.uib.no/nfi/rapport/?Keys=17061&language=no
Genesis and impact of Tsunamis on the European coasts – **GITEC.** Outline of project 2006

http://tsun.sscc.ru/htdbatl/ReferenceTXT.asp
List of reference of **GITEC** Tsunami – catalogue. Tinti S., Maramai A., Baptista M., Harbitz C., Izquierdo A. 1998.

10.3 Internet pages of research institutions and projects

www.pmel.noaa.gov/tsunami/
NOAA: National Oceanic & Atmospheric Administration (NOAA) Tsunami: – Research program, including a description and examples of the forecast model MOST (Method of Splitting Tsunami) and The National Tsunami Hazard Mitigation Program with information and a detailed link list.

http://ioc3.unesco.org/itic/
International Tsunami Information Centre (ITIC)

http://www.tsunami.org/
Pacific Tsunami Museum. Frequently asked questions (FAQ), Links to **Tsunami – Research institutions**.

http://www.state.me.us/doc/nrimc/mgs/explore/hazards/tsunami/jan05.htm
Tsunami in the Atlantic. Maine Geological Survey 2005

http://www.vedur.is/english/
Icelandic Meteorological Office including earthquake warnings.

http://hraun.vedur.is/ja/englishweb/
Warnings for **Iceland.** Icelandic Meteorological Office, March 2006

http://www.raunvis.hi.is/~alexandr/glaciorisk/index.html
Jökulhlaups. Mahlman, A., The Science Institute, University of Iceland Nov. 2002

http://www.newscientist.com/article.ns?id=dn2622
LOR02: Unique meteorite crater found under North Sea. Lorenz R. July 2002

http://www.geohazards.no/projects/offshoregeohazards.htm
Projects of the International Centre for Geohazards (ICG), Oslo. Project 6: **Offshore Geohazards**.

http://www.geohazards.no/projects/tsunamis.htm
ICG10: Projects at the International Centre for Geohazards (ICG), Oslo. Project 10: Tsunami, including maximum surface elevation caused by Mjølnir – impact.

http://cordis.europa.eu.int/ist/environment/infoday20060131.htm
Warning systems. Information Society Technologies (IST), Meeting Paris January 2006

http://www.gfz-potsdam.de/bib/pub/m/infoblatt_tsunami.pdf
GFZ Potsdam, Leaflet on Tsunami. Bormann, P. Mai 2005

http://www.ifm-geomar.de/index.php?id=gashydrate
Gas hydrate, IFM-GEOMAR Kiel 2005

10.4 Models

http://ocean.dmi.dk/models/cmod.html
DMImo: Description of BSH's models (Danish Version).

http://tsunami.jrc.it/model/simulation.pdf
ANN05: Comparison of model performance: Delft3d, MOST, INGV, JRC. Annunziato, A., Best, C., January 2005

http://www.gfdl.noaa.gov/
GFDL: Search for ETOPO2, Topography used by Nirupama et al. 2006

http://tsunami.jrc.it/model/model.asp
JRC – Model to compute travel times of Tsunami.

http://ioc3.unesco.org/ptws/21/documents/TsuModelMan-v3-ImamuraYalcinerOzyurt_apr06.pdf
TN106: Documentation of the models Tsunami-N1, -N2, -N3 and Tsunami-F1, -F2. Imamura, F., Yalçiner, A. C., Ozyurt, G. Version April 2006

http://www.dhisoftware.com/mike21/Description/m21bw/BW_Module.htm
MIK21: Brief description of the model MIKE21 BW of the DHI.

http://www.bauinf.uni-hannover.de/~milbradt/Martin/
MAR06: Model MARTIN, description of a preliminary version, Milbradt, P.

http://www.wldelft.nl/soft/intro/index.html
Description of the model **Delft3d** and its options.

http://www.telemacsystem.com/gb/default.html
Brief description of the model system **Telemac**.

www.baw.de/vip/abteilungen/wbk/Methoden/hnm/untrim/PDF/vd-untrim-2004.pdf
Documentation for model **UnTRIM**.

10.5 Tsunami – Simulations and benchmark problems

http://t14web.lanl.gov/Staff/clm/tsunami.mve/tsunami.htm
MAD04: Tsunami – Simulations including the North Atlantic. Mader 2004

http://www.math.uio.no/avdb/gitec/planok/
PEDpT: Exemplary Tsunami – Simulation from the source to bore formation at the coast. Pedersen, G.

http://www.oce.uri.edu/hawaii/workshop_scope1.pdf
Benchmark problem 3: **mass failure**. Grilli, S., Krby, J., Liu P., Brandes, H., Fryer, G. 2003

http://www.cee.cornell.edu/longwave/data/benchmark3/Pederson_BM3.pdf
Benchmark problem 3: **mass failure** and run-up using various models. Pedersen, G., June 2004

http://www.rcom.marum.de/Tsunami_Animation.html
WIN05: Tsunami Animation, North Sea. Winter Ch., February 2005

http://www.cee.cornell.edu/longwave/index.cfm?page=benchmark
BEN04: Formulation of various benchmark problems, The third international workshop on long-wave run up models. June 2004

www.cee.cornell.edu/longwave/data/benchmark1/Pederson_BM1.pdf
PEDup: Benchmark problem 1: run-up using several approaches. Pedersen, G., June 2004

10.6 Waves

http://www.fluidmech.net/msc/f_linkw.htm
CAR04: Links regarding waves, especially tsunami, solitons and bores. Cramer, M. S. 2004

www.math.uio.no/~johng/info/web/lotheor.pdf
Nonlinear Theory for surface waves. Pedersen, G., Summer school 2004 part1

http://www.math.uio.no/~johng/info/web/aptheor.pdf
Nonlinear Theory for surface waves. Pedersen, G., Summer school 2004 part2

http://mathworld.wolfram.com/news/2005-01-14/tsunamis/
WEI06: Mathematics for Tsunami. Weisstein, E. W. and Trott, M. January 2005.

http://www.pma.caltech.edu/Courses/ph136/yr2002/chap15/0215.2.pdf
Waves in Rotating Flows. Thorne, K. February 2003

http://people.uncw.edu/hermanr/Research/solitons.htm
Links on **soliton**, Herman, R. L. July 2005

http://www.fluidmech.net/gallery/waves/hjump.htm
Photographs of **bores** (and other waves)

Acknowledgements

This project was initiated by a lecture on tsunami in Europe held by H. Heinrich in January 2005. In early February 2005, the project and the first model computations using non-fitted models were presented at the BSH. During the meeting, J. Murawski outlined the history and theory of solitary waves. We would like to thank our two colleagues and all others who provided valuable contributions and pointed out useful tsunami literature to us. The project also benefited from the workshop "Tsunami - a hazard for our coasts?". On this occasion, we would also like to express our thanks to the participants and organisers of the workshop.

Appendix: List of symbols

$\vec{c}_g$	propagation velocity of a wave train
c_{g0}	reference propagation velocity
D	dissipation of energy
E	wave energy
E_{deep}	wave energy in deep water
f	arbitrary function
$\vec{F}$	friction force
F_h	- horizontal component
F_v	- vertical component
g	gravitational acceleration
h	undisturbed water depth
h_0	reference water depth
h_{deep}	reference deep water depth
Δh	characteristic change in bottom topography
H	wave height (twice the amplitude)
H_{deep}	deep water wave height
$\vec{i}$	unit vector in the direction of wave propagation
L	wave length
L_h	characteristic length for change in bottom topography
L_{deep}	deep water wave length
p	pressure
p_0	reference pressure
p_B	pressure (Boussinesq equations)
p_{hs}	pressure (hydrostatic equations)
p_η	surface pressure
p'	perturbation pressure (linear, non-hydrostatic)
p'_B	perturbation pressure (Boussinesq equations)
p'_{hs}	perturbation pressure (nonlinear, hydrostatic)
Q_E	net source function for wave energy
r	vertical coordinate
S	wave steepness
S_{deep}	deep water wave
t	time
T	wave period
T_{deep}	deep water wave period
T_{short}	short wave period
u	horizontal current velocity
u^+, u^-	partial solutions for u
u_b	solution at the boundary of external and internal domain
u_{ext}	solution in an external spatial area

u_{ext}^{+}, u_{ext}^{-}	partial solutions for u_{ext}
u_{int}	solution in an internal spatial area
$u_{\text{int}}^{+}, u_{\text{int}}^{-}$	partial solutions for u_{int}
U	Ursell parameter
$\vec{v}$	water velocity
$\vec{v}_h$	- horizontal component
$\vec{v}_v$	- vertical component
$\tilde{\vec{v}}$	„transport velocity “
w	vertical current velocity
x	horizontal Cartesian coordinate
z	vertical Cartesian coordinate
ϕ	gravitational potential
ϕ_G	tidal potential
η	surface elevation
η^{+}, η^{-}	partial solutions for η
η_0	initial surface elevation
η_0^{+}, η_0^{-}	partial solutions for η_0
η_b	solution at the boundary of external and internal domain
η_{ext}	solution in an external spatial area
$\eta_{exr}^{+}, \eta_{ext}^{-}$	partial solutions for η_{ext}
η_{int}	solution in an internal spatial area
$\eta_{\text{int}}^{+}, \eta_{\text{int}}^{-}$	partial solutions for η_{int}
κ	dissipation coefficient
$2\vec{\Omega}$	earth’s angular velocity
ρ	water density
ρ_0	reference density of water
σ	bottom slope
∇	Nabla
∇_h	- horizontal component

Berichte des Bundesamtes für Seeschiffahrt und Hydrographie

Verzeichnis der veröffentlichten Arbeiten

1	(1994)	Sy, A., Ulrich, J.	North Atlantic Ship-of-Opportunity XBT Programme 1990 - Data Report, 134 pp.
2	(1994)	Hagen, E., Mittelstaedt, E., Feistel, R., Klein, H.	Hydrographische Untersuchungen im Ostrandstromsystem vor Portugal und Marokko 1991 - 1992, 49 pp.
3	(1994)	Oliczewski, J., Schmidt, D.	Entwicklung einer Bestrahlungsapparatur zum photochemischen Aufschluß von Meerwasserproben zur Bestimmung von Schwermetallen, 70 pp.
4	(1994)	BSH [Hrsg.]	Das UN-Seerechtsübereinkommen tritt in Kraft: Inhalte und Konsequenzen für die Bundesrepublik Deutschland, 71 pp.
5	(1995)	BSH [Hrsg.]	Nationale Folgerungen aus dem Inkrafttreten des UN-Seerechtsübereinkommens, 103 pp.
6	(1995)	Haffer, E., Schmidt, D.	Entwicklung eines Probenvorbereitungsverfahrens zur Bestimmung von Arsen im Meerwasser mit der Totalreflexions-Röntgenfluoreszenzanalyse, 109 pp.
7	(1995)	BSH [Hrsg.]	Global Ocean Observing System - Statusbericht, 100 pp.
8	(1996)	Mittelstaedt, E., Meincke, J., Klein, H.	WOCE-Current measurements: The ACM8 array – Data Report, 150 pp.
9	(1996)	BSH [Hrsg]	GOOS Workshop - Anforderungen an ein wissenschaftliches Konzept für den deutschen Beitrag, 60 pp.
10	(1997)	Sterzenbach, D.	Entwicklung eines Analyseverfahrens zur Bestimmung von chlorierten Kohlenwasserstoffen in marinen Sedimenten und Schwebstoffen unter besonderer Berücksichtigung der überkritischen Fluidextraktion, 233 pp.
11	(1997)	Jonas, M., Richter, R.	Stand und Entwicklungstendenzen nautischer Systeme, Anlagen und Geräte an Bord von Seeschiffen, 37 pp.
12	(1997)	Wedekind, C., Gabriel, H., Goroncy, I., Främke, G., Kautsky, H.	"Meteor"-Reise Nr. 71/1985, Norwegen-Grönlandsee – Datenbericht. 44 pp.
13	(1998)	BSH [Hrsg]	HELCOM Scientific Workshop - The Effects of the 1997 Flood of the Odra and Vistula Rivers. 46 pp.
14	(1998)	Berger, R., Klein, H., Mittelstaedt, E., Ricklefs, K., Ross, J.	Der Wasseraustausch im Tidebecken Hörnum-Tief – Datenreport. 260 pp.
15	(1998)	Röske, F.	Wasserstandsvorhersage mittels neuronaler Netze. 212 pp.
16	(1998)	Ross, J., Mittelstaedt, E. Klein, H., Berger, R., Ricklefs, K.	Der Wasseraustausch im Tidebecken Hörnum-Tief – Abschlußbericht. 98 pp.
17	(1998)	Klein, H.	OPUS-Current Measurements: Mecklenburg Bight and Fehmarnbelt - Data Report, 150 pp.
18	(1999)	BSH [Hrsg]	Deutscher Programmbeitrag zum Globalen Ozeanbeobachtungssystem (GOOS), 67 pp.
19	(1999)	BSH [Hrsg]	German Programme Contribution to the Global Ocean Observing System (GOOS), 71 pp.
20	(1999)	Sztobryn, M., Stanislawczyk, I., Schmelzer, N.	Ice Conditions in the Szczecin and Pomeranian Bay During the Normal Period from 1961-1990, 36 pp.

21	(1999)	Nies, H., Karcher, M., Bahe, C., Backhaus, J., Harms, I.	Transportmechanismen radioaktiver Substanzen im Arktischen Ozean - Numerische und experimentelle Studien am Beispiel der Barents- und Karasee, 134 pp.
22	(2000)	Lorbacher, K.	Niederfrequente Variabilität meridionaler Transporte in der Divergenzzone des nordatlantischen Subtropen- und Subpolarwirbels – Der WOCE-Schnitt A2, 156 pp.
23	(2000)	Klein, H.	The Subsurface Eastern Boundary Current of the North Atlantic between 32°N and 53°N – Data Report, 240 pp.
24	(2000)	Klein, H.	Strömungen und Seegangsverhältnisse westlich der Insel Hiddensee - Datenreport, 59 pp.
25	(2001)	Goedecke, E.	Der hydrographische Aufbau in der Deutschen Bucht vornehmlich dargestellt auf Grund der vorliegenden Unterlagen über Temperatur, Salzgehalt und Dichte, 202 pp.
26	(2001)	Klein, H., Mittelstaedt, E.	Strömungen und Seegangsverhältnisse vor Graal-Müritz und in der Tromper Wiek - Datenreport, 162 pp.
27	(2001)	Klein, H., Mittelstaedt, E.	Gezeitenströme und Tidekurven im Nahfeld von Helgoland, 24 pp. und Anhang.
28	(2001)	Behnke, J., Berking, B., Herberg, J., Jonas, M., Mathes, S.	Functional Scope and Model of Integrated Navigation Systems - A Toolbox for Identification and Testing. 181 pp.
29	(2001)	Dick, S., Kleine, E., Müller-Navarra, S., Klein, H., Komo, H.	The Operational Circulation Model of BSH (BSHcmod) – Model description and validation. 49 pp.
30	(2002)	Sy, A. , Ulrich, J., Weichert, H.-J.	Upper Ocean Climate Ship-of-Opportunity Programme of BSH – A Status Report. 45 pp.
31	(2003)	Dahlmann, G.	Characteristic Features of Different Oil Types in Oil Spill Identification. 48 pp.
32	(2003)	Nies, H., Gaul, H., Oestereich, F., Albrecht, H., Schmolke, S., Theobald, N., Becker, G., Schulz, A., Frohse, A., Dick, S., Müller-Navarra, S., Herklotz, K.	Die Auswirkungen des Elbehochwassers vom August 2002 auf die Deutsche Bucht. 81 pp.
33	(2003)	Loewe, P., Becker, G., Brockmann, U., Frohse, A., Herklotz, K., Klein, H., Schulz, A.	Nordsee und Deutsche Bucht 2002 – Ozeanographischer Zustandsbericht
34	(2004)	Schulz, G.	Geomagnetic Results Wingst 1996, 1997, 1998 and 1999 including the complete Wingst data set since 1939 on CDrom
35	(2004)	Gouretski, V. V., Koltermann, K. P.	WOCE Global Hydrographic Climatology
36	(2004)	Gayer, G., Dick, S., Pleskachevsky, A., Rosenthal, W.	Modellierung von Schwebstofftransporten in Nord- und Ostsee
37	(2004)	Schmelzer, N., Strübing, K., Stanisławczyk, I., Sztobryn, M.	Die Eiswinter 1999/2000 bis 2003/2004 an der deutschen Nord- und Ostseeküste/ Ice Conditions in the Szczecin Lagoon and Pomeranian Bay During the Winters 1999 - 2002
38	(2005)	Loewe, P., Schmolke, S., Becker, G., Brockmann, U., Dick, S., Engelke, C., Frohse, A., Horn, W., Klein, H., Müller-Navarra, S., Nies, H., Schrader, D., Schulz, A., Theobald, N., Weigelt, S.	Nordseezustand 2003

39	(2005)	Sztobryn, M., Stigge, H.-J., Wielbińska, D., Stanisławczyk, I., Kańska, A., Krzysztofik, K., Kowalska, B., Letkiewicz, B. Mykita, M., Weidig, B.	Sturmfluten in der Südlichen Ostsee (westlicher und mittlerer Teil) Storm Surges in the Southern Baltic Sea (Western and Central Parts)
40	(2006)	Loewe, P., Schmolke, S., Becker, G., Brockmann, U., Dick, S., Frohse, A., Herrmann, J., Klein, B., Klein, H., Nies, H., Schrader, D. Schulz, A., Theobald, N., Weigelt, S.	Nordseezustand 2004
41	(2007)	Bork, I., Dick, St., Kleine, E., Müller-Navarra, S.	Tsunami – a study regarding the North Sea coast